METIS

Research and Innovation Action (RIA)

This project has received funding from the European Union's Horizon 2020 research and innovation programme under grant agreement No 945121

Start date : 2020-09-01 Duration : 57 Months

Ensembles of hazard consistent surface ground motions mainshock seismicity

Authors : Mrs. Paolo BAZZURRO (IUSS), Pablo García de Quevedo (IUSS), Nevena ?ip?i? (IUSS), Paolo Bazzurro (IUSS), Vinicius Alves Fernandes (EDF), Michail Korres (EDF), Irmela Zentner (EDF), Marco Pilz (GFZ)

METIS - Contract Number: 945121

Project officer: Katerina PTACKOVA

Document title	Ensembles of hazard consistent surface ground motions mainshock seismicity
Author(s)	Mrs. Paolo BAZZURRO, Pablo García de Quevedo (IUSS), Nevena ?ip?i? (IUSS), Paolo Bazzurro (IUSS), Vinicius Alves Fernandes (EDF), Michail Korres (EDF), Irmela Zentner (EDF), Marco Pilz (GFZ)
Number of pages	79
Document type	Deliverable
Work Package	WP5
Document number	D5.4
Issued by	IUSS
Date of completion	2025-02-20 18:50:57
Dissemination level	Public

Summary

This deliverable describes the ensembles of hazard-consistent ground motion records considered in the METIS project. The first section focuses on a brief summary of the methodology employed for ground motion selection, as well as all the characteristics and implications. Additionally, the work shows the results of the record selection at the rock level and the format and organization of the selection sets, together with some recommendations on record selection. Finally, the selected time-histories at rock level are used as input motion for site response analysis both under 1D and 2D hypotheses, integrating the geotechnical model of the METIS case-study site and expected uncertainties on soil layers. The produced datasets are available for further soil-structure interaction studies.

Approval

Date	By
2025-02-20 18:51:28	Mrs. Paolo BAZZURRO (IUSS)
2025-02-20 22:51:46	Dr. Irmela ZENTNER (EDF)

METIS

Seismic Risk Assessment for Nuclear Safety

Research & Innovation Action

NFRP-2019-2020

Hazard-consistent surface ground motion time histories for METIS case study

Deliverable D5.4

Version N°1

Authors:

Pablo García de Quevedo, Nevena Šipčić, Paolo Bazzurro (IUSS),

Vinicius Alves Fernandes, Michail Korres, Irmela Zentner (EDF)

Marco Pilz (GFZ)

Disclaimer

The content of this deliverable reflects only the author's view. The European Commission is not responsible for any use that may be made of the information it contains.

Document Information

Grant agreement	945121
Project title	Methods And Tools Innovations For Seismic Risk Assessment
Project acronym	METIS
Project coordinator	Dr. Irmela Zentner, EDF
Project duration	1st September 2020 – 31st May 2025 (57 months)
Related work package	WP5
Lead organisation	IUSS
Contributing partner(s)	EDF (site response), GFZ (site criteria), IUSS (record selection)
Dissemination level	open

History

Version	Submitted by	Reviewed by	Date	Comments
N°1	Irmela Zentner	Charisis Chatzigogos	June 2024	
		Tadeusz Szczesiak, Peter Rangelow	June 2024	
N°2	Irmela Zentner	Charisis Chatzigogos	November 2024	
		Tadeusz Szczesiak, Peter Rangelow	November 2024	

Table of Contents

List of figures

List of tables

Abbreviations and Acronyms

Acronym	Description
COV	Coefficient of variation
CS	Conditional Spectrum
CMS	Conditional Mean Spectrum
DB	Database
EQL	Equivalent Linear
FFBC	Free-field Boundary Condition
GMPE	Ground Motion Prediction Equation
GMR	Ground Motion record
IM	Intensity measure
IML	Intensity Measure Level
LHS	Latin Hypercube Sampling
NPP	Nuclear Power Plant
PGA	Peak Ground Acceleration
PSA	Pseudo-Spectral acceleration
PSHA	Probabilistic Seismic Hazard Assessment
Rjb	Joyner Boore distance
RotD50	median of response spectra of the two horizontal components projected onto all nonredundant azimuths
SDOF	Single degree of freedom
Vs30	Shear wave velocity in the first 30m
TF	Transfer function
WP	Work Package

Summary

This deliverable describes the ensembles of hazard-consistent ground motion records considered in the METIS project. The first section focuses on a brief summary of the methodology employed for ground motion selection, as well as all the characteristics and implications. Additionally, the work shows the results of the record selection at the rock level and the format and organization of the selection sets, together with some recommendations on record selection. Finally, the selected time-histories at rock level are used as input motion for site response analysis both under 1D and 2D hypotheses, integrating the geotechnical model of the METIS case-study site and expected uncertainties on soil layers. The produced datasets are available for further soil-structure interaction studies.

Keywords

Ground motions, record selection, site response, 2D, plane wave, variability, uncertainty, equivalent linear, soil column

1. Introduction

Choosing ground motion records on rock that are appropriate for the site under consideration is crucial for seismic risk assessment, as it provides a link between the seismic hazard with structural analysis for site-specific fragility computations.This task is a key aspect of WP5 in the METIS project, aiming to maintain hazard consistency. It involves selecting appropriate ground motions that are consistent with the rock hazard at the site of interest (Figure 2), as estimated in the WP4, and then driving these ground motions through the soil to obtain the corresponding surface motions. This process ensures that the derivation of reliable fragility curves (in WP6) use ground motions specifically suited for the site in question.

In the Deliverable D5.1 of the METIS project, it was established that the most convenient and robust approach for selecting rock hazard-consistent ground motions is the Conditional Spectrum method in either its original form (*CS*, Jayaram et al., 2011) or in one of its variants (e.g., *CS-MR,* Spillatura et al. 2021 and *GCIM,* Bradley, 2010). This method guarantees hazard consistency and offers realistic ground motions by assuming a more accurate spectral shape than that obtained through other traditionally used approaches, such as the uniform hazard spectrum (UHS). Additionally to the Conditional Mean Spectrum (*CMS*, Baker, 2011), the CS reflects the variability in the response spectrum, resulting in a more comprehensive representation of the ground motions that could potentially be experienced at the site. The ground motions selected for the case study site were obtained through the hazard analysis performed using the OpenQuake engine and the hazard model provided by WP4 (see METIS D4.6 for more information on METIS case study PSHA). The reference rock conditions were considered as being characterized by a *Vs30* of 1000m/s.

In the deliverable D5.3 of the METIS project the strategy for conducting 1D, 2D and 3D site response analyses were presented together with criteria for choosing the kind of site response analysis adequate for a given site.

From the criteria applied to the METIS case study site, it was concluded that the site can be considered a 1D site. General guidelines for standard practice of 1D ground response analysis are given in (Stewart, Afshari, & Hashash, 2014). Here we implement the approach for the consideration of uncertainty, variability and attenuation in equivalent linear (EQL) and nonlinear 1D site response presented and discussed in D5.3. We have proposed a generic framework for uncertainty quantification and propagation to define a reduced set of 1D columns that would: (i) well represent the mean and standard deviation of soil surface ground motion variability and (ii) be easily implemented for soil-structure interaction studies as the framework of the METIS project is oriented in integrating site effects in structural response analysis. Both the variability of input ground motion on rock as well as the uncertainty related to site data are considered and propagated. In addition, we perform 2D site response analysis to corroborate the 1D hypothesis from the site categorization.

The target Conditional Spectrum (CS) was created following the procedure detailed in Lin et al. 2013, which comprehensively considers all scenarios contributing to the hazard. This procedure has been recently integrated into the OpenQuake software (see METIS D4.4). Subsequently, the ground motion record selection was executed using the optimization methodology defined by Jayaram et al. 2011. This methodology enables the selection of different record sets that best match the target mean and dispersion within an acceptable tolerance (here measured as the sum of weighted square errors, *SSEs*), with multiple groups of ground motions per intensity level. Here, the selected ground motions were extracted from an extensive database compiled from the Engineering Strong-Motion (ESM) database (https://esm-db.eu) (Lanzano et al., 2019), NGA-West2 (NGA West 2 | Pacific Earthquake Engineering Research Center (berkeley.edu)) (Ancheta et al., 2014), New Zealand Strong-Motion database (Home - GNS Science) (here referred to as GNS) (Van Houtte et al., 2017), and the NEar-Source Strong-motion (NESS) (INGV/RELUIS NESS flat-file) (Sgobba et al., 2021). The database was described in more detail

in Deliverable D5.1. The selection was done for the *RotD50* combination of the horizontal components. The vertical component of the ground motion was not included in the selection procedure. It was scaled by the same amount as the two corresponding horizontal components, without any consideration of consistency since vertical hazard was not available for the case study site. These time histories are then considered as input motion for the site response analysis considering both ground motion variability and soil uncertainty.

In what follows we first present the METIS case study site and data in section 2. Then, in section 3, we describe the selected rock hazard consistent dataset and provide some recommendations and lessons learned. In section 4 we apply the site categorization criteria to the METIS case study site and perform site response analysis using the rock ground motion as input.

2. METIS case study

The METIS case study, illustrated in Figure 1, is located in the Tuscany region of Italy, with site coordinates of 42° 25' 26.4'' N and 11° 12' 7.2'' E. This zone is considered a low to moderate seismicity region, where historical data shows only 32 events with magnitudes above 5. The region has no information available about active fault structures and future seismicity was modelled via the smoothed seismicity approach. The full in-depth description of the modelled seismicity in the region can be found in Deliverable D4.6.

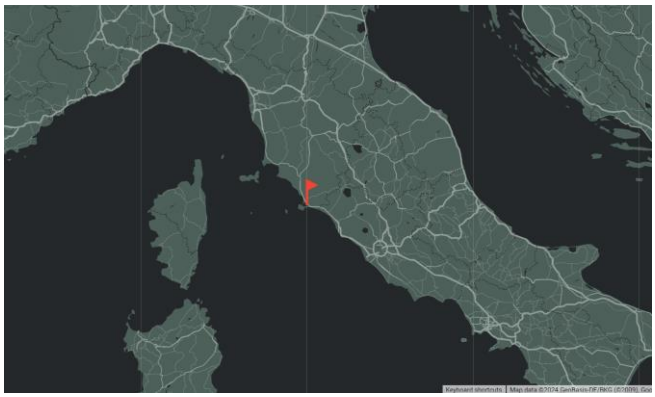

Figure 1: METIS Case study site

For consistency with record selection, hazard calculations at the rock level were performed for the METIS case study assuming a *Vs30* of 1000 m/s at bedrock level. The analysis was performed for several levels of intensity, for return periods going up to 100 000 years. This upper bound is considered high enough to cause strong motions that may damage the NPP structures and components. The detailed results of the hazard analysis, which can be found in Deliverable 4.6, are summarized here through the hazard curves for PGA and spectral accelerations at periods of 0.1s and 0.25s, as well as the uniform hazard spectra at two return periods (Figure 2).

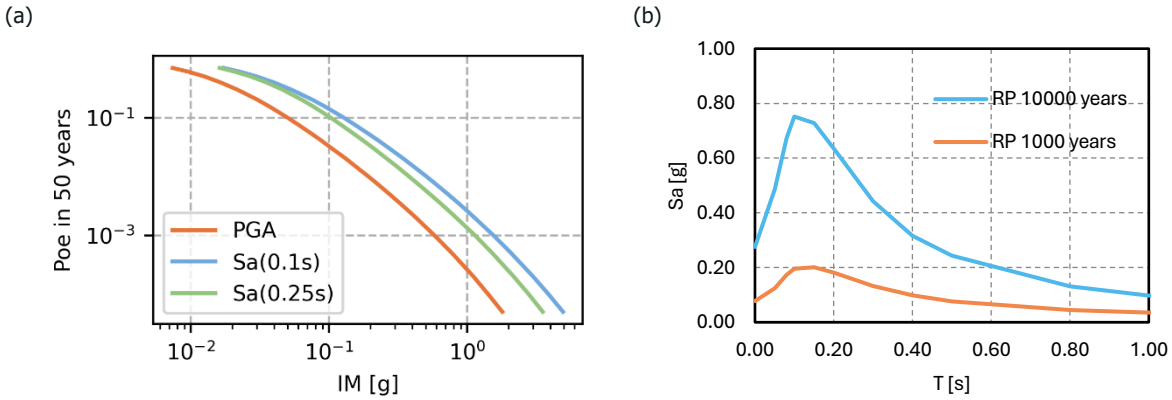

Figure 2: METIS Case study site (a) hazard curves and (b) Uniform hazard spectra

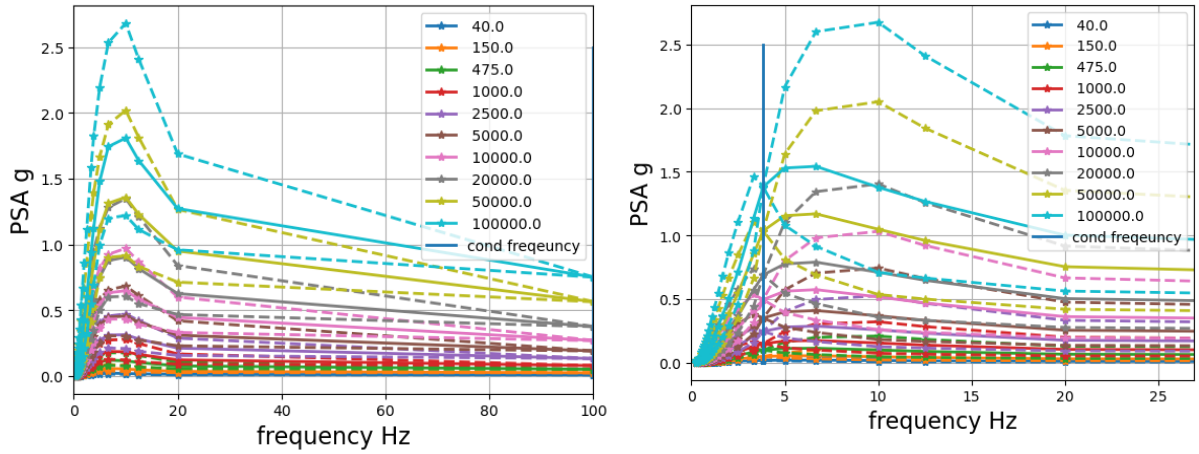

(a) PGA **(b) Sa(0.25 s)**

Figure 3: Target median (solid) and ±2σ spectra (dashed) derived from hazard for record selection. The dots are the conditional PSA values defined for the record selection procedure.

The target CMS and ±2σ intervals used for the record selection are shown in **Figure 7**as a function of frequency for two of the conditioning IMs, PGA and Sa(0.25s) and for the 10 return periods considered for record selection.

The soil properties at the site were characterized using borehole data indicating 4 different geotechnical layers. **Table 1** shows the soil characteristics and elastic properties of the layers along their corresponding depths, neglecting the first 2m of vegetation layer.

Layer		Depth (m)	Soil nature	Vs (m/s)	Poisson ratio (.)	Mass density $\rho(t/m^3)$
	2-1	0-5	Sand and gravel	509	0.4	1.75
	2-2	5-10	Silt and sand	390	0.475	1.70
	2-3	10-15	Sand and gravel	405	0.455	1.80
Layer 2	2-4	15-18	Sandy silt and sandy clay	605	0.425	1.85
	2-5	18-25	Gravelly sand	590	0.45	1.90
	2-6	25-30	Silty sand and silty clay	489	0.455	1.95
	2-7	30-33	Sand and sandstone	805	0.45	1.95
Layer 3		33-64	Silty clay	380	0.45	2.00
Layer 4		64-78	Silty sand and sandy silt	430	0.45	2.05
Layer 5		from 78	Silty clay	Vs(z)	0.455	2.00

Table 1: Soil profile at the METIS case study

The geotechnical and geophysical (cross-holes at 100m depth maximum) campaign performed at the site could not directly identify the bedrock layer. Geophysical down-hole measurements (**Figure 4**) identified a nearly flat interface between geotechnical layers previously identified (horizon A corresponding to the interface between layers 2 and 3 and horizon B the interface between layers 4 and 5). However, identified bedrock interface seems variable along the site, with an estimated maximum depth around 500-600m. The geological maps identified the bedrock as flysch rock, for which a reasonable hypothesis of Vs=1000 m/s is considered in this work, which is also in agreement with the Vs value considered for the PSHA established for the METIS case. Therefore, in this work the Vs profile at the last layer is defined by the following expression (Parolai, 2022): $Vs(z) = V_0(1+z)^n$, with Vs(78m)=417m/s and Vs(500m)=1000m/s, which gives n= 0.47 and V_0= 51.6 m/s.

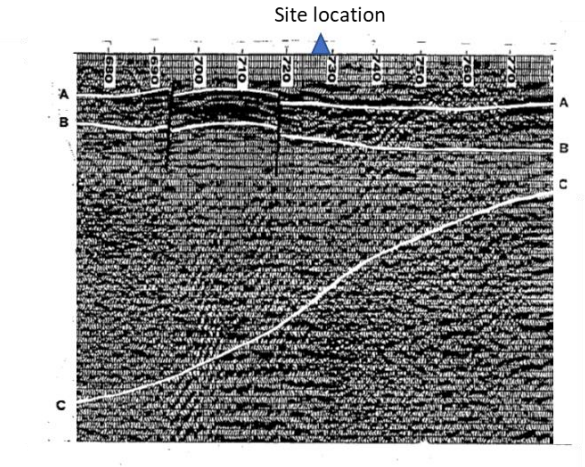

Figure 4: Synthetic view of one down-hole measurement performed at the site.

3. Ground motion selection on reference rock

3.1. Method and Dataset

This section summarizes the results of the record selection at rock level, performed through the procedures summarized in the previous subsection. Record selection was performed four times forthe conditioning IMs of *PGA*, *Sa*(0.1s), *Sa*(0.26s) and *AvgSA*(0.1:0.4s), which were deemed as the most relevant ones for structural analysis within the METIS project (Deliverable 6.3). Due to limitations on the existing variance-covariance matrix of spectral acceleration quantities, the *PGA* selection was done for a *Sa* at the conditioning period of 0.01s, given that this is the lowest period for which the correlation values are available (Baker and Jayaram, 2008). Additionally, record selection was performed for a period of 0.25s instead of 0.26s to avoid interpolation errors that can lead to imprecisions in the calculations of the spectral ordinates. The selection was done for a set of 10 intensity measure levels (*IMLs*), which are related to different probability of exceedance (POE) values in 50 years (or, alternative return periods), as described in Table 2.

Given the scarcity of available rock ground motions for high levels of intensity, simplifications were made by allowing ground motions recorded at non-rock sites, as well as scaling the amplitude of the signals. In particular, a lower bound of V*s30* of 400m/s was established, along with a maximum scaling factor of 10 at all IMLs except for the largest one, where the maximum scaling factor was set to 12. It is expected that the scaling factors can be reduced when a larger database is available. It is not expected that the scaling factors and non-rock site ground motion cause any considerable bias in the analysis results, as discussed in Deliverable D5.1. Additionally, the maximum error tolerance was set as 0.12, a value established through statistical tests as explained in METIS D5.1.

IML	POE in 50 years	Return Period	PGA [g]	Sa(0.1)[g]	Sa(0.25)[g]	AvgSa(0.1:0.4) [g]
1	0.7180	40	0.010	0.021	0.021	0.019
2	0.2855	150	0.025	0.054	0.052	0.049
3	0.0998	475	0.051	0.124	0.103	0.097
4	0.0488	1000	0.079	0.198	0.157	0.147
5	0.0198	2500	0.132	0.343	0.257	0.242
6	0.0100	5000	0.191	0.505	0.367	0.347
7	0.0050	10000	0.271	0.664	0.519	0.491
8	0.0025	20000	0.377	1.139	0.720	0.683
9	0.0010	50000	0.565	1.557	1.079	1.023
10	0.0005	100000	0.752	2.082	1.437	1.364

Table 2: The ten Intensity Measure Levels considered in the case study selection.

Given that downstream applications may afford different amounts of computational burden, the selection procedure was done in nine incremental sets, to provide flexibility during the analysis. This means that for each *IML*, there are nine groups of ground motion sets with increasing number of records per IML, starting with a set of 9 records, and then adding 2 for each group, ending up with a total of 25 records for the largest set. It must be noted that the larger sets contain all the records from the smaller sets and should not be combined, as the full group is hazard consistent and adding or removing records would hinder consistency. All these sets are consistent with the target CS within the considered tolerance. Figure 5 shows an example of the results of record selection at the same *IML5* (corresponding to 2500yr return period)) for a smaller set (11 ground motions) and for a larger set (25 ground motions). Note that this procedure was repeated exactly as described for all conditioning IMs with the exception of Sa(0.1s). For the Sa(0.1s) case, it was not possible to select incremental sets by simply adding two ground motions at the time to the previous set and obtain response spectra within the desired error tolerance. Therefore, in this case only, each set contains ground motions different than those selected for other IMLs.

It must be noted that no target duration was established for the rock record selection, and the accelerograms were selected with no limitations regarding this IM. This limitation may impact the results for duration sensitive components, such as those that are pushed into significant nonlinearities or are susceptible to degradation and damage accumulation. However, long duration ground motions should not be prevalent in the selection given the imposed spectral shape (as elaborated on in section 3.2). However, directly disaggregating the duration parameter depends on its availability within the GMPEs used in the hazard calculation, as well as the presence of a correlation structure to impose it during selection. The relevant duration can be deduced from then scenario obtained by disaggregation using available relationships. If duration is deemed critical, it should be included in the selection process. The record selection via the GCIM framework could also offer a more accurate approach to directly incorporate it. Alternatively, the CS-MR could also provide some improvements in this regard, as enforcing the causative parameters would lead to a selection of ground motions that reflect the duration of earthquakes with magnitudes and distances similar to those found by disaggregation.

Finally, a small number of near-field, pulse-like records can be identified within the selected dataset. These records, potentially featuring spikes in the velocity time-history indicative of fling effects, are an inherent aspect of hazard-consistent record selection across multiple intensity levels. Given their limited presence, their impact on the fragility results is expected to be minor, consistent with findings from previous studies (e.g., Kohrangi et al., 2018).

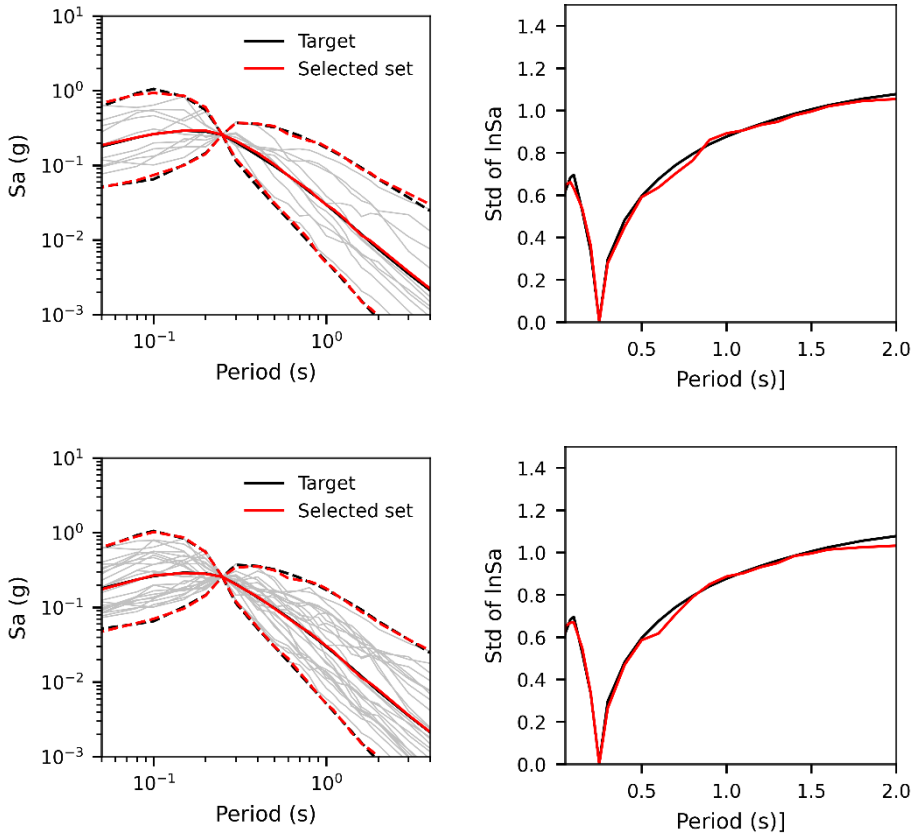

Figure 5: Target mean and dispersion of selected sets for *IML5* of the 11-record group (Top) and 25-record group (bottom) conditioned at Sa(0.25s).

3.1.1. Repository of the selected records

The selected records have been stored and saved as pickle files (.pkl) in a set of directories and subdirectories available in the project's Flexx repository. Additionally, python scripts are available to plot the results of the record selection procedure. For a better understanding of their format and contents, their structure and fields are detailed in Table 3. The ground motion acceleration files are stored within directories named *'IML_#'*, which contain all the ground motions at the indicated IML for each given conditioning *IM*. The different names of each record per set, time steps, scaling factors and other required data are contained within the mentioned file.

Level	Field name	Description
Level 1	Periods	List of considered periods of the spectrum
	Poes	List of probabilities of exceedance in 50 years

	imls	List of intensity measure values (Sa) in g per level
	IM_cond	Conditioning IM
	IM#	Directories from 1 to 10, containing the data per IML. *Detailed in level 2*
Level 2	Inside each IM directory there are 9 subdirectories, corresponding to the different number of records considered. *Detailed in level 3*	
Level 3	group	N followed by the number of records per IM in this group
	CS	subdirectories with the data for the group and IML. *See level 4.*
Level 4	Spectra	Contains the spectral acceleration values for each record, for the periods listed on the periods field
	Rec_h1	Names of the ground motion record files on the first horizontal direction
	Rec_h2	Names of the ground motion record files on the second horizontal direction
	Rec_v	Names of the corresponding vertical acceleration files
	SSEs	Matching error associated with this group and IML in %
	dt	Time step for each record
	nstp	Number of points for each record
	DB	Database of origin for each record file
	SF	scale factor applied to each record to match the target CS
	Mw	The magnitude of the earthquake causing the ground motion
	Rjb	Joyner Boore distance
	Vs30	Vs30 of the station at which the ground motion was recorded

Table 3: Description of fields and structure of the record selection files

3.2. Recommendations from D5.1 and comments on record selection

The recommendations and comments in this section are based on the record selection study described in Deliverable 5.1, only the main aspects of the tests performed there, and related conclusions are reported herein.

In CS-based hazard-consistent record selection, it is of paramount importance to be able to select ground motions that have the specified joint distributions of spectral accelerations. In an ideal case, an analyst would be able to choose from a sufficiently large number of ground motions that are naturally at the amplitude levels requested and have been recorded at sites with similar conditions of those present at the site. In this study the local soil conditions are selected to be reference rock of Vs30=1000m/s. Unfortunately, the existing databases of real ground motions do not have enough recordings to satisfy this request, especially for very high hazard levels. Therefore, one is left with two choices: either using the few existing ground motions recorded on the desired site conditions without enforcing hazard consistency or assembling hazard consistent sets of ground motions allowing two operations that may potentially affect the robustness of the results. These two operations are ground motion scaling and using ground motions not recorded on the desired site conditions. Previous studies (e.g. Tarbali and Bradley 2016) have shown that not enforcing hazard consistency has a very negative effect on the accuracy of the fragility curves that ensue.

In D5.1 we have investigated whether scaling and mixing soil conditions in CS-based record selection are legitimate operations, when done judiciously, or whether a bias is introduced in the structural responses by the use of these spurious ground motions. The first battery of tests on record selection had the objective of assessing the potential bias introduced by using records scaled by large factors selected according to the CS-based approach. To this end, two sets of 40 CS-based hazard-consistent ground motions were assembled for a given site: one containing records with exclusively high (7-10) scaling factors (HSF) and the other set with exclusively low (1-2) scaling factors (LSF). The accelerograms were selected using different conditioning IMs and ran through a suite of fixed-base nonlinear SDOF systems with different vibration periods of 0.2, 0.5, 1.0. 1.5 and 2.0s and two material constitutive laws, an elastic with hardening and a pinching model with degradation. Additionally, an MDOF system, representing a 5-story RC building was added to the testing set to evaluate any possible bias coming from MDOF systems, shown in Iñarritu et al. (2023). More details about the modeling approach and assumptions can befound in Vamvatsikos and Zeris (2010). For all cases, the response was evaluated in terms of maximum ductility (maximum inter-storey drift in the case of the MDOF). The ground motions were also subjected to comparative tests, by computing and comparing different intensity measures (PGA, $DS_{5\text{-}75}$, CAV and AI). Results showed that neither the IMs nor the responses and resulting fragility curves were significantly biased by using ground motions scaled by large factors, only observing small differences at severe levels of nonlinearity. Results of the responses for the MDOF case are summarized in **Figure 6**, while the rest can be found in D5.1 and Iñarritu et al. (2023). It must be noted that this investigation is conducted only for SDoF and simple MDOF placed on the ground and needs to be validated for more general cases.

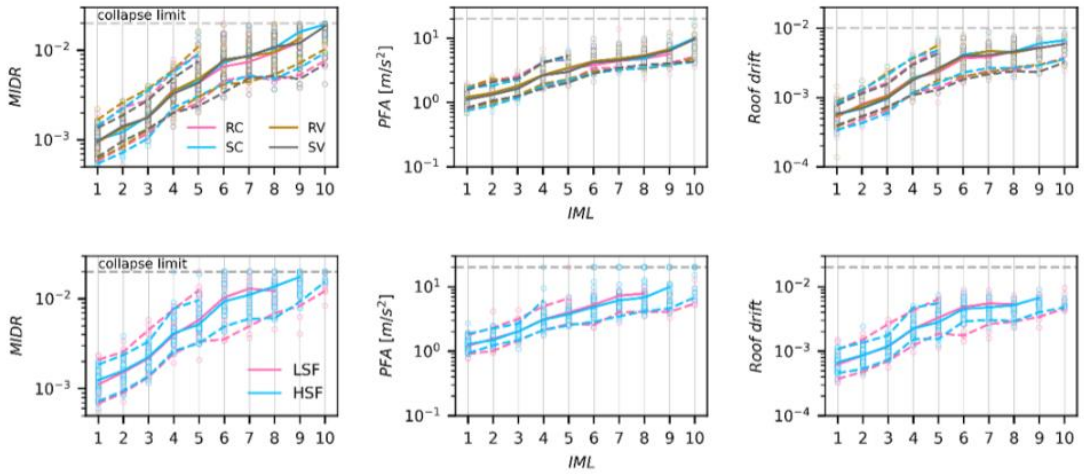

Figure 6: **Comparison of the response estimates obtained from MSA performed on the 5-story RC building. The figure shows the data points, the median (solid line) and 5th and 95th percentiles (dashedlines) of the MIDR (First column), PFA (second column), and roof drift (third column). Note: The first row shows the results obtained from different soil versus rock classifications, while the second row is related to the different scaling factor assumptions**

Similarly, a second battery of tests, using the same methodology and structures, investigated whether soil-recorded ground motions could be used with (or in lieu of) rock motions in CS-based site-specific record selection for rock conditions. This test is dictated by a practical need, namely the necessity to supplement the scarcely populated databases of existing rock ground motions especially at higher intensities. The same battery of tests described above was conducted here using two groups of ground motions: one with exclusively soil ground motions, classified using *Vs30*-based method and using several other metrics and proxies (referred to as complex method in D5.1), noted as SV and SC, respectively, and the other containing exclusively rock (following the same classification schemes) ground motions, noted as RV and RC. With the *Vs30* method ground motions that had vs30 values below 400m/s were classified as soil motions and those with *Vs30 values* above 800 m/s as rock ones. This strategy generates two groups of motions that are well distinct. Again, the results (detailed in Deliverable 5.1) did not show any significant impacts on the response statistics of the two groups. Some differences were only observed at very severely nonlinear response levels (i.e., high ductility levels). Additionally, it was important to investigate whether the selected soil ground motion groups exhibited systematically longer strong motion durations compared to rock motions, as represented by Ds_{5-75}. The results showed that, as expected, the soil groups had slightly longer median durations across all sets, along with higher dispersion and greater maximum values in most cases. However, this difference was smaller than the thresholds commonly used in the literature to differentiate between long and short-duration records. For instance, Chandramohan et al. (2016) defines short-duration records as those with Ds_{5-75} values below 25.0 seconds. Interestingly, the selected soil records had a significantly shorter mean duration compared to the full database. Specifically, the CS-selected soil records exhibited a mean duration of 8.9 seconds, a notable reduction from the 24.4 seconds observed in the full database.

These findings suggest that provided that hazard consistency is enforced via the CS approach one could apply scaling factors up to 10 and incorporate ground motions recorded at soil sites within the set of rock ones. Note that this conclusion arises from tests conducted by design for worst-case scenarios, where the datasets exclusively featured high scaling factors or solely comprised soil-recorded ground motions. Real applications will not consider such extreme cases. The selections would favour mildly-scaled rock ground motions that are supplemented by soil ground motions and largely scaled rock

motions very sparingly and only on an as needed basis. Given that the outcomes for these extreme scenarios exhibited no notable bias, one can infer that with a meticulous control over hazard consistency and spectral shape, the responses are expected not to manifest any statistically significant bias even when scaled ground motions and soil motions are included in the mix. While the simplified structures considered in these studies do not represent real nuclear structures, they enable us to perform large scale testing with the multiple ground motion groups considered.

Further details of these studies can be found in Deliverable D5.1.

When selecting ground motion records using CS, the match between the target and the selected sets should stay within an acceptable tolerance. Based on an additional battery of tests conducted in Deliverable D5.1, it was found that a sum of square errors below 0.12 can be considered to be an accurate match to the target CS when 25 periods participate in the computation of the sum of square errors, as done here. It is acknowledged that for an application to multimodal industrial structures, the list of frequencies needs to be adapted to the kind structure considered. Here, they were chosen among those already available in the databases. This threshold value, of course, depends on the number of vibration periods considered in the matching procedure, as a higher number of points would naturally yield higher acceptable threshold values of error. However, if so desired, an estimate of the acceptable tolerance value for different number of vibration periods can be computed by normalizing the values used for 0.12 (i.e., 0.12/25). As a comment of practical importance, it is recommended to only select records conditioning on spectral quantities at periods for which spectral ordinates are available in the database. Interpolation of response spectral ordinates may bias the results of selection. For instance, this was the case when attempting to select a group for a period of 0.26s, which led to a larger spread on the SaRotD50 values of the selected records. Herein the choice of the reference frequencies comes from the available data provided by the record databases (NGA, ESM, NESS), as the databases contain the RotD50 spectra for a set number of periods. Note, that a perfect match of the period of vibration of the structure with the period used in the CS approach is not needed to ensure statistically robust fragility curves.

To conclude, as discussed above, the accuracy of the match of the target joint spectral acceleration distribution imposed in the CS approach should be the top priority in record selection above scaling factors bounds or soil type limits of the selected motions. Relaxing those limitations (i.e., allowing some scaled and soil motions) is preferable to accepting a larger distribution mismatch (i.e., larger *error* values with only unscaled rock motions), as the consequences of using a hazard inconsistent set of ground motions for fragility computations are far worse.

3.3. Further Analysis of rock ground motion time histories selected for METIS case study and lessons learned

In this paragraph we provide a few further analyses of the target spectra and time histories selected for METIS case study and report on some issues encountered in the selection procedure.

In a first application of the record selection described in the previous sections, the Sa(0.26s) was considered as one of the conditioning IMs. This IM was selected to represent the fundamental frequency of a typical reactor model, such as the simplified reactor model used for preliminary analysis. For this conditioning IM the analysis of the time histories revealed significant discrepancies with respect to the

target. This is shown for the example of IML_7 (10 000-year return period) in **Figure 7.** For comparison the same result is also shown for the conditioning IMs PGA in **Figure 8**.

Additional analysis showed that the large misfit observed for Sa(0.26 s) conditioning was due to the fact that the Sa(0.26 s) RotD50 values were not available in databases but were obtained by interpolation between available values. The PGA RotD50 values were not interpolated (they are available in database), and the error is much smaller (**Figure 8**). However, there are still some misfits that might be due to discrepancies in the values provided in the database.

Based on these analyses, the SA(0.26s) results were discarded for further analysis and replaced by SA(0.25s) as described in section 3.1.1.

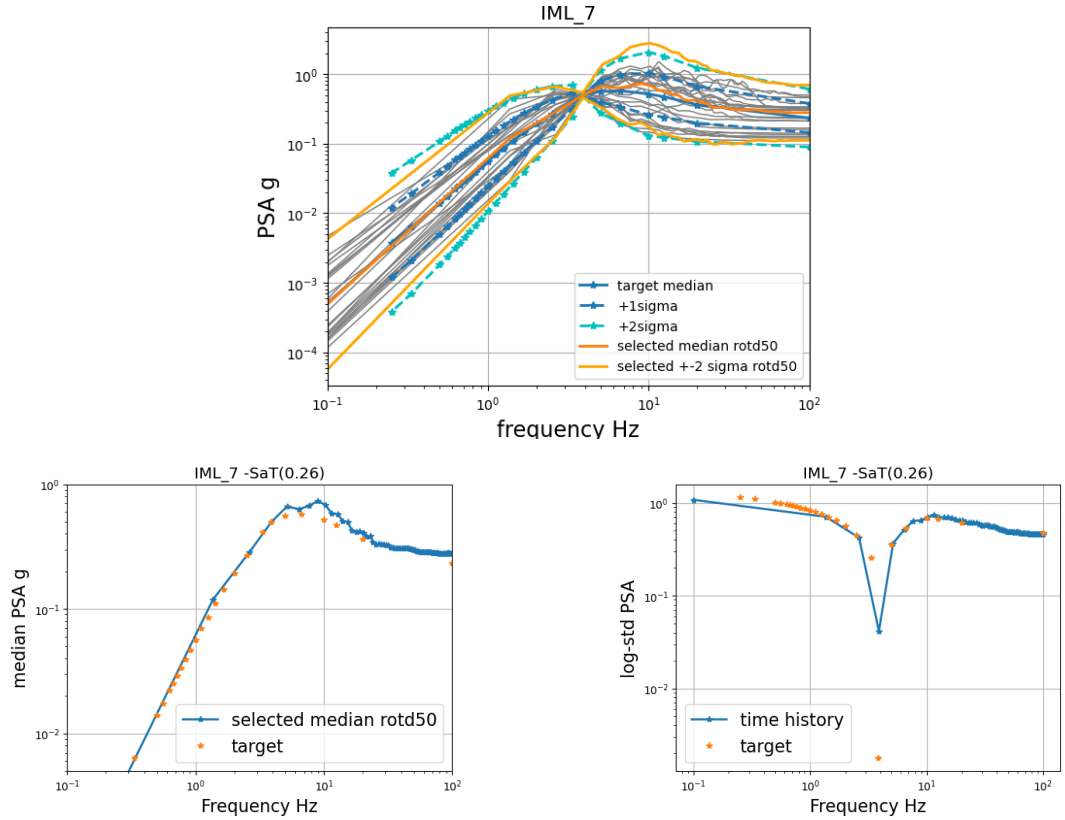

Figure 7: **Comparison of the target conditional PSA (median and log-std) to the statistics of selected records for 10 000-year return period (IML 7) for Sa(0.26 s) as an IM.**

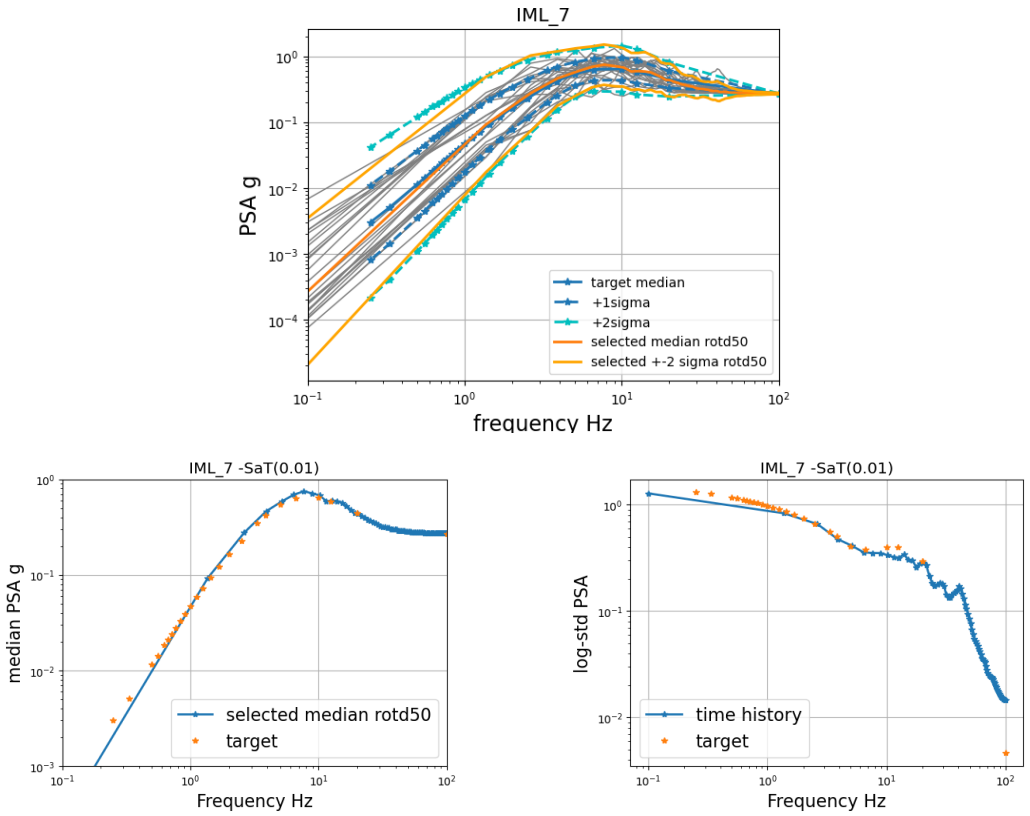

Figure 8: Comparison of the target conditional PSA (median and log-std) to the statistics of selected records for 10 000-year return period (IML 7) for PGA as an IM.

Scaling factors in the range (0.1-12) were allowed for to fit the target. The histogram of scaling factors applied to the 25 GMRs selected for the PGA conditioning and 10 000-year return period are shown in **Figure 9** below for illustration. Many time histories are 'regular' in overall shape but some exhibit very special features that might not be in agreement with the site and scenario. This is illustrated in **Figure 10** below.

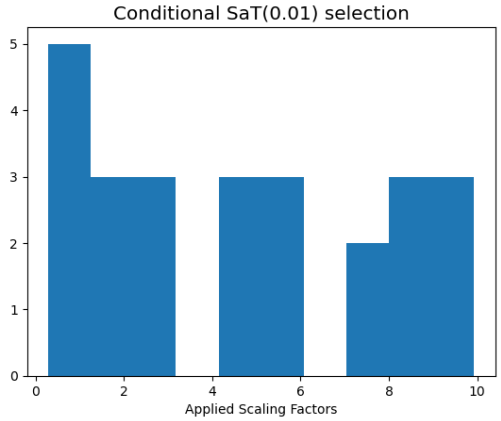

Figure 9: Scaling factors for 10 000-year return period for PGA (left).

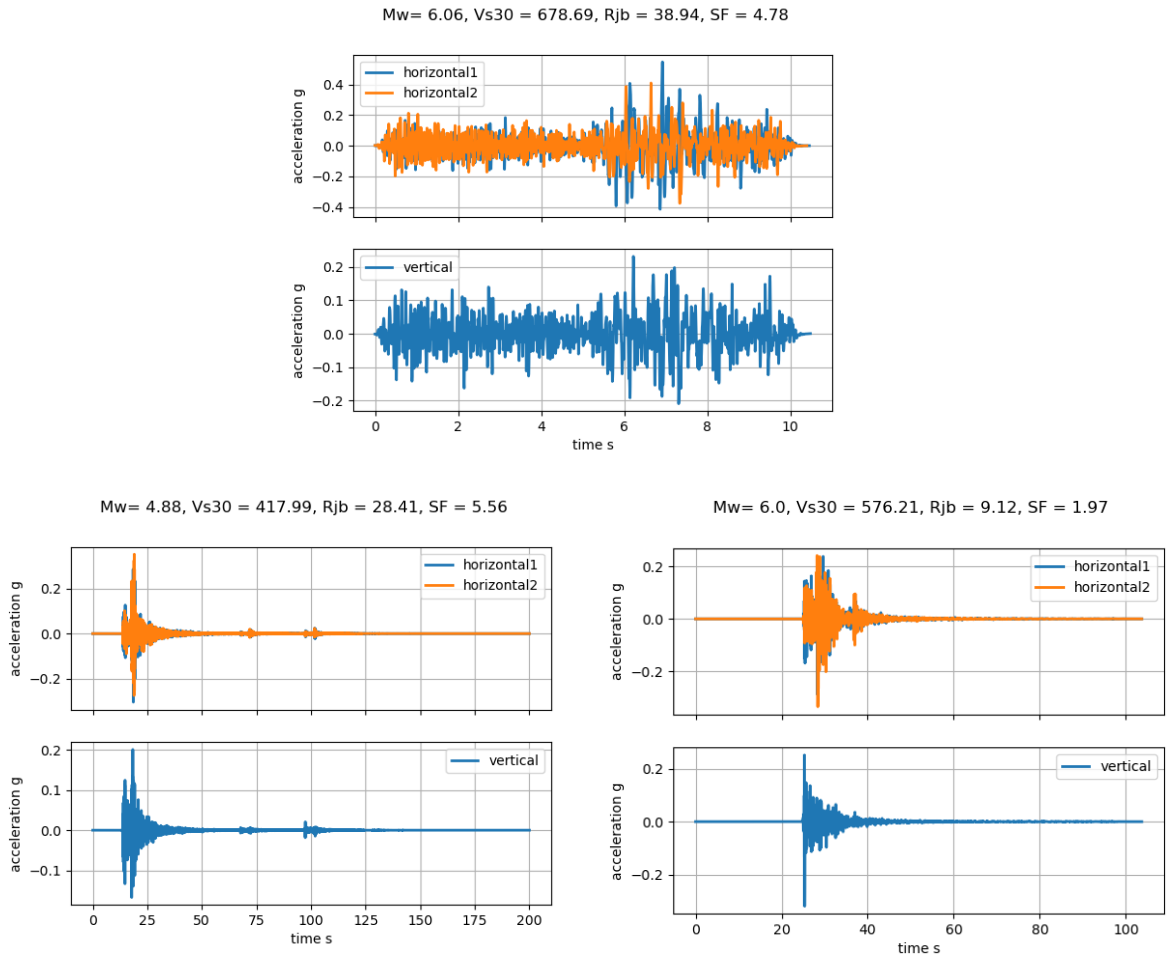

Figure 10: Examples of time histories selected from the database.

First insights and recommendations drawn from these analyses are:

- Need to compute RotD50 of selected ground motion and check their statistics and agreement with target, it is not recommended to interpolate the RotD50 values from the database.
- Need to visualize the selected ground motion time histories to assess their suitability to conduct risk assessment studies for the site under study. Some time histories may require further post-processing to focus the duration on the strong motion and exclude noise. Similarly, some of the ground motions coming from the existing databases have been reduced to the strong motion fase, which may influence the responses without any additional processing, this however, is only present in a small fraction of the records.
- The required scaling factors are quite high and earthquake scenario and site information could not be included in the selection process. The additional use of simulated ground motion time histories could help prevent from high scaling factors and avoid other gm features not in agreement with site-specific conditions.

- Constraints for the significant duration of the ground motion may be imposed for cases where severe nonlinearities are expected, as degradation due to cyclic loading may impact the fragilities. In these cases, hazard calculations should provide the target values of duration at each return period, and then imposed through other selection methods such as GCIM or CS-MR.
- Some of the records selected have pulse-like features. They represent near-field effects. The use of such ground motion requires more investigations. In particular, when a small set of records is selected then their presence could have an impact on nonlinear response.

4. Surface ground motions including site response

For the site response analyses we considered 5 intensity measure levels (IML) equivalent to 5 return periods: 2500, 5 000, 10 000, 20 000, 50 000 years. PGA and SA(0.25) are chosen as the conditioning IMs (see section 2).

4.1. Application of the criteria for 1D or multidimensional site response to METIS case study

When a site undergoes seismic shaking, local site effects have the consequences in terms of modifications in amplitude, frequency content and duration of ground-motion. These phenomena can be rather peculiar, and they vary from site to site depending on the local geologic and topographic site conditions. Classical approaches often overlook the effects of lateral variations, meaning that when the hypothesis of a laterally infinite body with horizontal layering vanishes, wave propagation cannot be modelled correctly as 1D and more sophisticated approaches are needed to capture 2D/3D site effects (i.e. topographic effects, slopes along with impedance contrasts, the geometry of the soft soil layers, basin-edge induced surface waves, 2D basin resonance effects). A first step consists in the definition of criteria that allow to decide whether 1D or multidimensional site response analysis are required for the site under study and these criteria have been outlined and described in Deliverable 5.3. In summary, the criteria allow an assessment of sites which are more likely to be affected by multidimensional site effects indicating that more complex ground-motion modelling is required. The scheme is based on single-station ground motions at surface stations only. The scheme is benefitting from the fact that no additional site-specific information nor recordings at nearby reference sites are required.

For the test site, we have selected 26 weak ground motions leading to linear-elastic behaviour of the ground with the best-possible azimuthal coverage to identify any azimuthal-dependent amplification in the frequency band between 0.2 and 20 Hz. The sample events cover a distance range between 11 and 106 km. Most of the events are located to the east and north-east of the test site with only few events covering the western azimuths, leaving an azimuthal gap of around 170°. The events used, however, reflect the real seismotectonic setting as good as possible. The maximum PGA is ~0.1 m/s. This is appropriate since here we are mainly interested in the identification of topological or geometrical site effects such as non-horizontal layering, basin effects etc., and not the nonlinear site response that is considered in section 4.2.

For the test data, we obtain an index of I = 0.31 (with 0 indicating a fully 1D behaviour while an index of 1 represents the certainty of significant horizontal variability at this site), meaning that the site tends to be 1D with some minor influence of 3D effects. A small aggravation factor could be used to consider

the occurrence of 2D/3D site effects. Please keep in mind that our approach does not allow us to distinguish whether the measured 3D effects are caused by topographic or basin effects or, for example, by basin-edge induced surface waves.

4.2. 1D site response analysis for METIS case study: data and models

This section describes the modeling approach adopted in this study for integrating uncertainties and variability on 1D soil columns equivalent linear (EQL) response, following the modeling approach and recommendations described in METIS D5.3. The EQL is based on an iterative procedure of linear elastic simulations in frequency domain, soil dynamic properties being updated at each iteration based on 65% of the maximum shear strain attained during shaking at each soil layer. The 1D soil column hypothesis consists of vertically propagating seismic shear waves on a laterally stratified soil. Given the large variability and depth on bedrock interface identified at the site, two bedrock depths are considered on a parametric basis: 200m and 400m.

The following modelling strategy is considered in this study to obtain soil surface ground motion:

- Deconvolution of rock motions selected at the free-field to the equivalent outcropping rock motions at different bedrock depths (200m or 400m) by considering a homogeneous rock with Vs 1000m/s and damping ratio of 1%,

- Convolution of the obtained outcropping rock time-histories through a 1D soil column representing the site to obtain free-field motions to be used for soil-structure interaction analysis.

Both the variability of input ground motion on rock as well as the uncertainty related to site data are considered and propagated in this study.

4.2.1. Best-estimate model

The dynamic soil properties (variation of normalized secant shear modulus (G/G_{max}) and damping (D) relative to shear strains) were partially characterized (maximum shear strains around 3.10^{-4}) by resonant column tests on soil specimens from layers 2 and 3 (**Figure 11**, **Figure 12**). However, as the soil is expected to be subjected to larger shear strains during extreme shaking, models for both $G/G_{max}(\gamma)$ and $D(\gamma)$ are considered to cover a larger shear strain range, as follows:

- Normalized secant shear modulus: adjustment from a standard hyperbolic model: $\frac{G}{G_{max}} = \frac{1}{1+\left(\frac{\gamma}{\gamma_r}\right)^a}$
- Damping: adjustment for both Darandeli (2001) and Zhang et al. (2004) models, and the mean damping curve from these two models is considered.

This study considers the same normalized secant modulus and damping from layer 2 to layer 4, and from 3 to layer 5, as no data was provided for layers 4 and 5. This hypothesis is based on similarities on soil nature (**Table 1**), although these deep layers are not expected to be subjected to large non linearities during shaking.

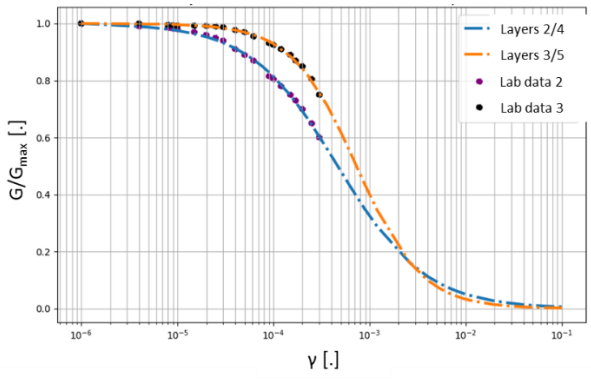

Figure 11: Normalized secant modulus curves for geotechnical layers.

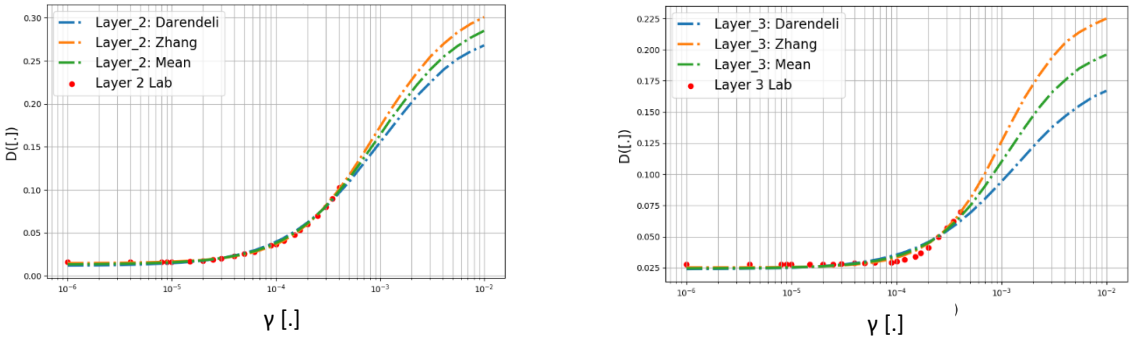

Figure 12: Damping curves for geotechnical layers.

4.2.2. Soil uncertainty quantification and propagation

We adopt a generic framework for consideration of uncertainty and propagation of uncertainties via Latin Hypercube sampling, see **Figure 13** below and Deliverable D5.3 for more details on methods used on uncertainty quantification and sampling strategy.

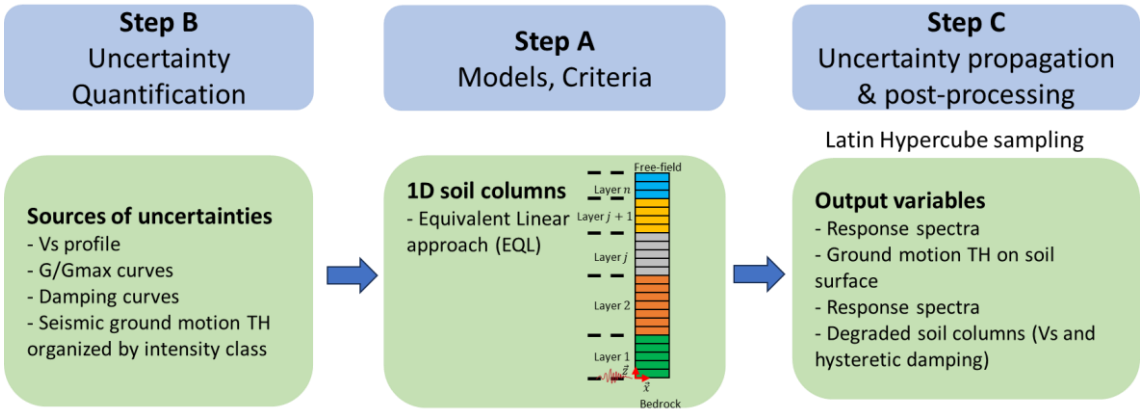

Figure 13: Uncertainty propagation scheme.

The correlated Vs values are modelled by lognormal distribution where the correlation depends on the vicinity of the layers, i.e. adjacent layers have higher Vs correlation than more distant ones. β_{Vs} is chosen at 0.175, which allows associating the deterministic interval (0.5, 2) to 2.3%-97.7% confidence intervals of the lognormal distribution. Variability in the last layer is parametrized by the variability in Vs(78m), for which median value is given by Vs(z) previously described and β=0.1. No variability is introduced for Vs value at the bedrock, as seismic hazard and record selection was established for Vs=100m/s and includes already the variability in the ground motion. Uncertainty in the layer heights is not accounted for, as results are not expected to be very sensitive to small variations of layering. **Figure 14** shows a sample of 100 soil profiles together with the median and +-1 sigma intervals for both H=200m and 400m hypothesis.

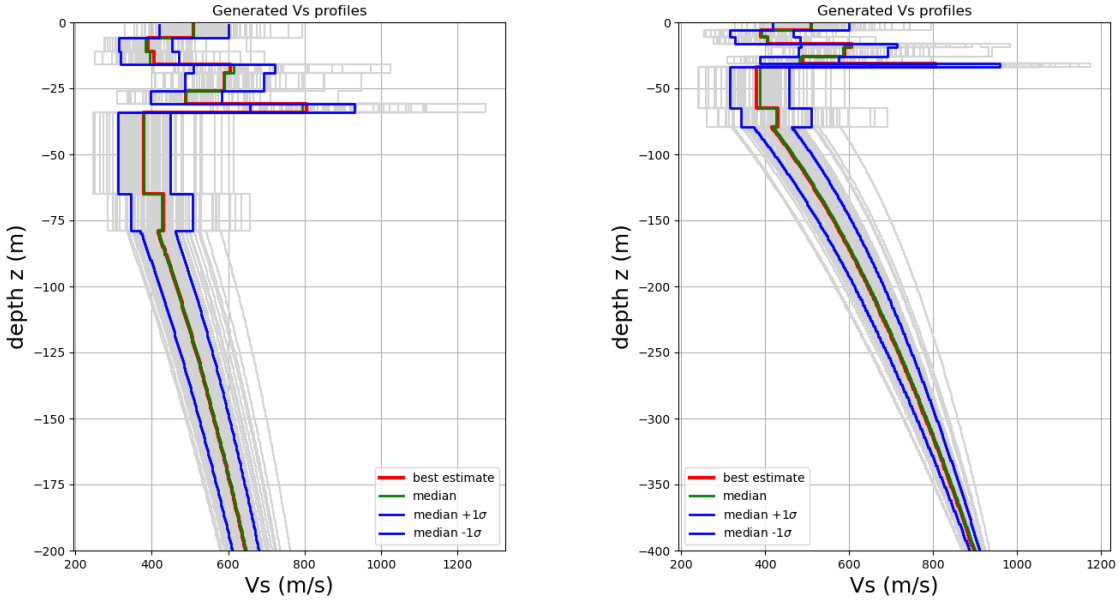

Figure 14: Randomized Vs profiles with bedrock at 200m depth (left) or 400m depth (right).

A lognormal distribution is assumed for the sampling of the damping (D) curves while a truncated Gaussian distribution was chosen for the G/G_{max} curves due to their specific properties. A negative correlation of -0.5 is introduced to account for the increasing damping with decreasing modulus. **Figure 15** shows the standard deviation from Darendeli (2001) for generic and different specific soil types. We adopted the lower specific values for layer 3,4 and 5 of our soil profiles. An example of randomized nonlinear properties for layer 2 is presented on **Figure 16**.

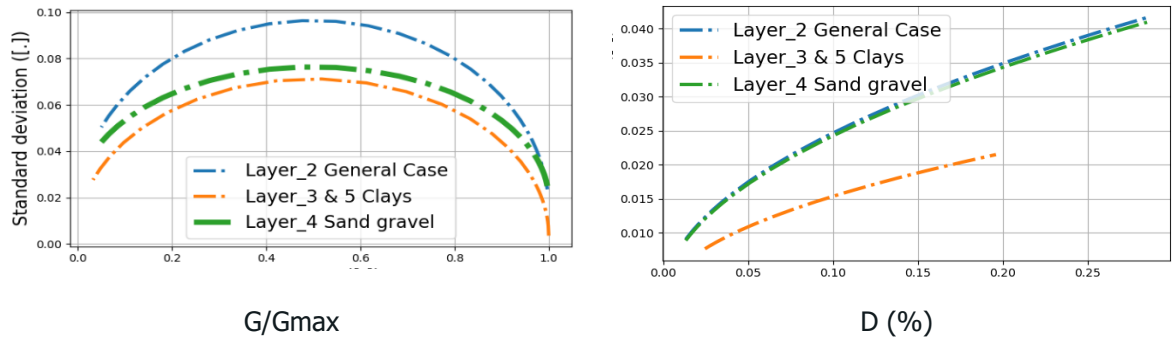

Figure 15: Generic and specific soil class standard deviation from Darendeli (2001) layer numbers refer to METIS case study.

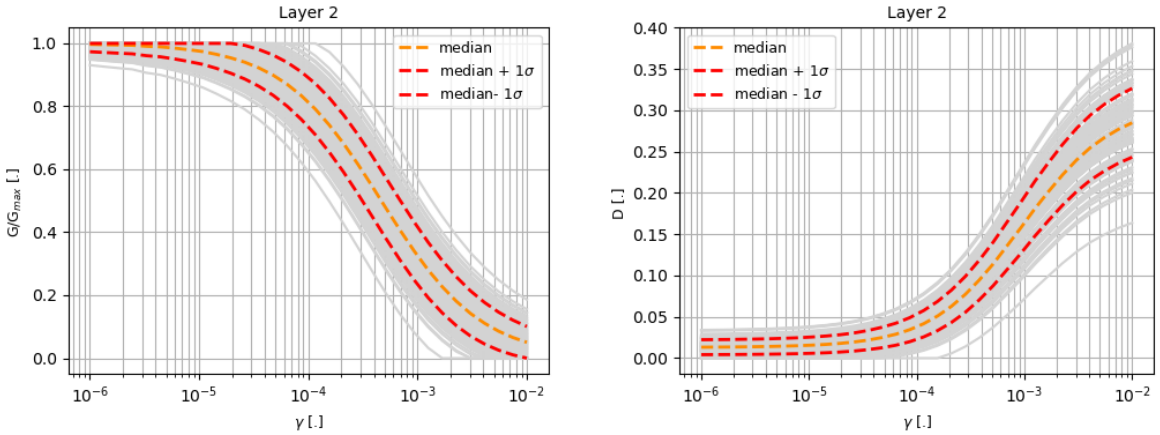

Figure 16: Example of randomized soil nonlinear properties (layer 2).

For this application we identified a sample size of N=100 to well represent soil uncertainty, as illustrated in **Figure 15** below but this must be assessed for more examples to deduce general conclusions. For the uncertainty propagation, we pair each of the 100 soil columns with one time history from the set. Since 100 soil columns for 25 time histories are available (for each horizontal direction), each time history is used 4 times. The results for this LHS-type design are compared to the full factorial design where each time history is paired with each soil column. The results confirmed the acceptability of the reduced design.

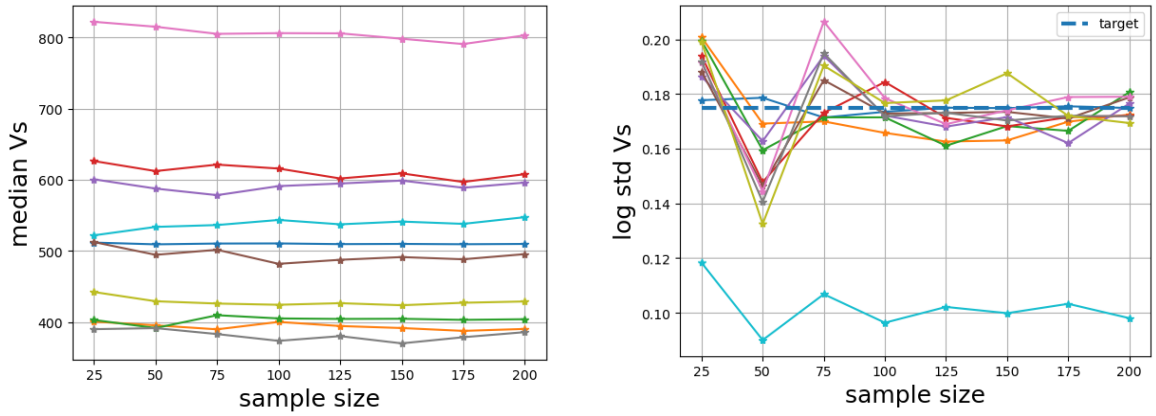

Figure 17: Convergence of median and log-std of the soil layer Vs-values as a function of N. The different coloured curves correspond to the different layers.

4.3. 1D site response analysis for METIS case study: numerical results

The 3-direction free-field time histories consistent both with rock hazard and soil column properties necessary as input data for soil-structure interaction (SSI) studies were computed for all IMLs and conditioning periods, under hypothesis of soil column depth of 200m or 400m and whether uncertainties or best-estimate soil properties are considered. A total of 7500 numerical simulations were performed consisting of:

- 5 IMLs x 3 directions x 2 conditioning periods x 25 time-histories x 2 bedrock depths = 1500 soil column calculations for best-estimate properties and
- 5 IMLs x 3 directions x 2 conditioning periods x 100 soil columns (4 x 25 time histories) x 2 bedrock depths = 6000 soil column calculations integrating uncertainties.

The output data necessary for soil-structure interaction and fragility analysis have been stored in a set of directories and subdirectories available on FLEXX repository. Documentation on input data and hypotheses as well as the output data format is also provided with the data.

4.3.1. Deconvolution strategy

In this section we assess the impact of deconvolution strategy and soil column depth on free-field signals, both in terms of the uncertainty on bedrock depth (hypothesis of H=200m or 400m) and bedrock damping. Indeed, bedrock depth and damping have a direct impact on the high frequency content of deconvolved signals, as reported on **Figure 18** (left) for elastic transfer functions for deconvolution under different damping hypothesis. In turn, the median amplitude of the obtained free-field spectral accelerations a for one set of free-field motions (X direction and one set of selected time histories – 2500 years r.p.) are clearly affected by the deconvolution (**Figure 18** – right). Smaller damping on rock compared to the one on soil, specially at the last soil layer (layer 5), leads to higher differences between H=200 and H=400m soil columns. In this work we choose to keep a physical value of D=1% for the rock damping, lower than small strain damping on the soil column and therefore

leading to differences in free-field motion computed for the H=200 and H=400m soil columns hypothesis.

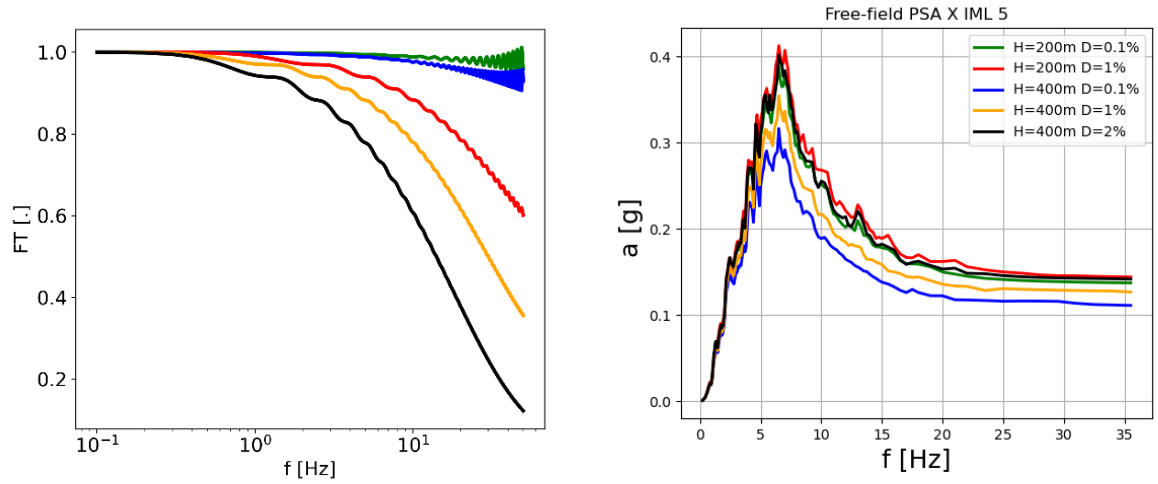

Figure 18: Elastic transfer functions for deconvolution on rock (Vs=1000m/s) columns with H=200m and H=400m and different damping characteristics (left) and response spectra for convolution on soil columns (right).

The deconvolution results for 2500 years return period on both horizontal components are presented in **Figure 19**, and compared to the conditional spectra anchored at PGA and used for time histories selection (based on RotD50). As previously discussed, the impact of the deconvolution on the obtained input motions for soil column analysis is mainly relevant for deep soil profiles.

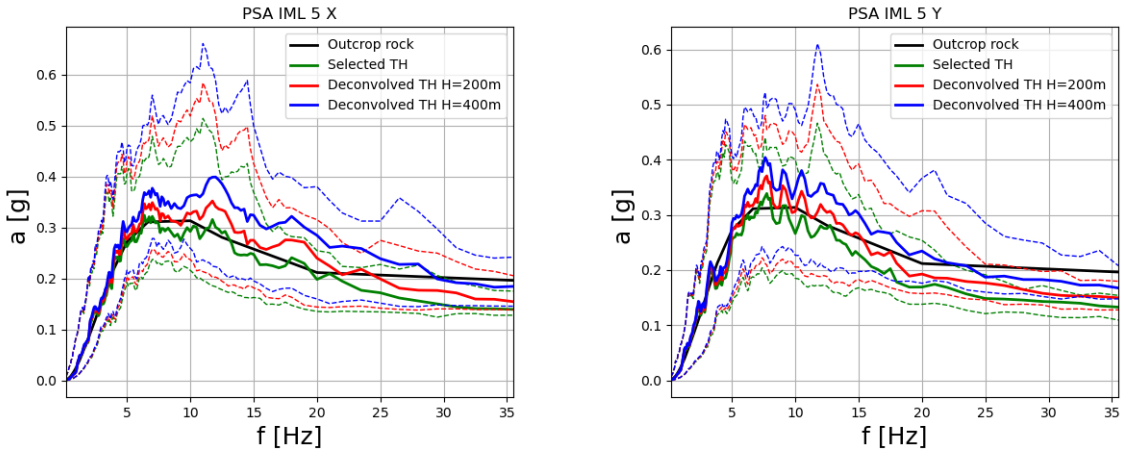

Figure 19: Pseudo-spectral accelerations a in units of g are plotted for horizontal components (X: left and Y: right) of deconvolved bedrock input motions for return period of 2 500 years and a soil columns of H=200m, 400m, considering CMS anchored at PGA. Solid line: median; dashed line: 15% and 85% quantiles

4.3.2. Best-estimate soil column results

In this section we briefly describe the results for free-field spectral accelerations for both horizontal and vertical components. The horizontal components are obtained by Linear Equivalent approach, whereas

the vertical free-field motion is obtained without any soil properties reduction. **Figure 20** and **Figure 21** presents the results for 2 500 years (left) and 50 000 years (right) return periods, for a soil column hypothesis of H=200m and CMS anchored at PGA and T=0.25s, respectively. Figure axis are in log-log to better visualize differences between outcrop rock and soil spectral accelerations at low frequencies. As expected, pseudo-spectral accelerations for both horizontal directions at the soil follow a consistent similar response, although the time-histories selection procedure enforced hazard consistency for RotD50 combination of the horizontal components rather than for each horizontal component separately. Differences between rock and site pseudo-spectral accelerations are mainly due to: (i) site amplification at low frequencies (cf. **Figure 22** for site amplification function) and (ii) soil damping which leads to a reduction pseudo-spectral accelerations at the high-frequency range. In this sense, obtained median PGA values from the 1D soil column model are lower than the PGA at rock.

The vertical component presents a large variability, as: (i) no consideration of consistency with the vertical ground motion hazard is proposed in this work and (ii) soil modulus reduction and damping are considered only for horizontal components, the convolution of the vertical one being performed for the elastic soil column.

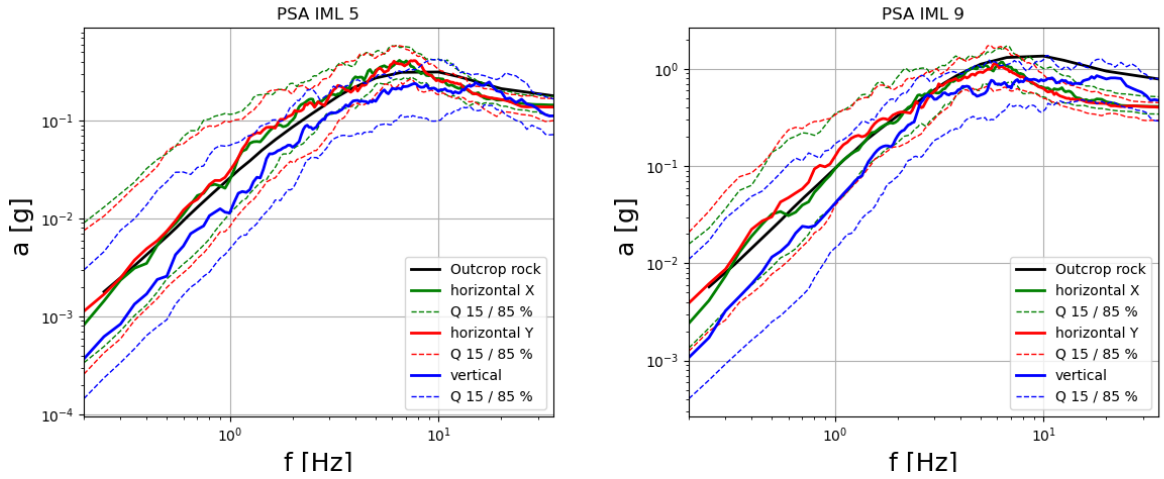

Figure 20: Pseudo-spectral accelerations a in units of g are plotted for horizontal and vertical components for return period of 2 500 (left) and 50 000 (right) years, considering best-estimate soil column and CMS anchored at PGA. Solid line: median; dashed line: 15% and 85% quantiles.

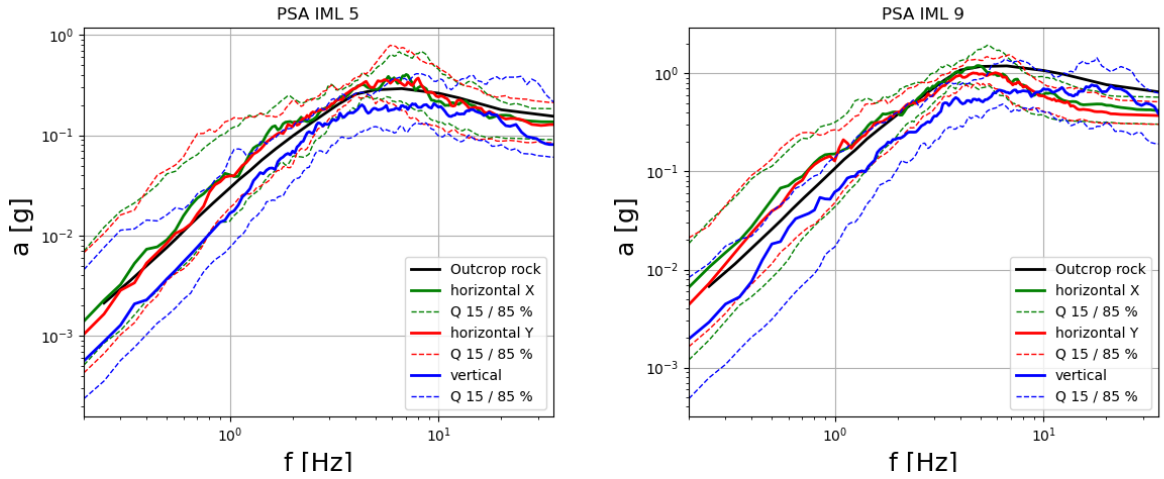

Figure 21: Pseudo-spectral accelerations a in units of g are plotted for horizontals and vertical components for return period of 2 500 (left) and 50 000 (right) years, considering best-estimate soil column and CMS anchored at T=0.25s. Solid line: median; dashed line: 15% and 85% quantiles.

For all considered cases, maximum equivalent shear strains for best-estimate soil columns were lower than 0.35%, although extreme case of IML 9 (50000 years return period) presented 3 out of 50 numerical simulations per anchoring CMS period (2 horizontal directions x 25 TH) with maximum shear strains larger than 0.15%. Maximum strains are obtained on layers 3 and 4, which are the more prone to nonlinearity as (i) layer 3 is adjacent to Vs inversion at the interface with layer 2 and (ii) layer 4 has a rapid G/G_{max} reduction with shear strains.

4.3.3. Impact of soil column uncertainties

The numerical simulations performed show that the introduction of uncertainties in the soil column (Vs profile and nonlinear properties) directly impacts the bedrock to surface transfer function (TF) (**Figure 22**) as: (i) smaller resonance peaks for the median TF values are observed and (ii) higher TF variability is obtained in comparison to the best estimate profile only, although differences reduce when considering high return periods (right-hand side). However, median and 15%/85% quantiles for the spectral accelerations at the surface are less impacted by the variability at the soil column (**Figure 23**). Slight lower median values and consistently lower 15% quantile are obtained for return period of 50 000 years, as higher nonlinearities are attained for some simulations, leading to lower spectral accelerations. Indeed, including soil variability led to a higher number of soil columns presenting maximum shear strains larger than 0.15%, or locally higher than 0.5% (6 out of 400 simulations for 20000 years return period and 23 out of 400 simulations for 50000 years return period). Excluding these extreme cases do not significantly change the median spectral acceleration at the surface (**Figure 23**), although 15% quantile increases. In both Figures, the PSA response are shown for the response in x-direction for illustration.

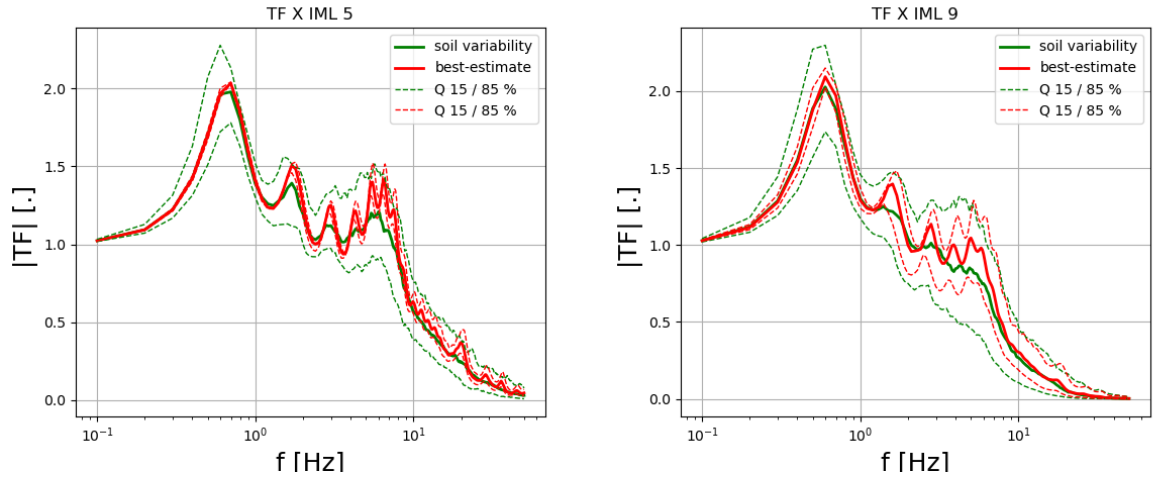

Figure 22: Bedrock to surface transfer function for return period of 2 500 (left) and 50 000 (right) years for CS anchored at PGA. Solid line: median; dashed line: 15% and 85% quantiles.

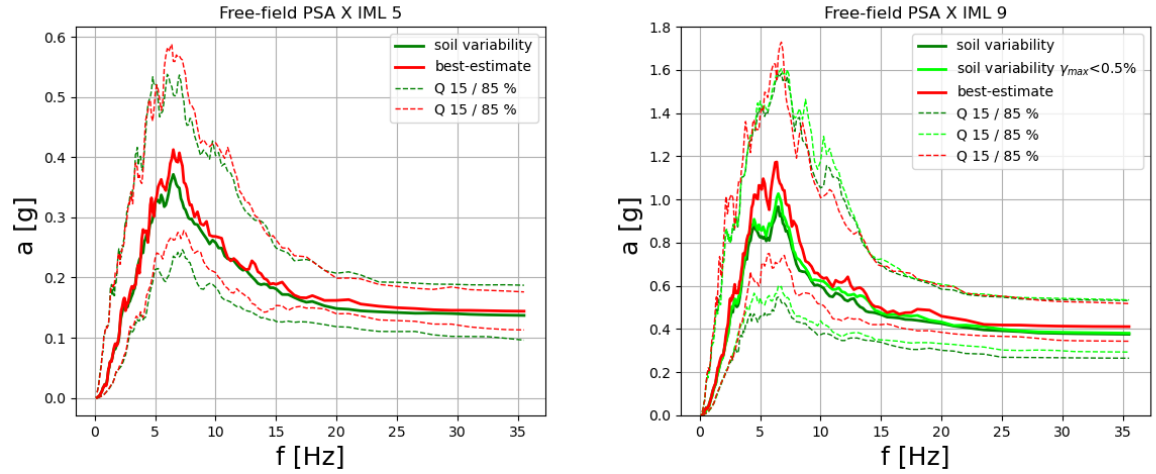

Figure 23: Pseudo-acceleration for return period of 2 500 (left) and 50 000 (right) years when considering uncertainties in the soil column for CS anchored at PGA. Solid line: median; dashed line: 15% and 85% quantiles.

The relative impact of introducing uncertainties in the soil column compared to the variability of input time histories only is analysed by comparing the coefficient of variation (ratio between standard deviation and mean value, COV) value for RotD50 of the horizontal components for all IMLs and both conditional periods (PGA and T=0.25s). **Figure 24** shows that considering soil variability leads to consistent higher COV values when considering all IMLs for all frequencies. As expected, COV is lowest at the conditional period/frequency, as the selection procedure described on section 3 imposes to select time histories by exactly matching the defined rock PSA at that frequency. **Figure 25** shows that COV is consistently larger by at least a factor 2 at the conditional frequency when introducing soil column uncertainties, this result being directly linked to the β values of lognormal distributions considered for both Vs profile and nonlinear soil properties.

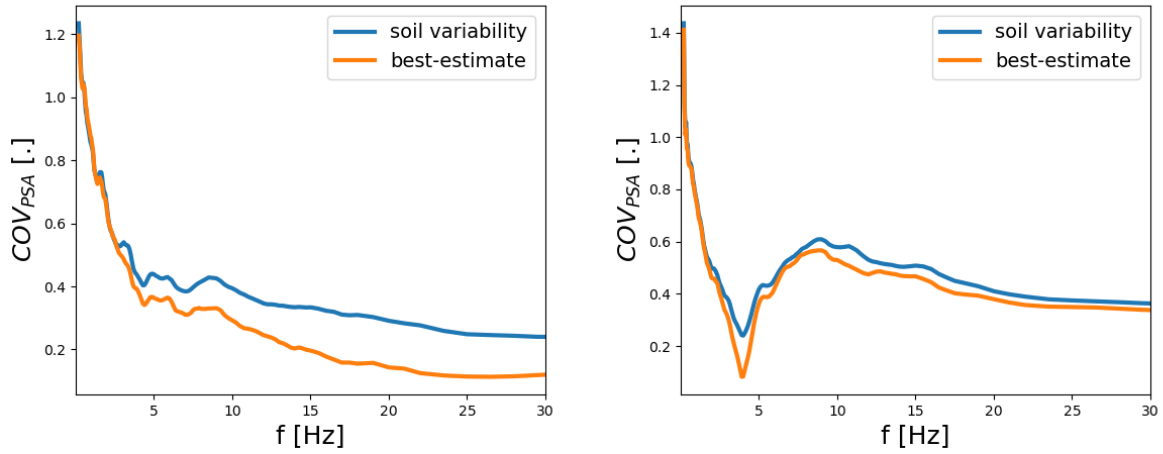

Figure 24: Comparison of best estimate and best-estimate + uncertainty case for soil variability: Mean value of the coefficient of variation of all IMLs for Rotd50 PSA for both conditioning periods (PGA – left, T=0.25s – right).

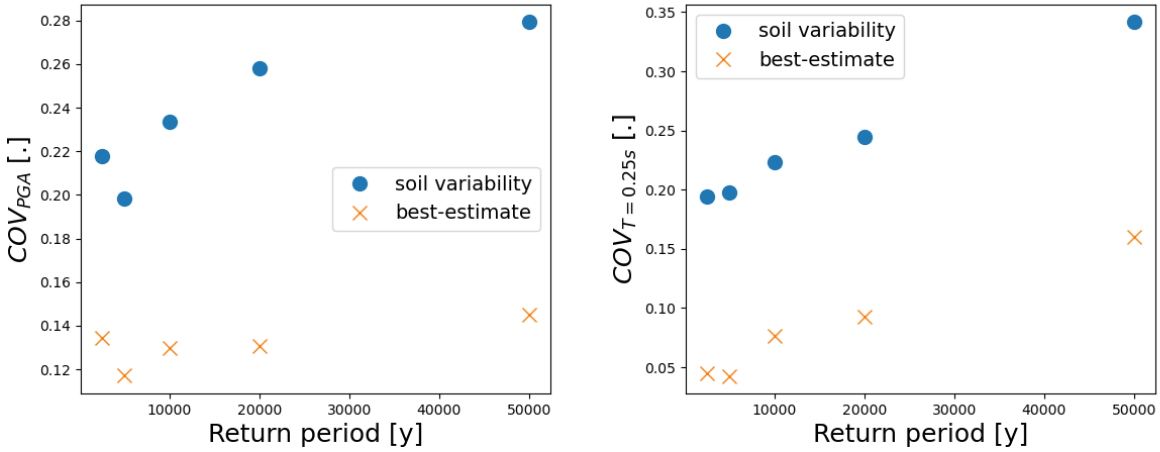

Figure 25: Coefficient of variation of Rotd50 PSA at the selected period (PGA – left, T=0.25s – right) for all IMLs.

4.4. Comparative studies with 2D site response

In this section we describe and assess an approach that allows for the consideration of multi-dimensional site effect analysis using the so called Free-Field Boundary Condition (FFBC). It is most common in practical applications that information concerning the seismicity of the region of interest are constrained to a PSHA analysis performed for the reference bedrock, while information concerning the form of the complete wave field is quite scarce. In this context, it is common practice to evaluate site amplification using a plane wave excitation of vertical incidence generally applied at the bottom of the computational domain, while the motion along the lateral sides is not known beforehand. A simple solution to introduce the lateral ground motion, initially proposed by (Zienkiewicz, et al., 1989), is the FFBC, where the

excitation imposed on the lateral sides is the one obtained from the wave propagation in a 1D soil column as schematically represented in Figure 26.

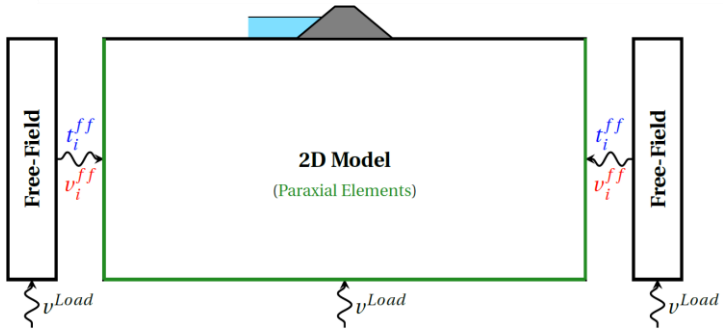

Figure 26: Schematic representation of the free-field boundary condition (FFBC).

The definition of the dynamic excitation in code_aster is ensured via the use of paraxial elements. The traction vector t_i^{ff} and the incident velocity field v_i^{ff} are obtained from the 1D soil column wave propagation. These are the necessary fields needed to correctly construct the free-field excitation on the lateral boundary (Korres et al. 2022).

It is worth noticing that the 1D columns can be solved prior to the construction of the dynamic excitation which is then transferred to the lateral boundary for the 2D dynamic analysis. This implies that no interaction takes place between the 1D column and the 2D profile as information is transferred unidirectionally from the 1D column to the 2D domain. This implies that the wave field generated in the 2D model does not affect the free-field ground motion of the 1D propagation, a simplifying assumption that might be too approximate depending on the complexity of the 2D analysis. Nevertheless, it can be justified in certain cases if the columns are placed at some distance from the central region of the model.

4.4.1. Overall strategy and assumptions for the 2D analysis

The aforementioned methodology is applied to the 2D soil profile of the METIS case-study (**Figure 4**) by considering the best-estimate soil properties equivalent to the soil column with H=200m. However, contrary to the 1D analysis, no material damping is considered in this case (cf. §4.4.3 for a discussion on the influence of soil material damping). The spatial variation of the Young's modulus for the 2D soil profile of **Figure 4** and the best-estimate properties is presented in **Figure 27** (left).

Provided that the efficiency of the FFBC approach is highly influenced by the distance between the geology of interest and the lateral boundary of the model, a first comparison is performed using a simplified Ricker excitation to identify the appropriate size for the 2D model. For this purpose, a hypothesis is made for the lateral extension of 2D soil profile (**Figure 27**) assuming horizontal layer stratification in both sides of the model. The latter was mainly motivated from the lack of further information allowing to extend the 2D profile more appropriately as well as to the fact that the site is located close to the seacoast and thus the horizontal extension of the model remains plausible. Consequently, three model sizes are examined as presented in **Figure 27**: (i) Small model (100 m length), corresponding to the known 2D profile, and (ii) Medium (500 m length) and Large (900 m length) model, allowing to evaluate the convergence of the numerical solution at the site of interest. Finally, it is worth mentioning that provided the complex geological 2D profile, the 1D soil column is different for the two sides of the model.

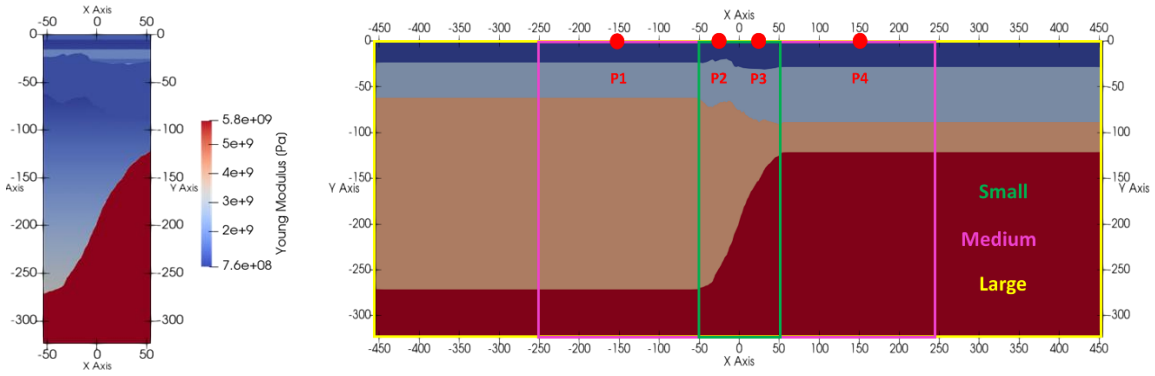

Figure 27: Spatial variability of the Young's modulus for the small model (left), and the three different sizes of the 2D soil profile (right).

Once the 2D model size is fixed, a comparison is performed between the 1D and 2D site response, using the previously described ground motion database proposed for the METIS case study. The purpose of this analysis is to evaluate the "1D character" of the site of interest and evaluate the spatial variability of the ground motion deriving from the 2D analysis.

4.4.2. Results and comparison with the 1D soil column

The influence of the size of the model is examined at first. Three models are compared adopting the same boundary conditions: plane wave excitation with vertical incidence imposed at the base of the model and the free-field motion obtained from the 1D soil column imposed at the lateral side. The characteristics of each model in terms of mesh discretization as well as the computational time are provided in Table 4, along with the characteristics of the 1D column.

Table 4. General information for the different numerical models.

Model	Nb of Elements	Nb of DOFs	CPU Time [min]
1D Column	200	1 K	1
2D Small	5 K	28 K	3.5
2D Medium	26 K	151 K	10
2D Large	47 K	280 K	25

Numerical results for the three model sizes are presented in **Figure 28**, and for a point located at the site of interest (surface and the center of the model). It is worth noticing that the *Small* model (green line in **Figure 28**) provides a different response compared to the other two model sizes for the convergence in terms of site response. Two main reasons can be the source for this important difference in terms of site response:

- The free-field motion imposed at the boundary steams from an 1D propagation on a horizontally stratified soil column which is incompatible with the wave front generated by the 2D geology. The applied free-field motion is different on the left and right-hand sides of the model as the soil 1D profile is not the same. The proximity of the absorbing boundaries to the variable bedrock profile in depth is an important point and we compare different model sizes to assess adequacy of the results in the points of interest. Therefore, the proximity of the boundary to the 2D geological profile plays a negative role on the global response even more due to the lack of material damping in the present study.
- As illustrated in the acceleration wave field presented in **Figure 29**, the 2D soil profile modifies locally the vertical incidence of the wave front leading to an inclined wavefront following the geological profile. Paraxial elements are known to perform better for angles of incident waves that remain close to 90^0 (Modaressi et al. 1994). In this context, different angles of incidence may decrease their absorption capacity and lead to spurious reflections on the domain of interest. This phenomenon is less present as the boundary remains farther from the complex geology.

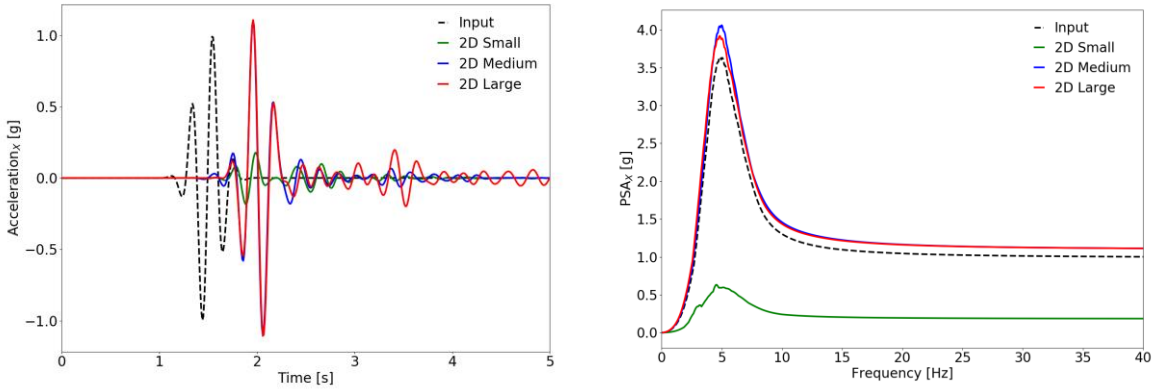

Figure 28: Horizontal component of the site response and a simplified Ricker excitation: acceleration time history (left), and 5% damped spectral acceleration (right).

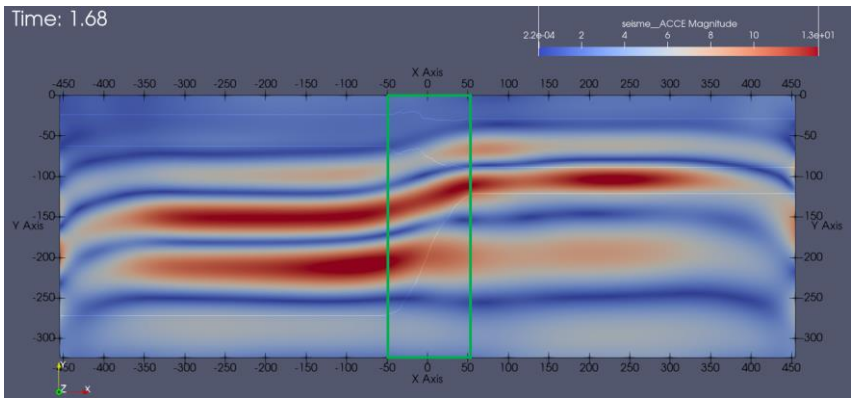

Figure 29: Acceleration field at 1.68s. The green rectangle at the center represents the size of the small model.

Provided the small differences between the Medium and Large size models, the Medium size model is chosen so as to examine the 2D site response compared to the 1D soil analysis.

Since the 2D analyses are conducted as linear elastic with no material damping, numerical results are presented here only for the return period of 2 500 years for all 25-acceleration time-histories corresponding to the x component. Comparison between the undamped 1D and the 2D (point at the center at the surface) site response is presented on the left-hand side of Figure 30, in terms of mean value (solid line) and standard deviation (dashed line). According to **Figure 30**, site amplification is rather similar between the 1D and the 2D case and thus the assumption of 1D propagation is justified for the case of interest, confirming the result from section 4.1. There are only slight differences with higher amplitudes for the 2D case in the range between 10Hz and 20 Hz.

Nevertheless, it is worth noticing that contrary to the 1D analysis, the 2D simulation also accounts for the spatial variability of the seismic ground motion. At the right side of **Figure 30**, we compare the results for one of the seismic signals and different stations at the surface of the 2D profile (see also right-hand side of **Figure 27**), where we observe that the response is different depending on the location of the point at the surface (distance of 300m between point 1 and 4). The latter is an important element that needs to be considered as the variability of the ground motion may lead to more complex seismic motion to which the structure will be subjected to, compared to a simplified wave motion steaming from a plane wave solution and 1D soil column hypothesis.

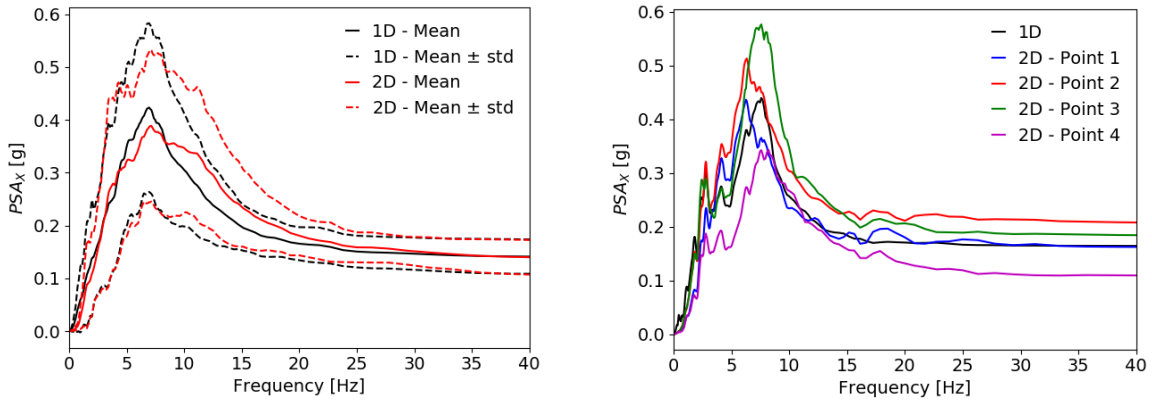

Figure 30: Horizontal component of the 5% damped spectral acceleration: Comparison 1D vs 2D (left), Spatial variability of the seismic ground motion (right).

4.4.3. Influence of the attenuation on the 2D profile

This part examines the influence of attenuation in the 2D site response. In the traditional 1D linear equivalent analysis presented in section 4.2.1, soil attenuation is considered through shear strain dependent damping presented in **Figure 12**. The present analysis for the 2D soil profile considers soil attenuation through the use of Rayleigh damping, calibrated for the best-estimated small-strain soil damping ($\xi_1 = 1.5\ \%, \xi_2 = 2.7\%, \xi_3 = 1.4\%, \xi_4 = 1\%$ for each layer). Even though it does not consist of an ideal way to represent soil attenuation, it is used here for demonstration purposes and further work should consider a nonlinear constitutive law to evaluate energy dissipation in the soil medium.

Rayleigh parameters (α and β) are calibrated here in a large frequency band between 0.2 and 25 Hz to cover a larger spectrum for the attenuation. Parameters are calibrated for small-strain damping only and not to intended to model material damping expressed by D-gamma curves. Numerical results are summarized in Figure 31 along with the undamped 2D response and the 1D response. As expected, the influence of soil attenuation led to a generalized decrease of the complete spectrum observed at the surface and the center of the 2D profile. Similar results are observed on the spatial variability of the ground motion. The right part of Figure 31, examines the evolution of the difference of the response spectrum between points 2 and 3 locate at the surface (Figure 27), and for the same scenario presented in Figure 30 (right). The closer this difference tends to zero, the smaller the spatial variability of the ground motion. As it can be observed in Figure 31 (right), soil attenuation leads to lower values for the examined scenario.

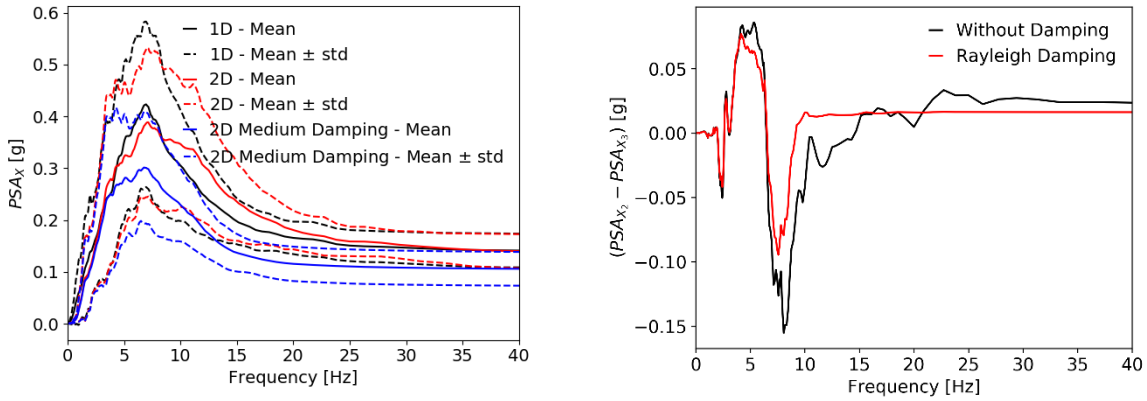

Figure 31. Horizontal component of the 5% damped spectral acceleration. (left), difference between spectral acceleration of point 2 and 3 (Figure 27).

4.5. Recommendations

- The estimated soil variability should cover the uncertainties related to the soil profile and nonlinear properties. In this work these are constrained by the available data at the site, modelling hypothesis (fixed Vs at bedrock) and literature data. A link to usual practice and deterministically assumed coefficients of variation can also help in the uncertainty quantification step.
- The conducted analysis highlighted that it is required to have the deconvolution step for better consistency of bedrock input motion in order to account for the soil column depth. Introducing the deconvolution decreases inconsistencies when considering different soil column heights in cases where there is no significant contrast to bedrock. In this work we assumed two different hypotheses: shallow (200m) and deep (400 m) bedrock depth. Bedrock spectral accelerations are higher for the deep soil column; nevertheless, rock attenuation being lower than soil, deep soil columns lead to lower pseudo-spectral accelerations than shallow ones. This work didn't directly address the case where there is no identified bedrock depth, but the deconvolution step seems appropriate in such cases as large differences would be considered for the bedrock depth.
- In cases when evaluating the impact of variable bedrock profile by 2D wave propagation analysis, free-field boundary conditions should not be placed directly next to the variable

bedrock profile. In the numerical simulations performed in this work, a model 2 times larger at each side than the variable bedrock profile is sufficient.

- The choice of using recordings from real earthquakes for time-histories selection invariably leads to signals with different total duration and possibly different time-steps. The 1D site response being performed in frequency domain, this was not a main issue and therefore this work didn't focus in providing recommendations on this point. However, metadata is provided so time steps can be harmonized among time histories, although total duration would certainly remain different given the large variability in this point from selected time-histories (**Figure 10**). Very long signals are certainly an issue for nonlinear structural time domain analysis, for which the numerical simulation cost is directly linked to the signal total duration.

5. Conclusions

METIS project implemented the hazard consistent record selection for the case study site. The records are the input for site response and for fragility and response assessment of structures, systems and components for METIS case study.

Bedrock record selection for horizontal time-histories was performed using the CS approach, in which a distribution of spectral shapes is imposed that represent the expected hazard at a given site for a given return period. This method was applied for the METIS case site, considering a Vs of 1000 m/s, following the PSHA results. The target spectrum was defined to consider all ruptures and GMPEs, following the Lin et al., (2013) methodology implemented in OpenQuake. The sets were selected for 10IMLs, for the IMs Sa(0.01s), used to define PGA, Sa(0.1s), Sa(0.25s), used instead of 0.26s and for AvgSa(0.1:0.4s). Vertical motions were obtaining by sampling applying the same scaling factor defined for the horizontals, without any consideration of consistency with vertical ground motion hazard since vertical hazard was not available for the case study site.

Different sizes, in terms of number of records were selected to give the users more freedom in terms of number of analyses, with the organization and contents of the record repositories described in section 3.1.1. The adopted selection strategy required rather high scaling factors (0.1-10), the scaling factors can be considerably reduced when selecting only single sets of ground motion of size 25-30. Here, the required scaling factors are quite high and earthquake scenario and site information could not be included in the selection process. The additional use of simulated ground motion time histories could help prevent from high scaling factors and avoid other ground motion features not in agreement with site-specific conditions.

However, in D5.1, the authors found that the CS- selected record sets can be allowed to contain some ground motions with higher scaling factors than those allowed conventional in non CS-based applications, more so at the highest intensity levels, to achieve a good match of the target spectra. Similarly, some recorded soil ground motions, corresponding to the target spectrum and distribution can be included in the set without introducing any bias on the SDOF studied in D5.1. Based on these tests, the most critical aspect for hazard-consistent bedrock record selection is to match well the mean and distributions of the target spectra. The results showed that no bias is introduced into the fragility, and the only slight differences are observed at very high levels of nonlinearity, which is rare for nuclear SSCs. In some particular cases, additional features, such as strong motion duration or other properties linked to waveforms can impact strongly nonlinear response. For this purpose, the inclusion of additional selection criteria such as duration, as well as other seismological parameters related to the scenario and the site should be included in future studies, provided that the hazard analysis for these parameters is plausible.

Given the large amount of different components present on a nuclear power plant, with different sensitivities to several IMs, such as spectral accelerations at different periods, more efficient IMs such

as AvgSA could be implemented to simplify the selection. This way, a single IM is capable of predicting the behavior of multiple SSCs.

The bedrock records selected were used as input motion for site response analysis studies based both on 1D and 2D modelling hypothesis. A geotechnical model for the site was defined based on the available data and by considering reasonable hypotheses on nonlinear properties and bedrock depth. Following recommendations from Deliverable D5.3, uncertainties were integrated and propagated on 1D site response analysis, providing a database with 3-component free-field motions and associated soil equivalent properties for further soil-structure interaction studies. Although for a reduced dataset maximum shear strains were locally higher than 0.5% for 50000 years return period, these are not expected to impact further steps of the METIS case-study using the produced data. The obtained results confirmed that integrating uncertainties on soil properties lead consistently to higher coefficients of variation (COV) for the RotD50 free-field motion at the CMS anchoring period for selected rock time-histories. The large variability obtained for vertical motions at the free-field is a consequence of both the time-histories selection procedure, which didn't apply any constraint in the vertical motion, and the hypothesis of obtaining 1D site response with elastic properties for the vertical direction.

In a similar way as the 1D analysis, the selected bedrock recordings were used as input excitation for the 2D site response analysis. Input excitation is introduced as a Free-Field Boundary Condition as discussed in Deliverable D5.3 and the influence of the size model on the horizontal response of the 2D profile is examined at first for a simplified Ricker excitation. Following the definition of the domain size, the 1D and 2D analysis are compared for the selected records database and the best-estimate soil profile. Obtained results demonstrate that in the present case the 1D and 2D response are similar for the horizontal component at the same bedrock depth. This result enforces the conducted 1D numerical analysis, although the observed spatial variability of the seismic ground motions obtained from the 2D model cannot be directly accounted for in the 1D analysis. Finally, a 2D analysis using a Rayleigh model to represent soil attenuation as a first simplified approach is examined in the last part, and as expected a decrease of the obtained response spectrum is observed in the site of interest. In future work, a nonlinear constitutive model will be used to represent soil damping more appropriately.

6. Bibliography

METIS

Rood, A. (2024). METIS case study PSHA: openquake hdf5 output files for Conditional Spectra [Data set]. Zenodo. https://doi.org/10.5281/zenodo.10664586

METIS D4.6 - Preparation of the METIS hazard study case and application. Authors: Chartier, T., & Rood, A. (2024). Zenodo. https://doi.org/10.5281/zenodo.10529417

METIS D4.4 - New PSHA methodologies: code developments and documentation. Authors: Pagani, M., et al. (2024).

METIS D5.1 Methodology for site-specific rock-hazard-consistent record selection for mainshock-only seismicity. Authors: Sipcic, García de Quevedo Iñarritu, Alvarez-Sanchez, Kohrangi, Bazzurro (2022)

METIS D5.3 - Strategies for site response modelling - Development of surface ground motions from rock-hazard consistent ground motions. Authors: - Korres, M., Alves Fernandes V., Zentner, I. & Pilz, M., (2024). Zenodo. https://doi.org/10.5281/zenodo.10598198

Others

Ancheta, T. D., Darragh, R. B., Stewart, J. P., Seyhan, E., Silva, W. J., Chiou, B. S. J., Wooddell, K. E., Graves, R. W., Kottke, A. R., Boore, D. M., Kishida, T., & Donahue, J. L. (2014). NGA-West2 database. Earthquake Spectra, 30(3), 989–1005. https://doi.org/10.1193/070913EQS197M

Baker, J. W. (2011). Conditional mean spectrum: Tool for ground-motion selection. Journal of Structural Engineering, 137(3), 322–331. https://doi.org/10.1061/(ASCE)ST.1943-541X.0000215

Baker, J. W., & Cornell, C. A. (2006). Spectral shape, epsilon and record selection. Earthquake Engineering and Structural Dynamics, 35(9), 1077–1095. https://doi.org/10.1002/eqe.571

Baker, J. W., & Jayaram, N. (2008). Correlation of spectral acceleration values from NGA ground motion models. Earthquake Spectra, 24(1), 299–317. https://doi.org/10.1193/1.2857544

Baker, J. W., & Lee, C. (2018). An Improved Algorithm for Selecting Ground Motions to Match a Conditional Spectrum. Journal of Earthquake Engineering, 22(4), 708–723. https://doi.org/10.1080/13632469.2016.1264334

Boore, D. M., & Atkinson, G. M. (2008). Ground-motion prediction equations for the average horizontal component of PGA, PGV, and 5%-damped PSA at spectral periods between 0.01 s and 10.0 s. Earthquake Spectra, 24(1), 99–138. https://doi.org/10.1193/1.2830434

Bradley, B. A. (2010). A generalized conditional intensity measure approach and holistic ground-motion selection. Earthquake Engineering & Structural Dynamics, 39, 1321–1342. https://doi.org/10.1002/eqe

Darendeli, M. B. (2001). *Development of a new family of normalized modulus reduction and material damping curves.* Ph.D. dissertation, The university of Texas at Austin.

Iñarritu P.G.Q., Šipčić N, Alvarez-Sanchez L, Kohrangi M, Bazzurro P. (2023) A closer look at hazard-consistent ground motion record selection for building-specific risk assessment: Effect of soil characteristics and accelerograms' scaling. Earthquake Spectra.;39(3):1683-1720. doi:10.1177/87552930231173713

Jayaram, N., Lin, T., & Baker, J. W. (2011). A Computationally efficient ground-motion selection algorithm for matching a target response spectrum mean and variance. Earthquake Spectra, 27(3), 797–815. https://doi.org/10.1193/1.3608002

Kaiser, A., Van Houtte, C., Perrin, N., Wotherspoon, L., & McVerry, G. (2017). Site characterisation of GeoNet stations for the New Zealand Strong Motion Database. Bulletin of the New Zealand Society for Earthquake Engineering, 50, 39–49. https://doi.org/10.5459/bnzsee.50.1.39-49

Kiani, J., Camp, C., and Pezeshk, S., (2018). On the number of required response history analyses. Bulletin of Earthquake Engineering, 16(11), 5195–5226. Springer Netherlands. DOI: 10.1007/s10518-018-0381-1

Kohrangi, M., Vamvatsikos, D., and Bazzurro, P., (2017). Site dependence and record selection schemes for building fragility and regional loss assessment. Earthquake Engineering and Structural Dynamics, 46(10), 1625–1643. DOI: 10.1002/eqe.2873

Kohrangi, M., Vamvatsikos D., and P. Bazzurro (2018). "Pulse-Like Versus Non-Pulse-Like Ground Motion Records: Spectral Shape Comparisons and Record Selection Strategies", Earthquake Engineering and Structural Dynamics, September, https://doi.org/10.1002/eqe.3122.

Korres, M., Lopez-Caballero, F., Alves Fernandes, V., Gatti, F., Zentner, I., Voldoire, F., ... & Castro-Cruz, D. (2023). Enhanced seismic response prediction of critical structures via 3D regional scale physics-based earthquake simulation. Journal of earthquake engineering, 27(3), 546-574.

Lanzano, G., Sgobba, S., Luzi, L., Puglia, R., Pacor, F., Felicetta, C., D'Amico, M., Cotton, F., & Bindi, D. (2019). The pan-European Engineering Strong Motion (ESM) flatfile: compilation criteria and data

statistics. Bulletin of Earthquake Engineering, 17(2), 561–582. https://doi.org/10.1007/s10518-018-0480-z

Laurendeau, A., Bard, P. Y., Hollender, F., Perron, V., Foundotos, L., Ktenidou, O. J., & Hernandez, B. (2018). Derivation of consistent hard rock (1000 < VS < 3000 m/s) GMPEs from surface and down-hole recordings: analysis of KiK-net data. Bulletin of Earthquake Engineering, 16(6), 2253–2284. https://doi.org/10.1007/s10518-017-0142-6

Li, W., & Assimaki, D. (2010). Site- and Motion-Dependent Parametric Uncertainty of Site-Response Analyses in Earthquake Simulations. Bulletin of the Seismological Society of America, 100, 954–968.

Lin, T., Harmsen, S. C., Baker, J. W., & Luco, N. (2013). Conditional spectrum computation incorporating multiple causal earthquakes and ground-motion prediction models. Bulletin of the Seismological Society of America, 103(2 A), 1103–1116. https://doi.org/10.1785/0120110293

Lin, T., Haselton, C. B., & Baker, J. W. (2013). Conditional spectrum-based ground motion selection. Part I: Hazard consistency for risk-based assessments. Earthquake Engineering & Structural Dynamics, 42, 1847–1865. https://doi.org/10.1002/eqe

Modaressi, H., & Benzenati, I. (1994). Paraxial approximation for poroelastic media. Soil Dynamics and Earthquake Engineering, 13(2), 117-129.

Pagani, M., Monelli, D., Weatherill, G., Danciu, L., Crowley, H., Henshaw, P., Butler, L., Nastasi, M., Panzeri, L., Simionato, M., & Vigano, D. (2014). OpenQuake Engine : An Open Hazard (and Risk) Software for the Global Earthquake Model. Seismological Research Letters, 85(3), 692–702. https://doi.org/10.1785/0220130087

Passeri, F., Foti, S., & Rodriguez-Marek, A. (2020, September). A new geostatistical model for shear wave velocity profiles. Soil Dynamics and Earthquake Engineering, 136, 106247. doi:https://doi.org/10.1016/j.soildyn.2020.106247

Rodriguez-Marek, A., Rathje, E. M., Bommer, J. J., Scherbaum, F., & Stafford, P. J. (2014, June). Application of Single-Station Sigma and Site-Response Characterization in a Probabilistic Seismic-Hazard Analysis for a New Nuclear Site. Bulletin of the Seismological Society of America, 104, 1601–1619. doi:https://doi.org/10.1785/0120130196

Sgobba S., Pacor F., Felicetta C., Lanzano G., D'Amico M. C., Russo E., Luzi L. (2021). NEar-Source Strong-motion flatfile (NESS), version 2.0 [Data set]. Istituto Nazionale di Geofisica e Vulcanologia (INGV). https://doi.org/10.13127/ness.2.0

Shome, N., & Cornell, C. A. (1999). Probabilistic Seismic Demand Analysis of Nonlinear Structures. Reliability of Marine Structures. In Program Technical Report RMS-35. Standford University.

Spillatura, A., Kohrangi, M., Bazzurro, P., and Vamvatsikos, D., (2021). Conditional spectrum record selection faithful to causative earthquake parameter distributions. Earthquake Engineering and Structural Dynamics, 50(10), 2653–2671. DOI: 10.1002/eqe.3465

Stewart, J. P., Afshari, K., & Hashash, Y. M. (2014). Guidelines for performing hazard-consistent one-dimensional ground response analysis for ground motion prediction. *Peer Rep, 16*, 117.

Tarbali, K., and Bradley, B. A. (2016) The effect of causal parameter bounds in PSHA-based ground motion selection. Earthquake Engng Struct. Dyn., 45: 1515–1535. doi: 10.1002/eqe.2721.Toro, G. R. (1995). Probabilistic models of site velocity profiles for generic and site-specific ground-motion amplification studies. Technical Rep, 779574.

Vamvatsikos D and Zeris C (2010) Influence of uncertain vertical loads and accelerations on theseismic performance of an RC building. In: 3rd FIB international congress, Washington, DC, 29May 2 June 2010

Van Houtte, C., Bannister, S., Holden, C., Bourguignon, S., & McVerry, G. (2017). The New Zealand Strong Motion Database. Bulletin of the New Zealand Society for Earthquake Engineering, 50(1), 1–20. https://doi.org/10.5459/bnzsee.50.1.1-20

Zhang J, Andrus RD, Juang CH. Normalized Shear Modulus and Material Damping Ratio Relationships. J Geotech Geoenviron Eng. avr 2005;131(4):453-64.

Zienkiewicz, O. C., Bicanic, N., & Shen, F. Q. (1989). Earthquake input definition and the trasmitting boundary conditions. Advances in computational nonlinear mechanics, 109-138.

7. Appendix

7.1. Example of bedrock selected ground motions

The following figures and tables show the case with 15 time histories per stripe for the PGA selection.

7.1.1. IML1

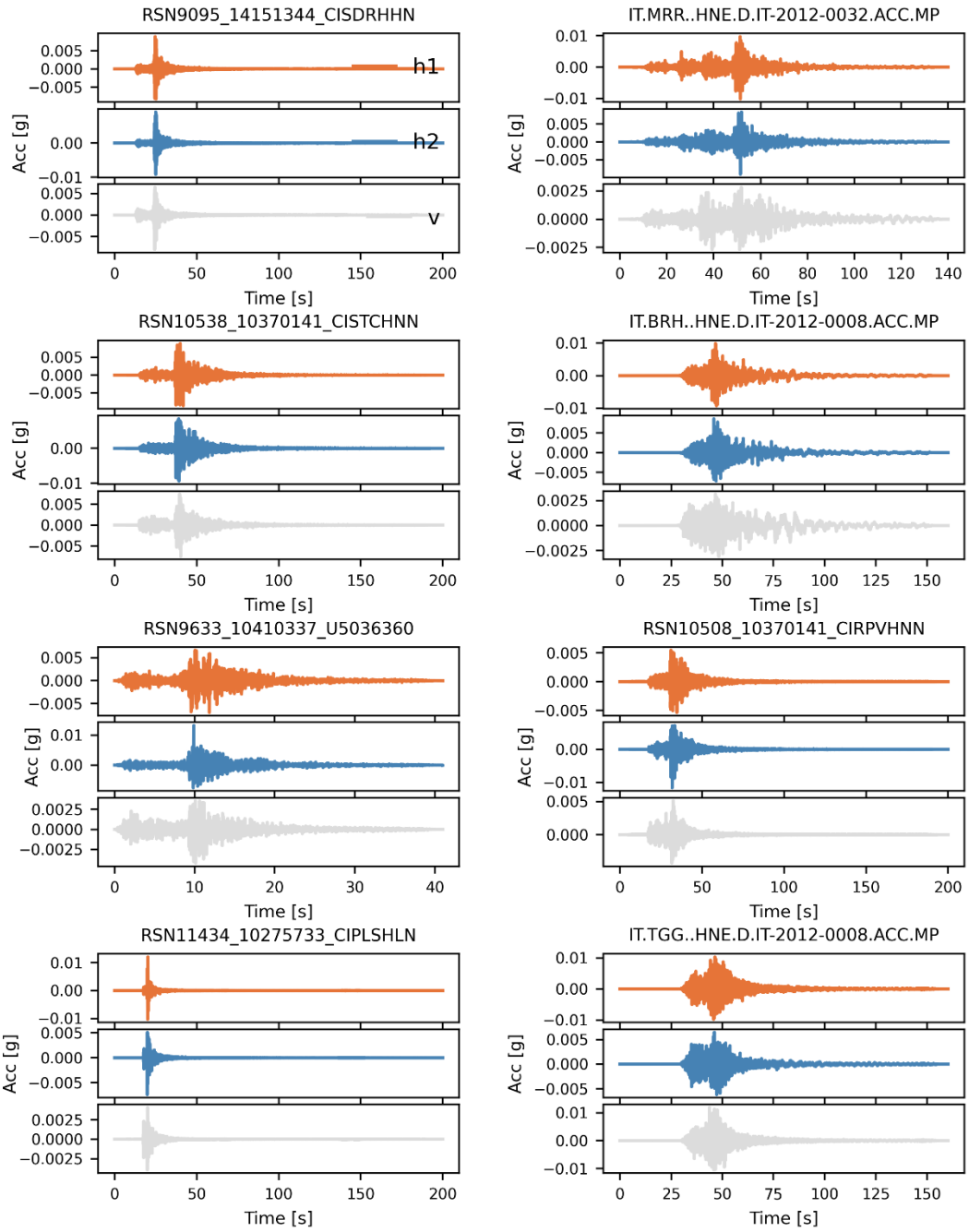

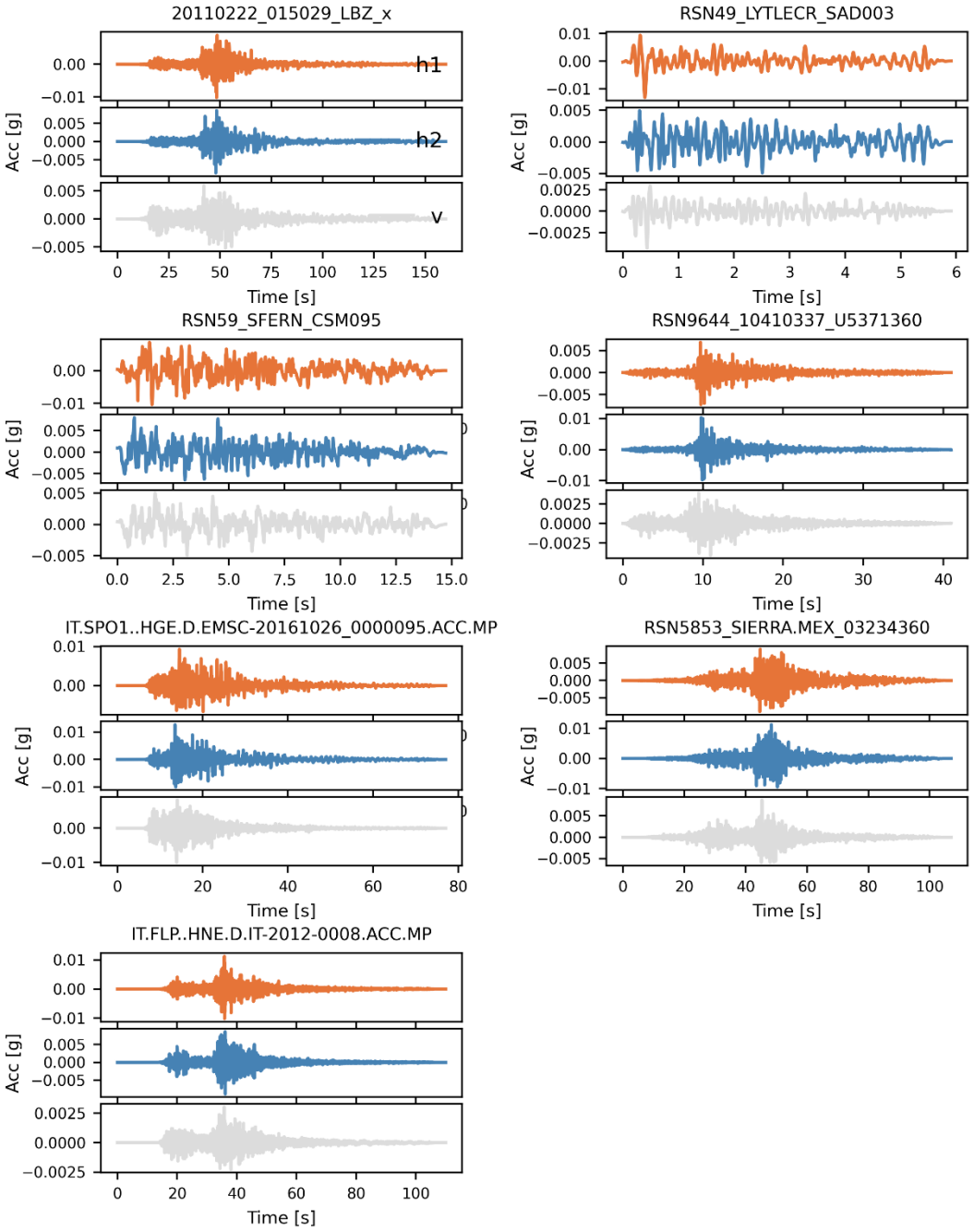

Figure 32: Set of 15 3-component waveforms of the selected ground motions at bedrock for PGA (Sa[0.1s]) for IML1

7.1.2.IML2

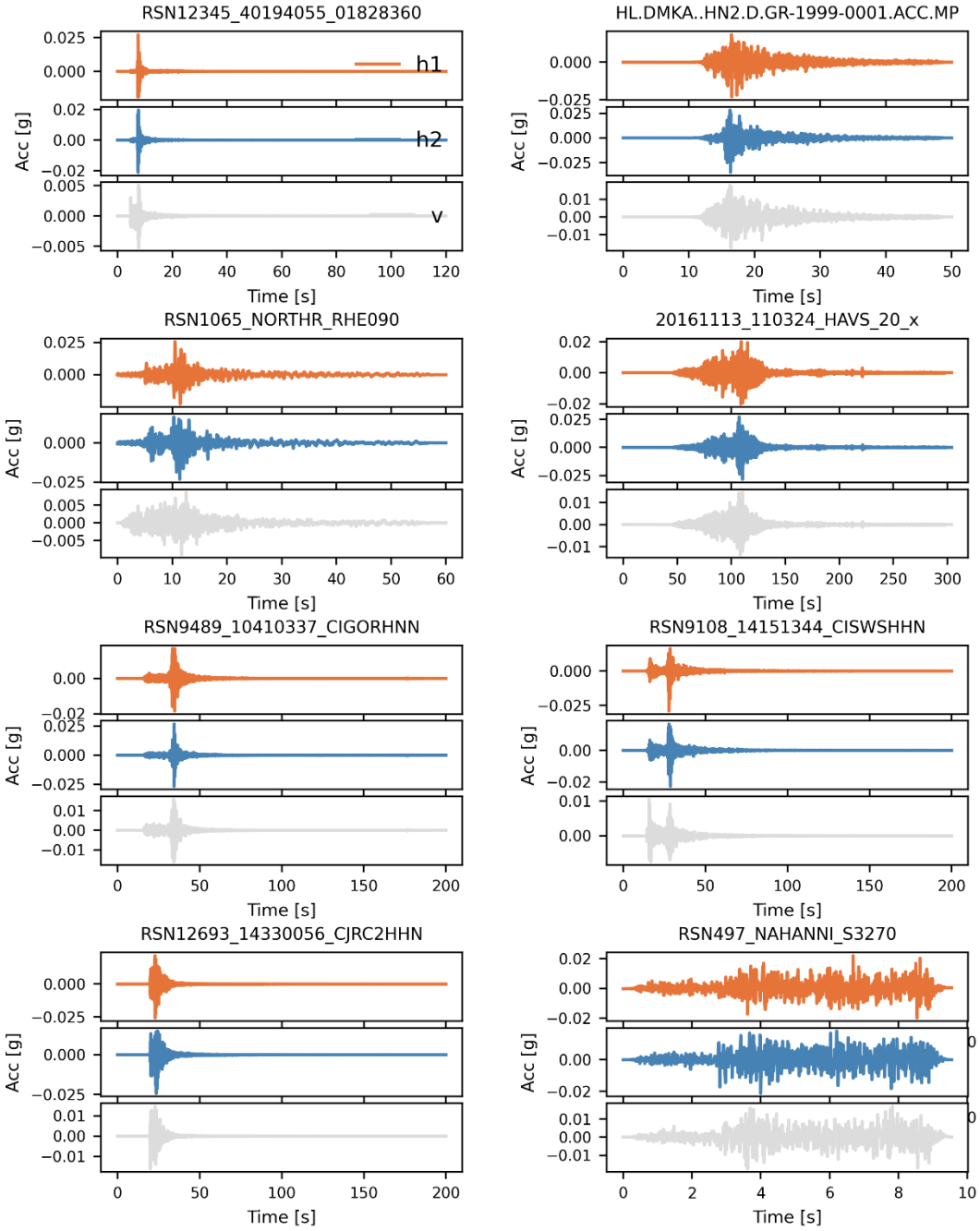
RSN12345_40194055_01828360
h1
h2
v
Acc [g]
Time [s]
HL.DMKA..HN2.D.GR-1999-0001.ACC.MP
RSN1065_NORTHR_RHE090
20161113_110324_HAVS_20_x
RSN9489_10410337_CIGORHNN
RSN9108_14151344_CISWSHHN
RSN12693_14330056_CJRC2HHN
RSN497_NAHANNI_S3270

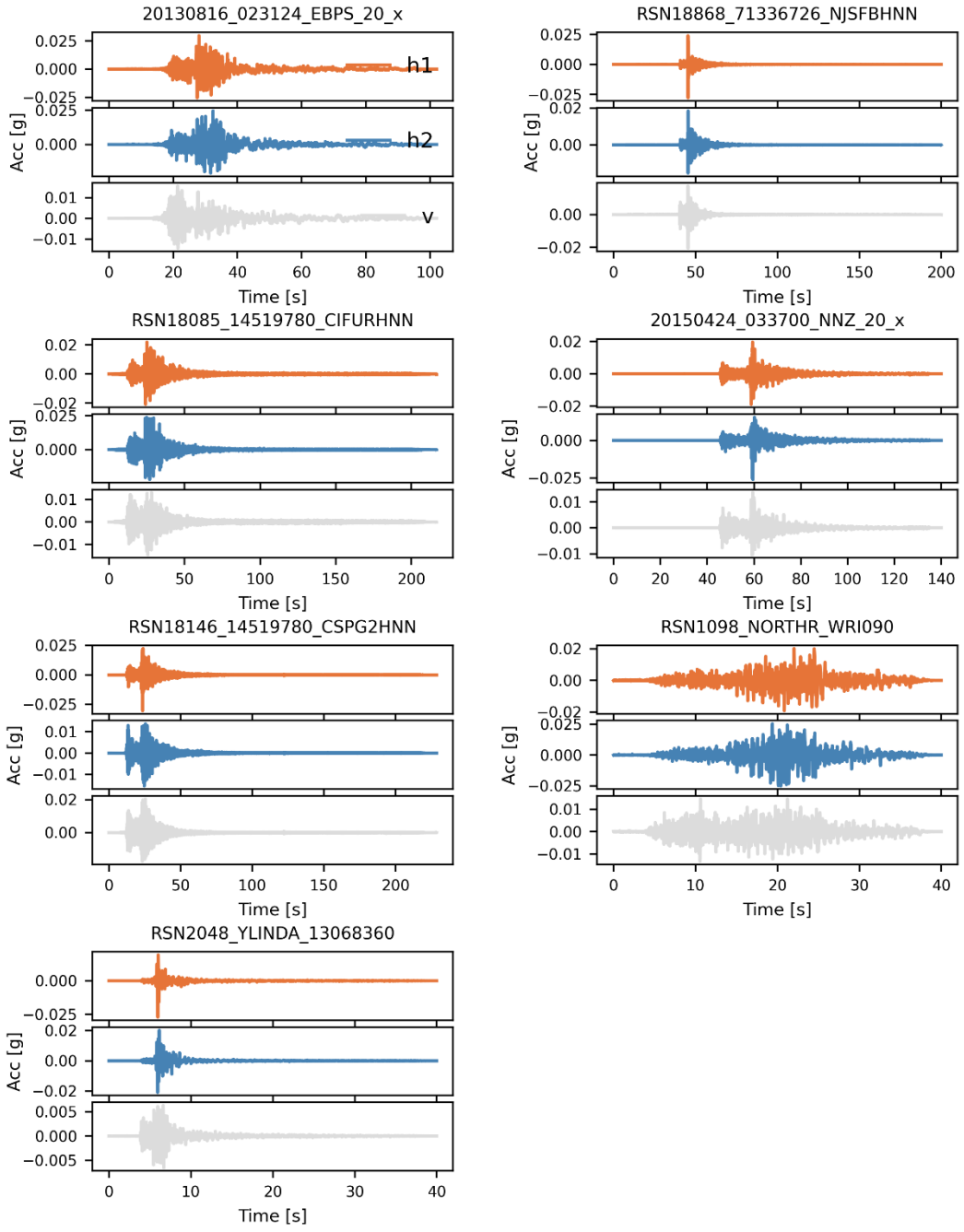

Figure 33: Set of 15 3-component waveforms of the selected ground motions at bedrock for PGA (Sa[0.1s]) for IML2

7.1.3.IML3

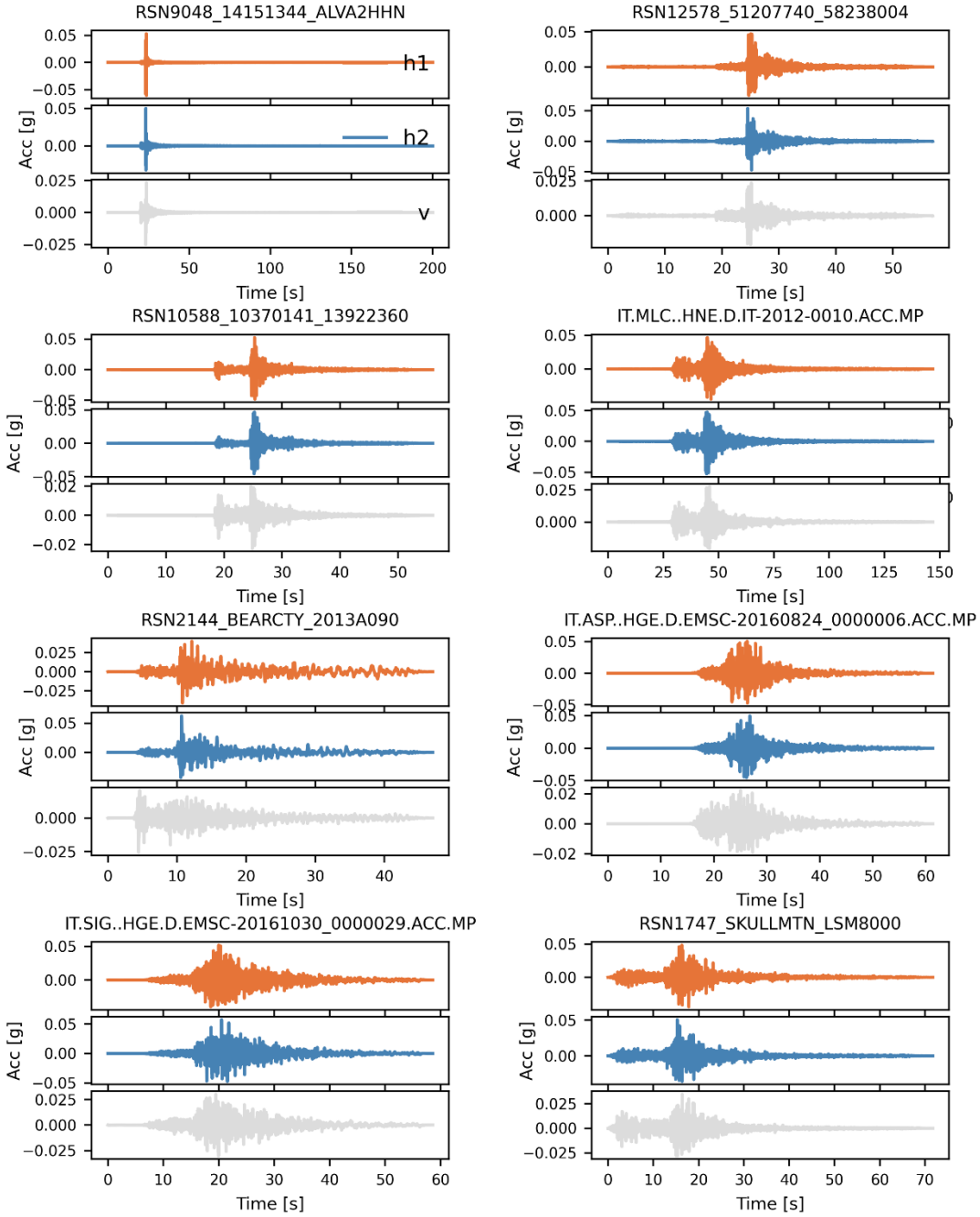
RSN9048_14151344_ALVA2HHN
h1
h2
v
Acc [g]
Time [s]
RSN12578_51207740_58238004
RSN10588_10370141_13922360
IT.MLC..HNE.D.IT-2012-0010.ACC.MP
RSN2144_BEARCTY_2013A090
IT.ASP..HGE.D.EMSC-20160824_0000006.ACC.MP
IT.SIG..HGE.D.EMSC-20161030_0000029.ACC.MP
RSN1747_SKULLMTN_LSM8000

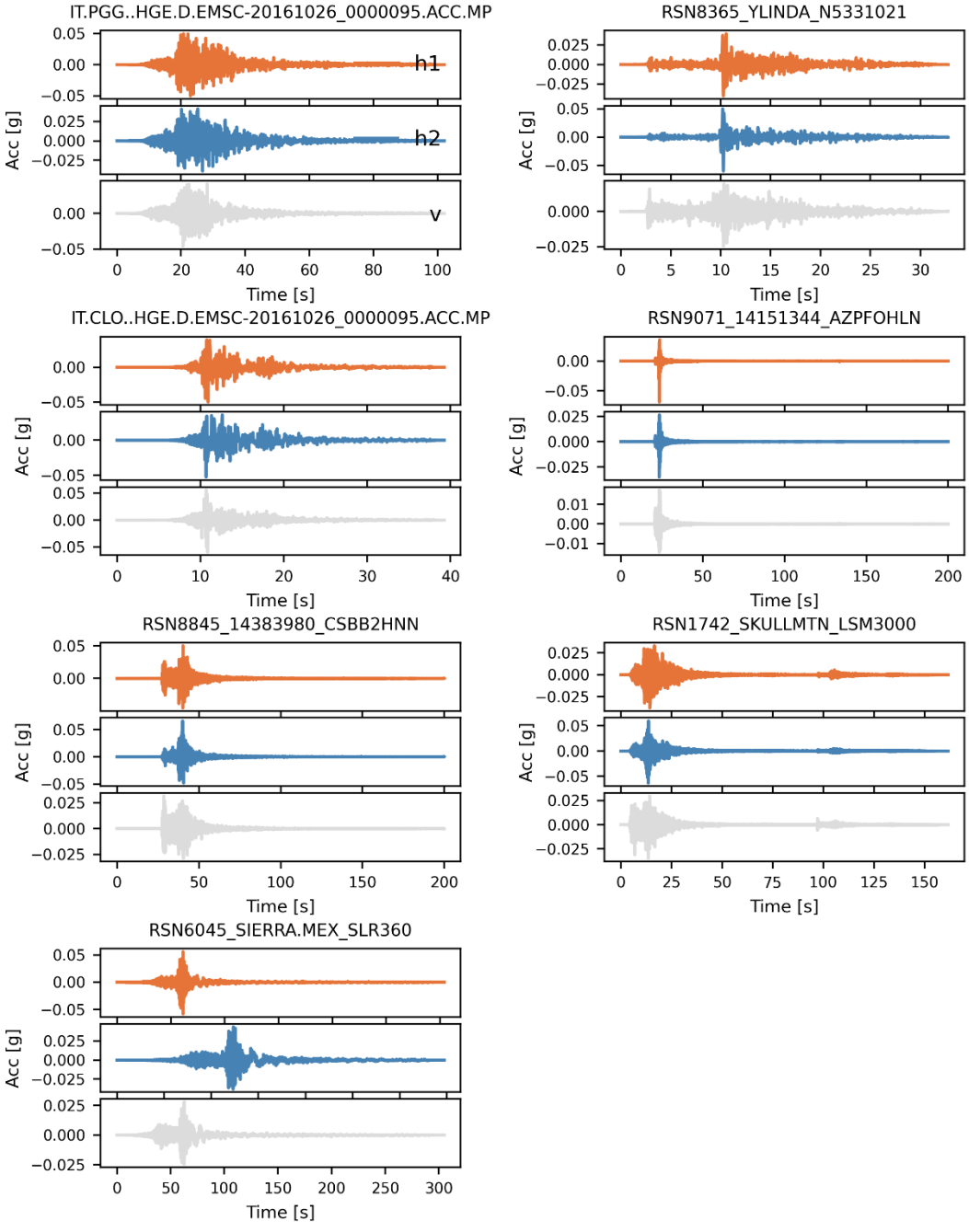

Figure 34: Set of 15 3-component waveforms of the selected ground motions at bedrock for PGA (Sa[0.1s]) for IML3

7.1.4.IML4

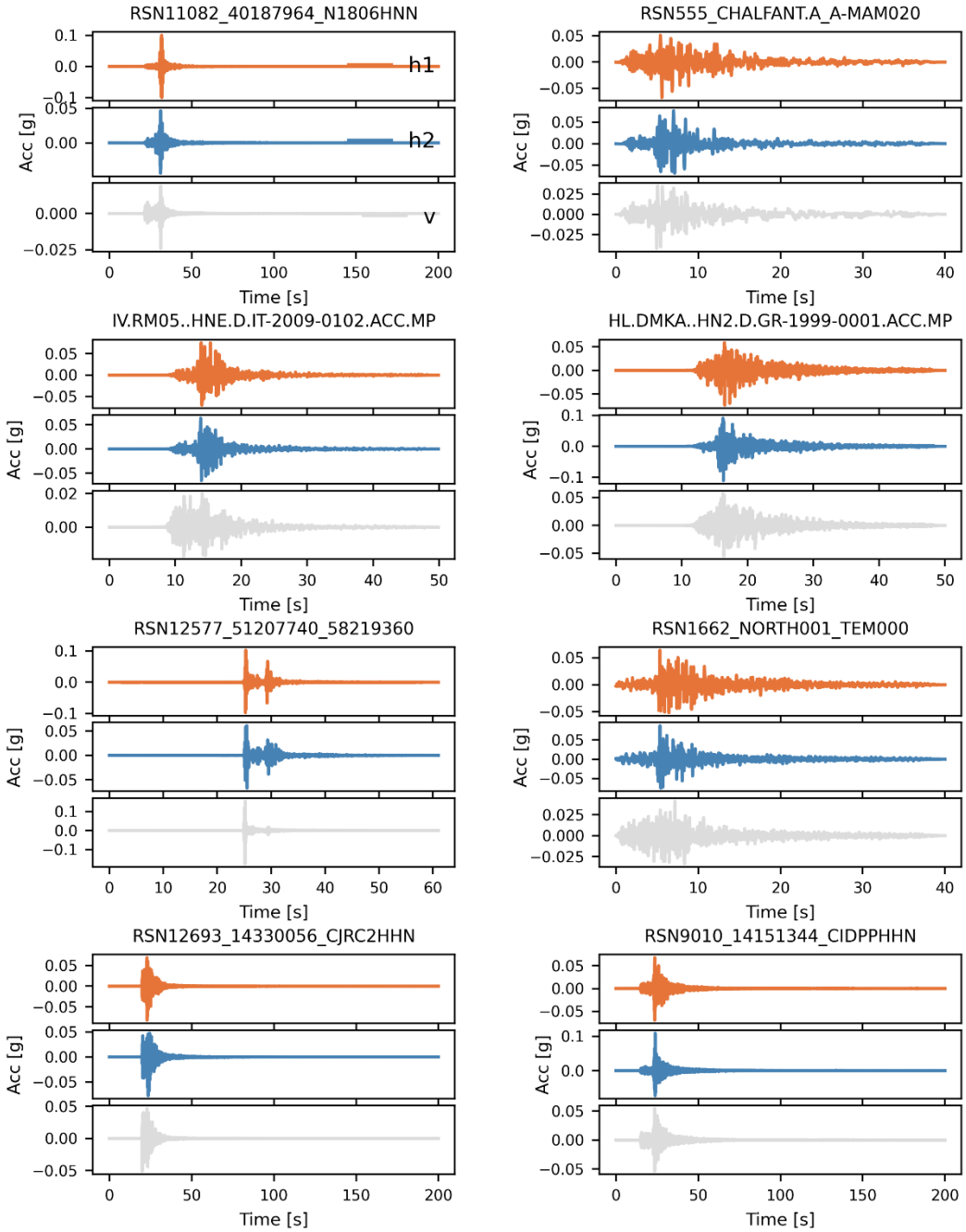
RSN11082_40187964_N1806HNN
h1
h2
v
Acc [g]
Time [s]
RSN555_CHALFANT.A_A-MAM020
IV.RM05..HNE.D.IT-2009-0102.ACC.MP
HL.DMKA..HN2.D.GR-1999-0001.ACC.MP
RSN12577_51207740_58219360
RSN1662_NORTH001_TEM000
RSN12693_14330056_CJRC2HHN
RSN9010_14151344_CIDPPHHN

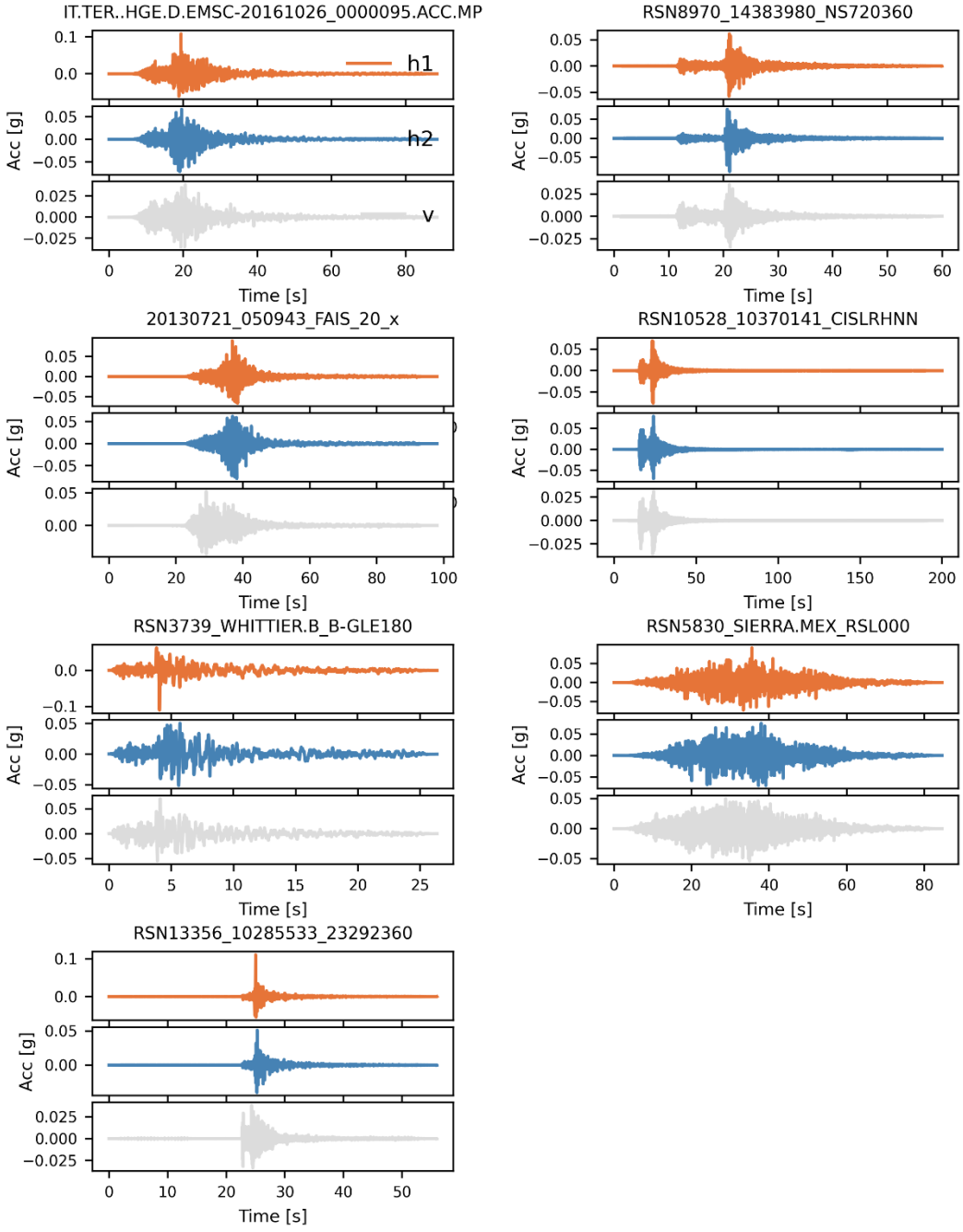

Figure 35: Set of 15 3-component waveforms of the selected ground motions at bedrock for PGA (Sa[0.1s]) for IML4

7.1.5.IML5

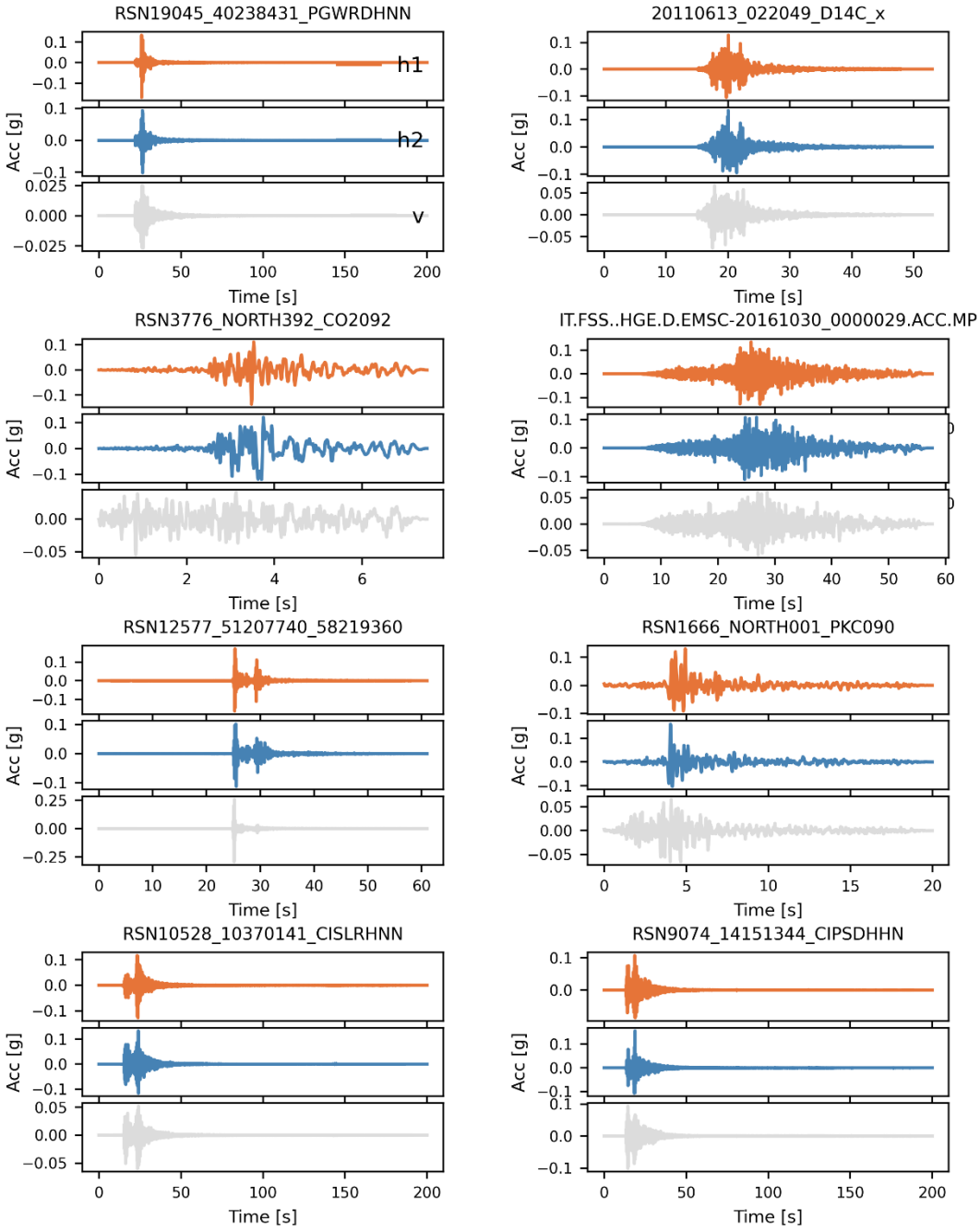
RSN19045_40238431_PGWRDHNN
h1
h2
v
Acc [g]
Time [s]
20110613_022049_D14C_x
RSN3776_NORTH392_CO2092
IT.FSS..HGE.D.EMSC-20161030_0000029.ACC.MP
RSN12577_51207740_58219360
RSN1666_NORTH001_PKC090
RSN10528_10370141_CISLRHNN
RSN9074_14151344_CIPSDHHN

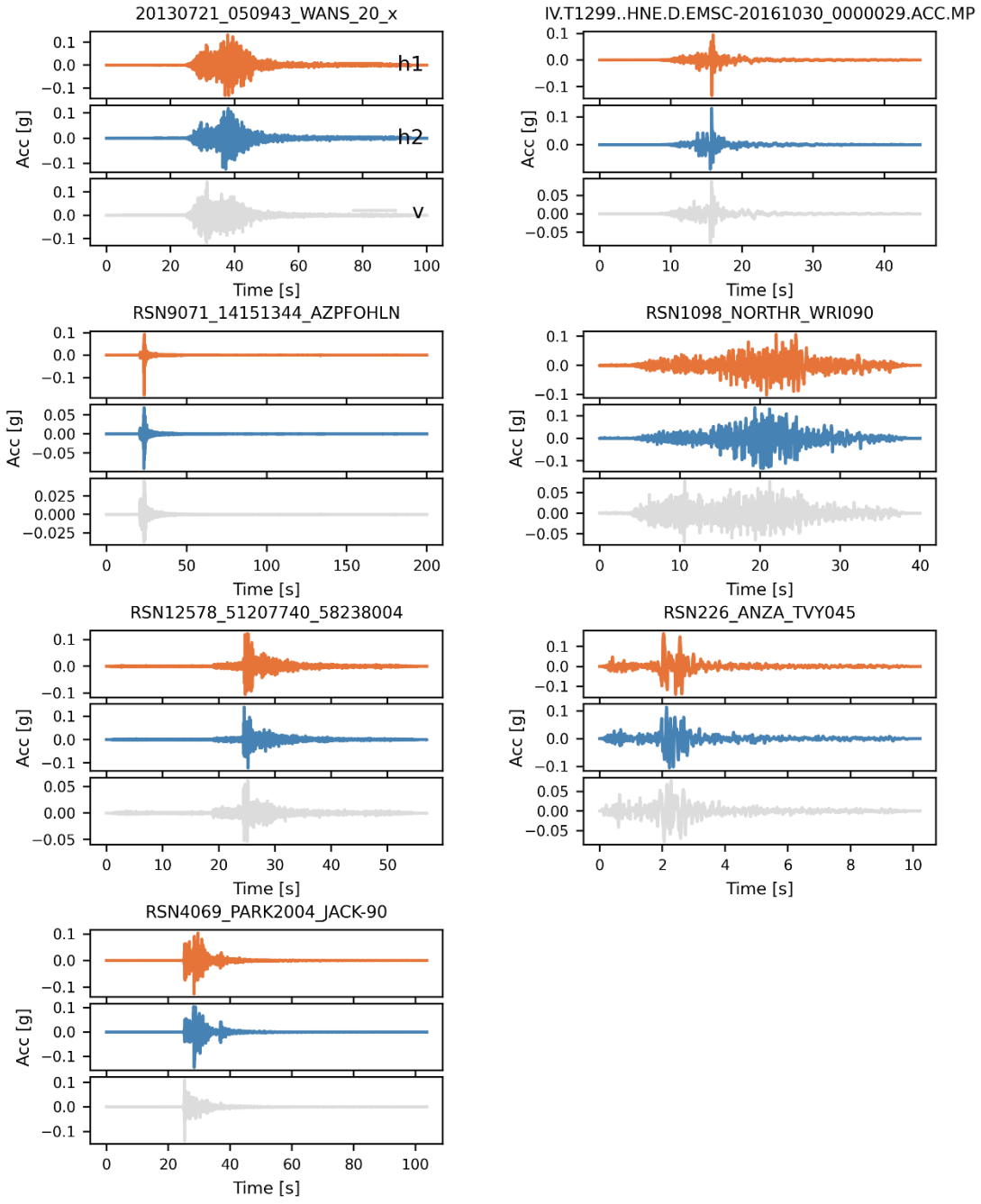

Figure 36: Set of 15 3-component waveforms of the selected ground motions at bedrock for PGA (Sa[0.1s]) for IML5

7.1.6.IML6

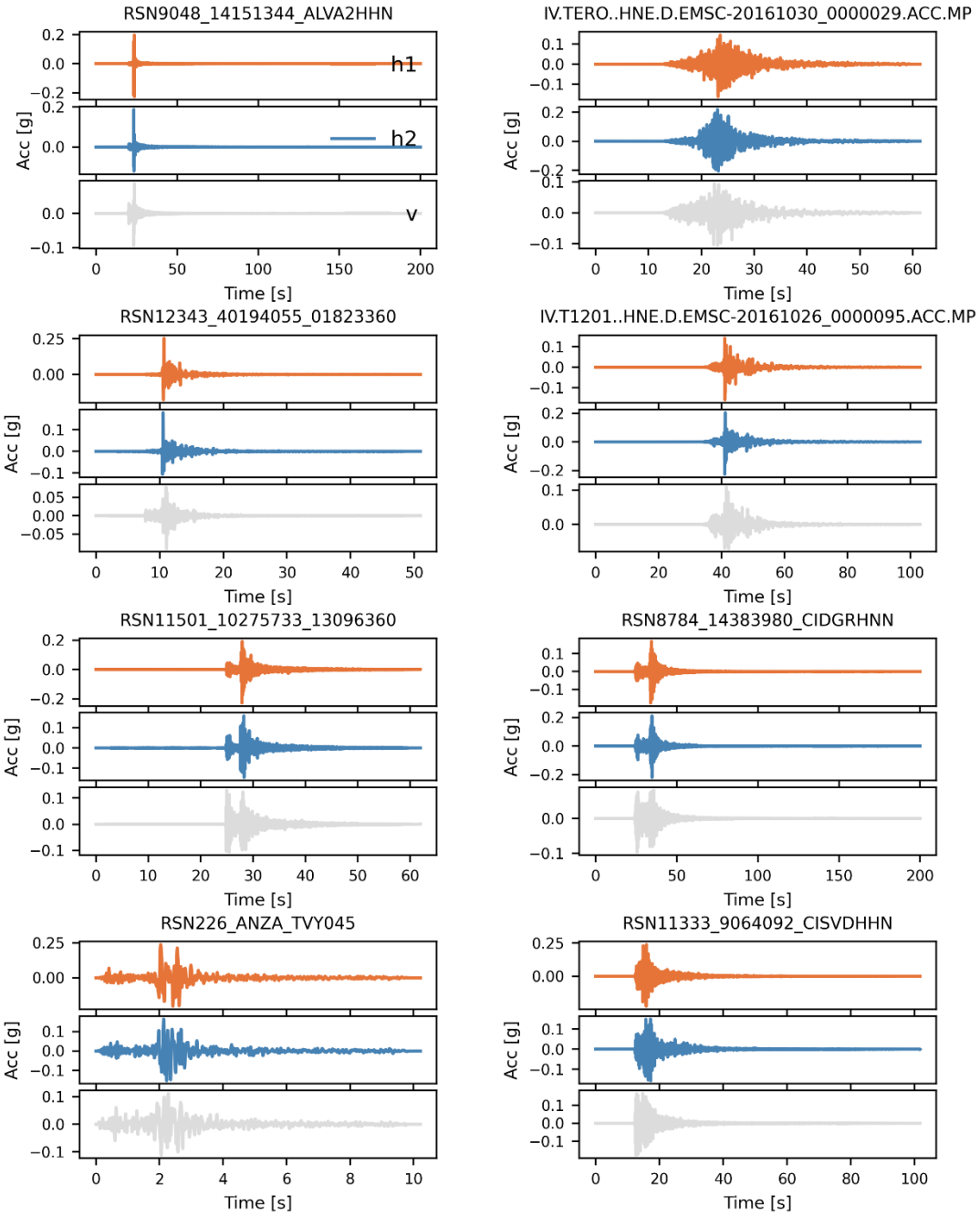
RSN9048_14151344_ALVA2HHN
h1
h2
v
Acc [g]
Time [s]
IV.TERO..HNE.D.EMSC-20161030_0000029.ACC.MP
RSN12343_40194055_01823360
IV.T1201..HNE.D.EMSC-20161026_0000095.ACC.MP
RSN11501_10275733_13096360
RSN8784_14383980_CIDGRHNN
RSN226_ANZA_TVY045
RSN11333_9064092_CISVDHHN

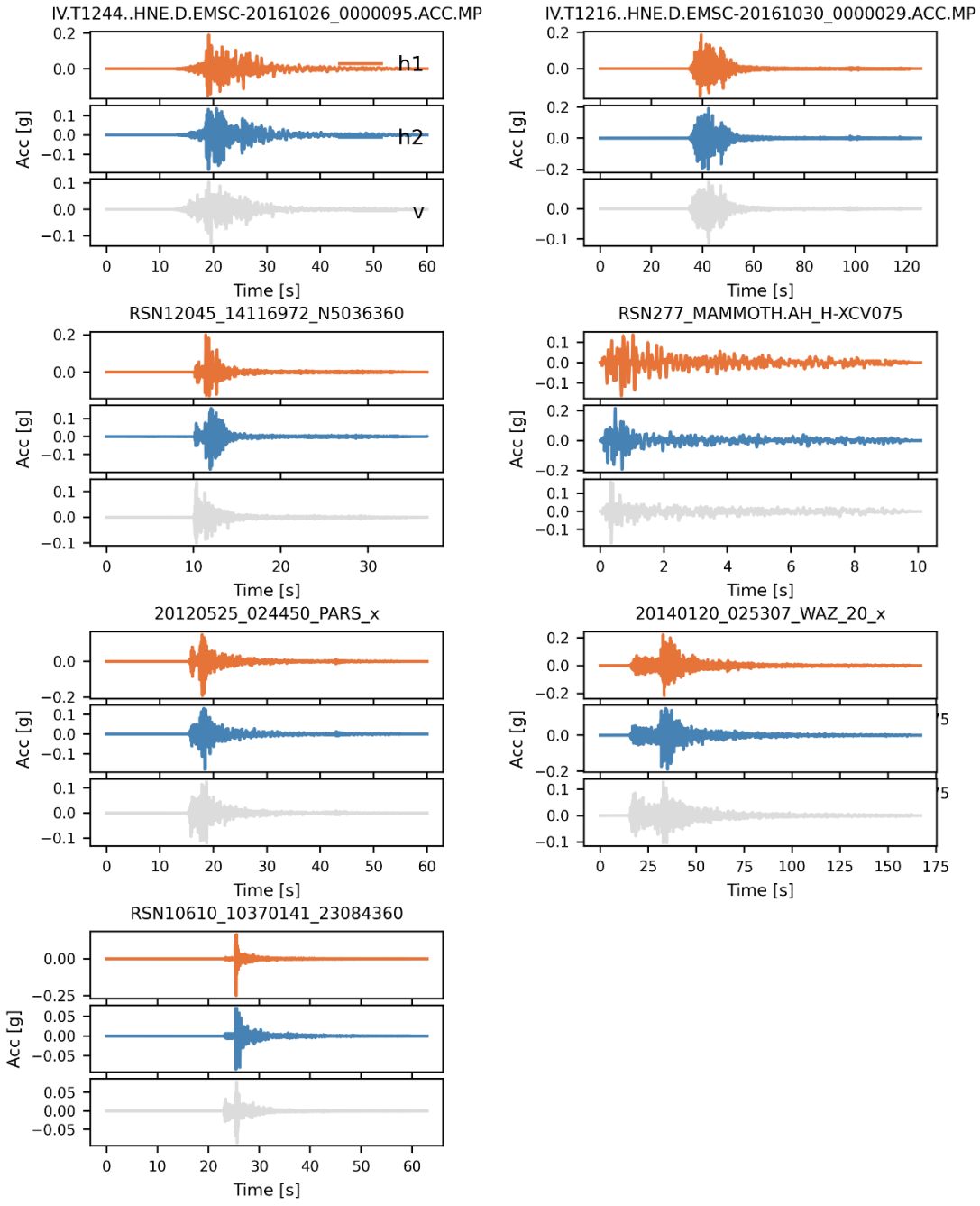

Figure 37: Set of 15 3-component waveforms of the selected ground motions at bedrock for PGA (Sa[0.1s]) for IML6

7.1.7.IML7

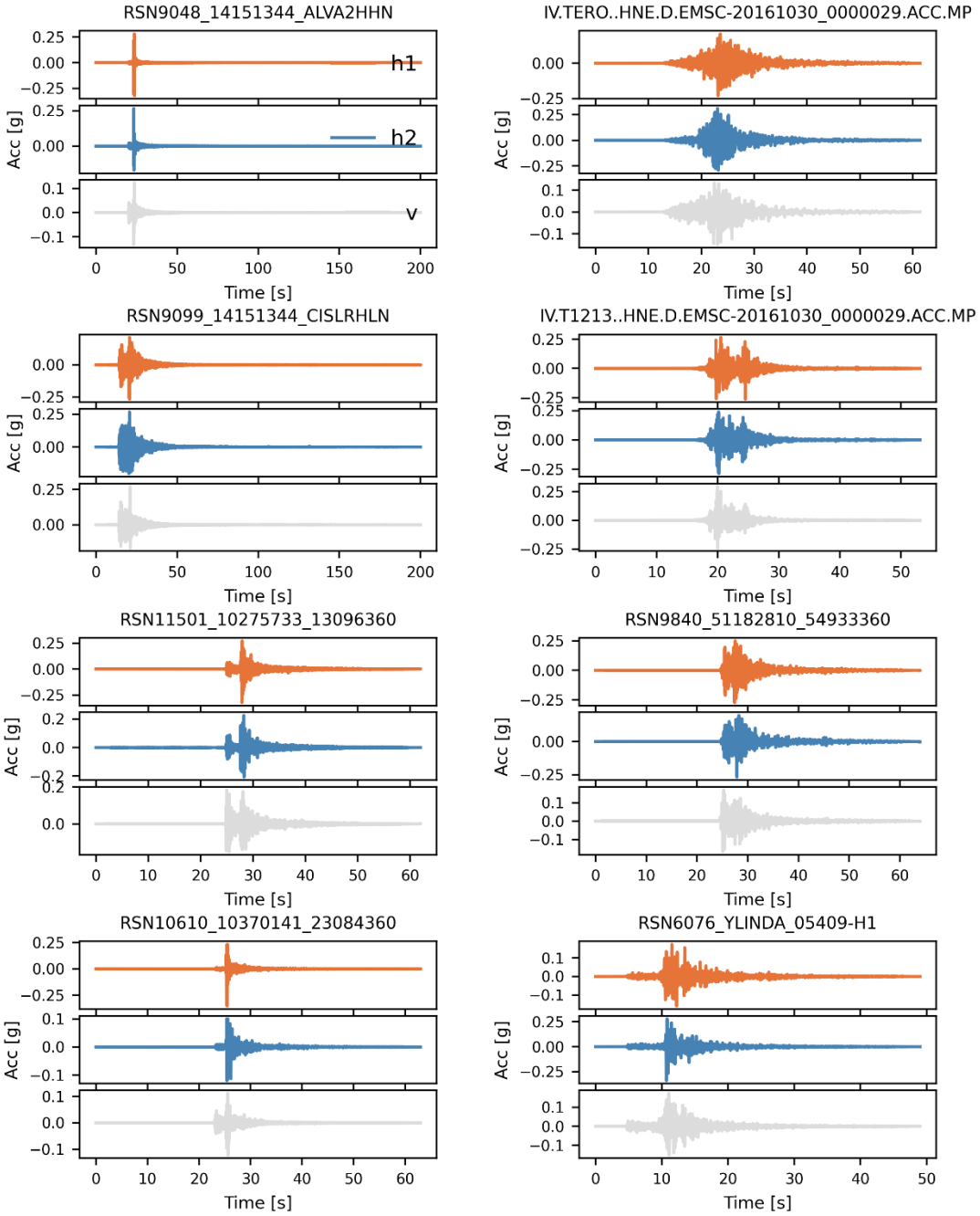
RSN9048_14151344_ALVA2HHN
h1
h2
v
Acc [g]
Time [s]
IV.TERO..HNE.D.EMSC-20161030_0000029.ACC.MP
Acc [g]
Time [s]
RSN9099_14151344_CISLRHLN
Acc [g]
Time [s]
IV.T1213..HNE.D.EMSC-20161030_0000029.ACC.MP
Acc [g]
Time [s]
RSN11501_10275733_13096360
Acc [g]
Time [s]
RSN9840_51182810_54933360
Acc [g]
Time [s]
RSN10610_10370141_23084360
Acc [g]
Time [s]
RSN6076_YLINDA_05409-H1
Acc [g]
Time [s]

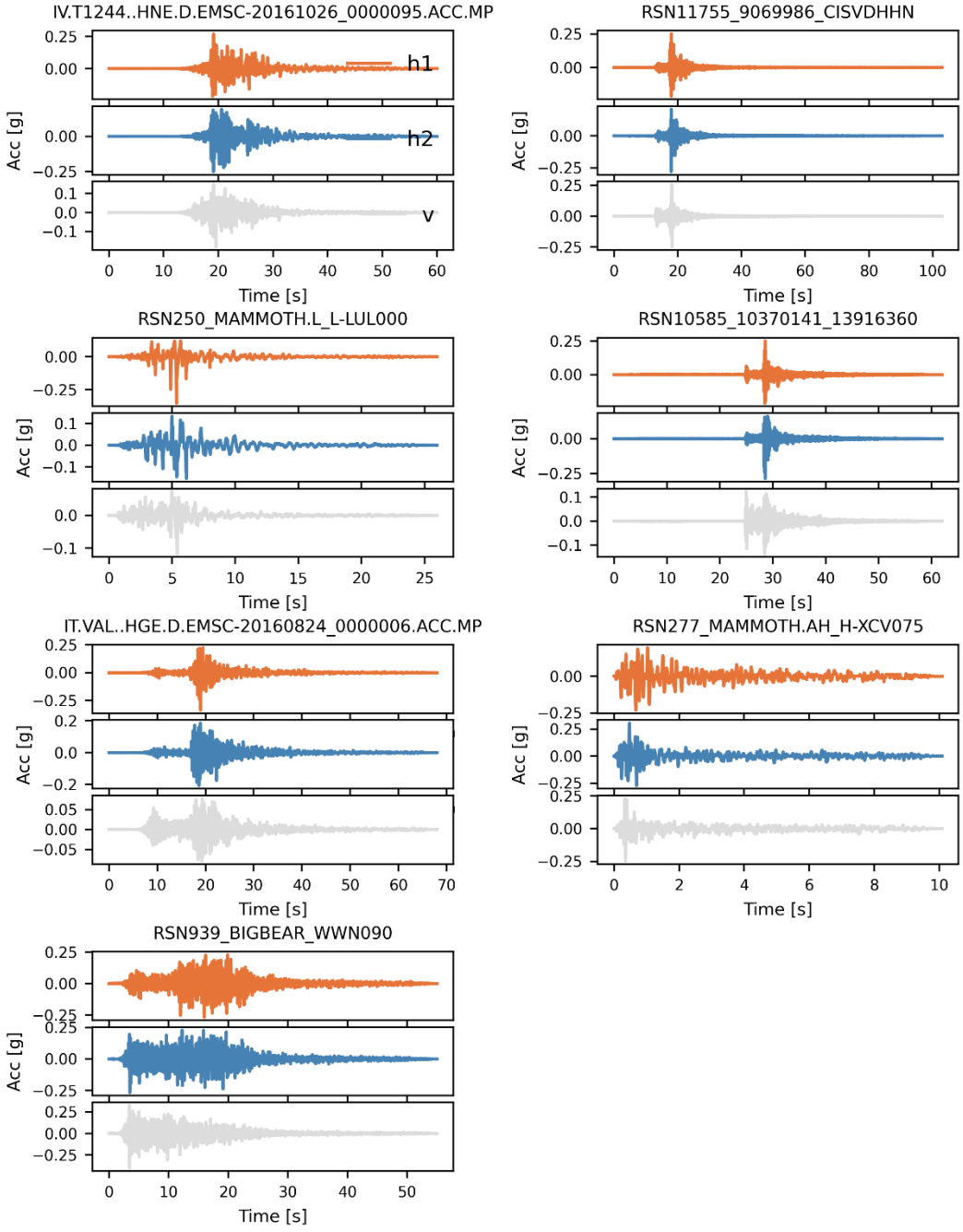

Figure 38: Set of 15 3-component waveforms of the selected ground motions at bedrock for PGA (Sa[0.1s]) for IML7

7.1.8.IML8

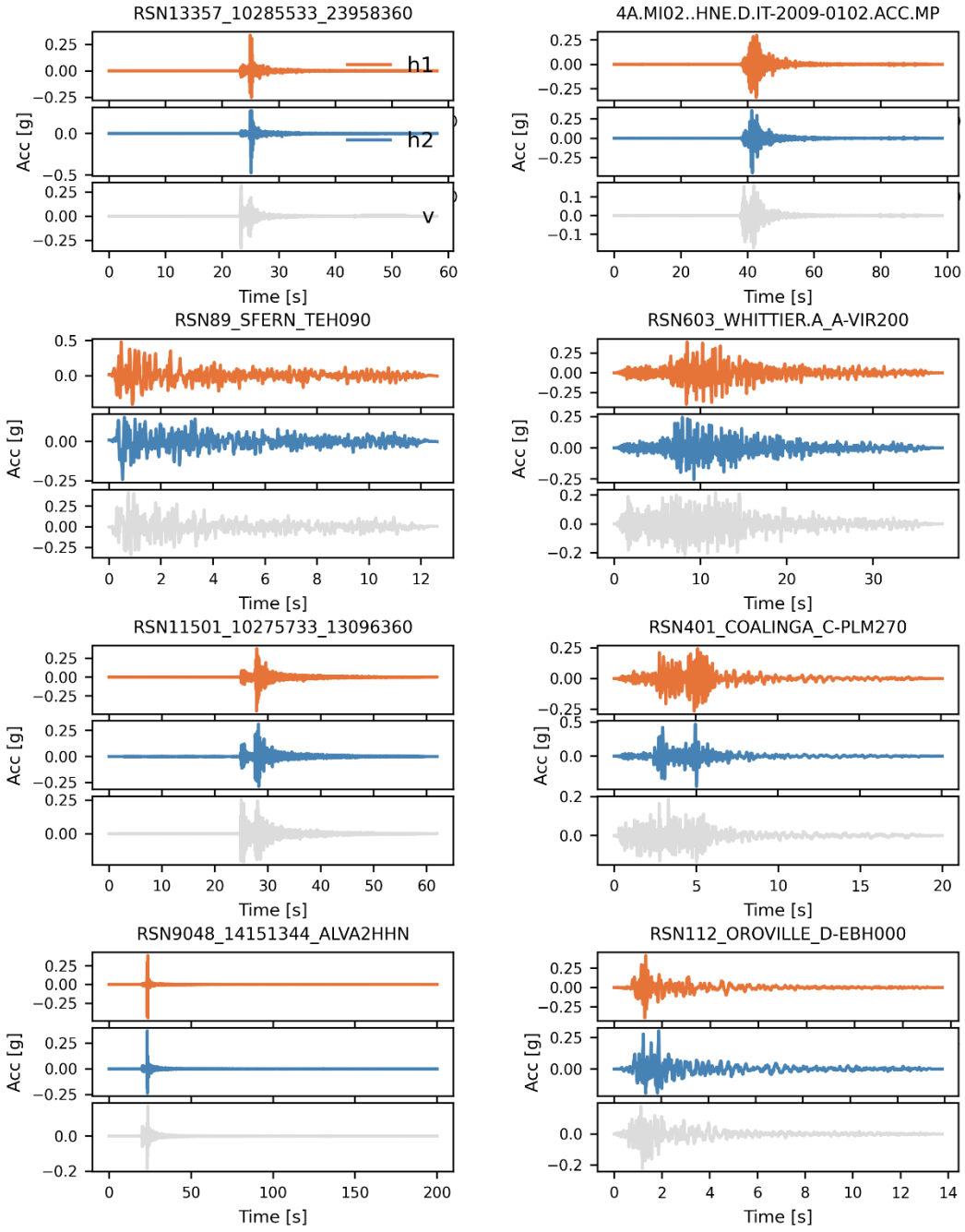
RSN13357_10285533_23958360
h1
h2
v
Acc [g]
Time [s]
4A.MI02..HNE.D.IT-2009-0102.ACC.MP
RSN89_SFERN_TEH090
RSN603_WHITTIER.A_A-VIR200
RSN11501_10275733_13096360
RSN401_COALINGA_C-PLM270
RSN9048_14151344_ALVA2HHN
RSN112_OROVILLE_D-EBH000

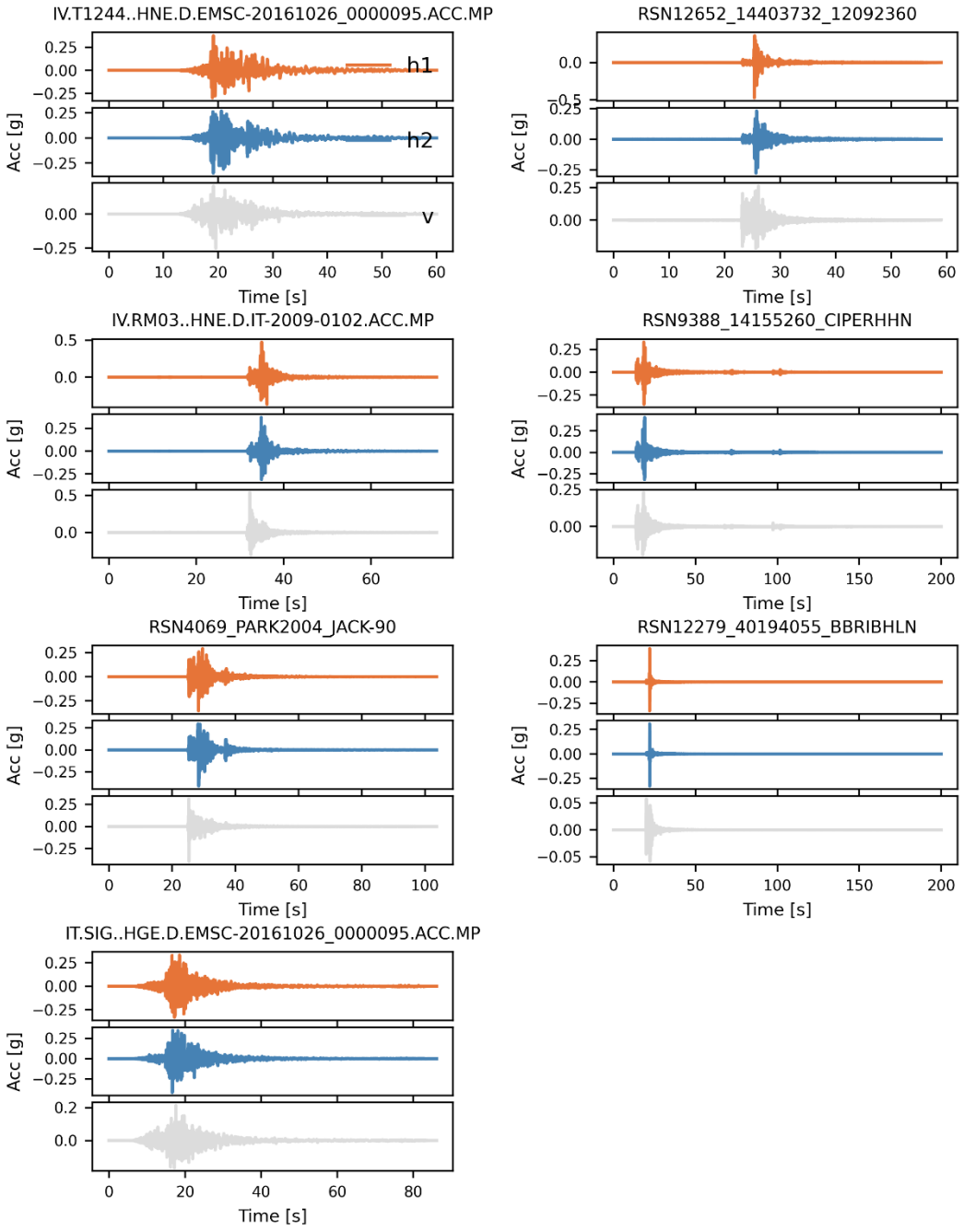

Figure 39: Set of 15 3-component waveforms of the selected ground motions at bedrock for PGA (Sa[0.1s]) for IML8

7.1.9.IML9

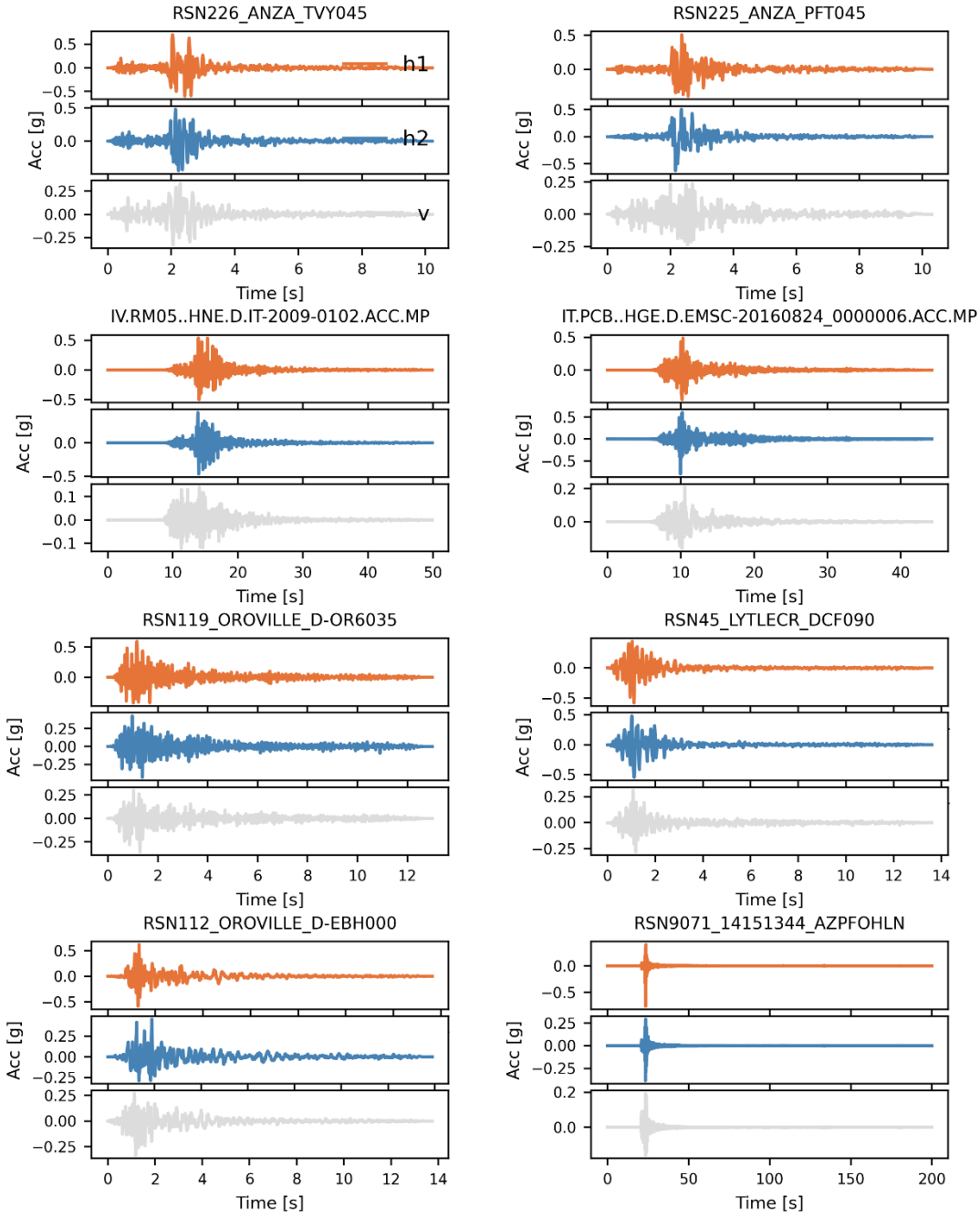
RSN226_ANZA_TVY045
h1
h2
v
Acc [g]
Time [s]
RSN225_ANZA_PFT045
IV.RM05..HNE.D.IT-2009-0102.ACC.MP
IT.PCB..HGE.D.EMSC-20160824_0000006.ACC.MP
RSN119_OROVILLE_D-OR6035
RSN45_LYTLECR_DCF090
RSN112_OROVILLE_D-EBH000
RSN9071_14151344_AZPFOHLN

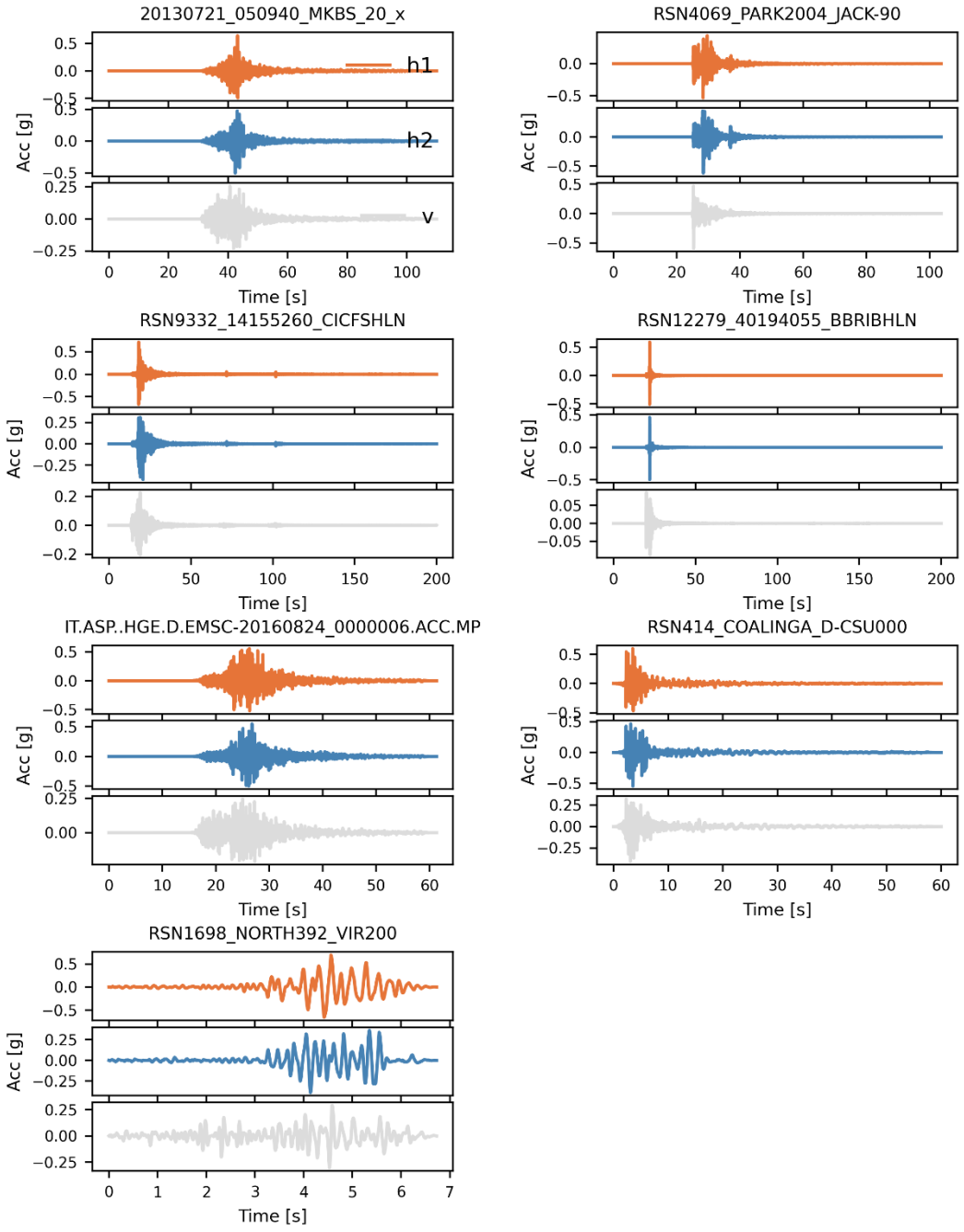

Figure 40: Set of 15 3-component waveforms of the selected ground motions at bedrock for PGA (Sa[0.1s]) for IML9

7.1.10. IML10

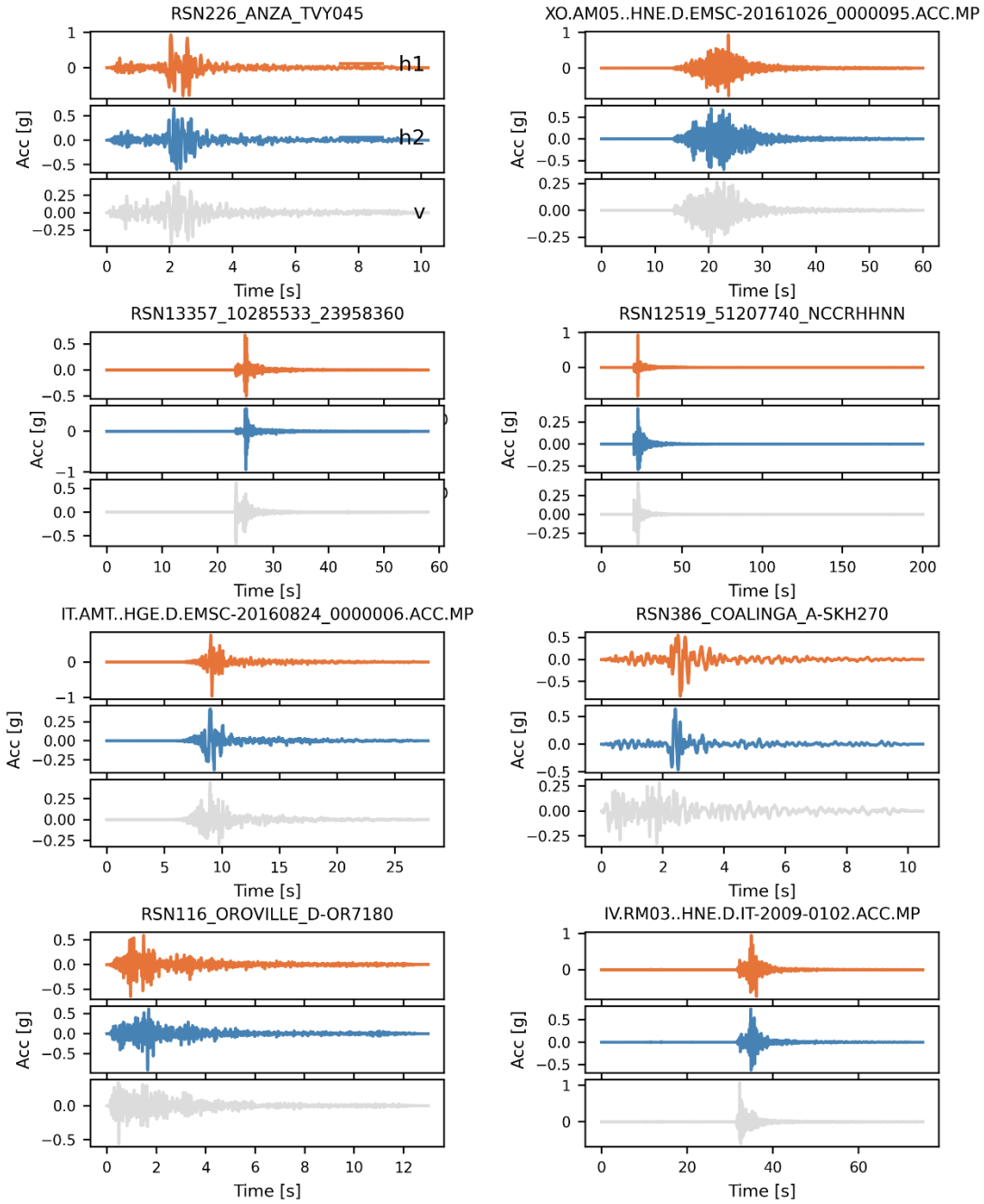
RSN226_ANZA_TVY045
h1
h2
v
Acc [g]
Time [s]
XO.AM05..HNE.D.EMSC-20161026_0000095.ACC.MP
RSN13357_10285533_23958360
RSN12519_51207740_NCCRHHNN
IT.AMT..HGE.D.EMSC-20160824_0000006.ACC.MP
RSN386_COALINGA_A-SKH270
RSN116_OROVILLE_D-OR7180
IV.RM03..HNE.D.IT-2009-0102.ACC.MP

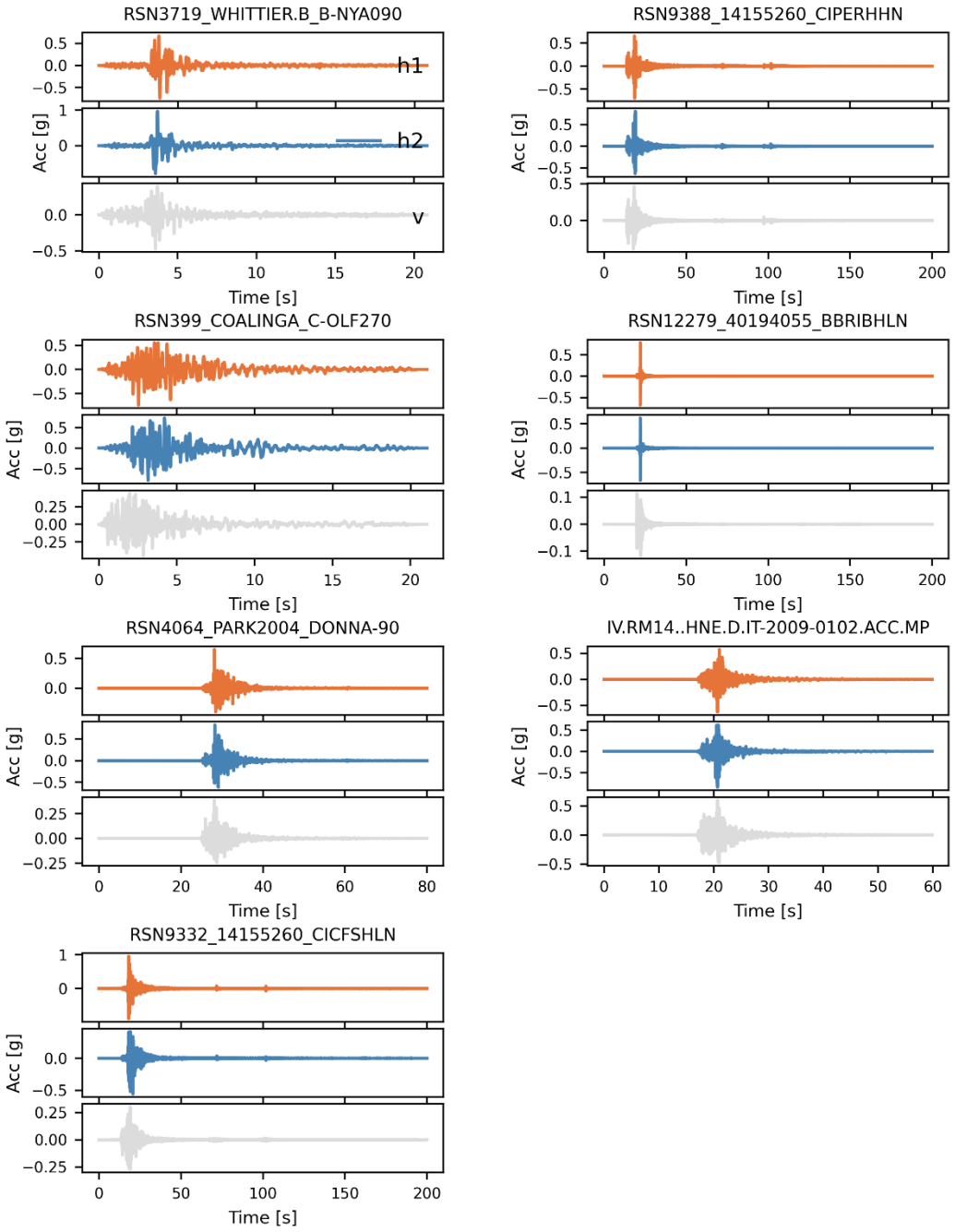

Figure 41: Set of 15 3-component waveforms of the selected ground motions at bedrock for PGA (Sa[0.1s]) for IML10

7.2. Selected records and causative Parameters

IML	rec_h1	rec_h2	rec_v	Mw	Rjb [km]	Vs30 [m/s]	DB
1	RSN9095_14151344_CISDRHHN	RSN9095_14151344_CISDRHHE	RSN9095_14151344_CISDRHHZ	5.2	93.4	827	NGA
1	IT.MRR..HNE.D.IT-2012-0032.ACC.MP	IT.MRR..HNN.D.IT-2012-0032.ACC.MP	IT.MRR..HNZ.D.IT-2012-0032.ACC.MP	5.5	98.9	915	ESM
1	RSN10538_10370141_CISTCHNN	RSN10538_10370141_CISTCHNE	RSN10538_10370141_CISTCHNZ	4.45	173.7	490	NGA
1	IT.BRH..HNE.D.IT-2012-0008.ACC.MP	IT.BRH..HNN.D.IT-2012-0008.ACC.MP	IT.BRH..HNZ.D.IT-2012-0008.ACC.MP	6.1	69.3	521	ESM
1	RSN9633_10410337_U5036360	RSN9633_10410337_U5036090	RSN9633_10410337_U5036-UP	4.7	90.1	631	NGA
1	RSN10508_10370141_CIRPVHNN	RSN10508_10370141_CIRPVHNE	RSN10508_10370141_CIRPVHNZ	4.45	108.5	530	NGA
1	RSN11434_10275733_CIPLSHLN	RSN11434_10275733_CIPLSHLE	RSN11434_10275733_CIPLSHLZ	4.73	11.7	699	NGA
1	IT.TGG..HNE.D.IT-2012-0008.ACC.MP	IT.TGG..HNN.D.IT-2012-0008.ACC.MP	IT.TGG..HNZ.D.IT-2012-0008.ACC.MP	6.1	63.9	797	ESM
1	20110222_015029_LBZ_x	20110222_015029_LBZ_y	20110222_015029_LBZ_z	5.63	211.8	1000	GNS
1	RSN49_LYTLECR_SAD003	RSN49_LYTLECR_SAD273	RSN49_LYTLECR_SADDWN	5.33	42.1	667	NGA
1	RSN59_SFERN_CSM095	RSN59_SFERN_CSM185	RSN59_SFERN_CSMDWN	6.61	89.4	813	NGA
1	RSN9644_10410337_U5371360	RSN9644_10410337_U5371090	RSN9644_10410337_U5371-UP	4.7	95.9	496	NGA
1	IT.SPO1..HGE.D.EMSC-20161026_0000095.ACC.MP	IT.SPO1..HGN.D.EMSC-20161026_0000095.ACC.MP	IT.SPO1..HGZ.D.EMSC-20161026_0000095.ACC.MP	5.9	34.4	533	ESM
1	RSN5853_SIERRA.MEX_03234360	RSN5853_SIERRA.MEX_03234-90	RSN5853_SIERRA.MEX_03234-UP	7.2	139.4	477	NGA
1	IT.FLP..HNE.D.IT-2012-0008.ACC.MP	IT.FLP..HNN.D.IT-2012-0008.ACC.MP	IT.FLP..HNZ.D.IT-2012-0008.ACC.MP	6.1	131.5	417	ESM
2	RSN12345_40194055_01828360	RSN12345_40194055_01828090	RSN12345_40194055_01828-DN	4.23	13.7	415	NGA
2	HL.DMKA..HN2.D.GR-1999-0001.ACC.MP	HL.DMKA..HN3.D.GR-1999-0001.ACC.MP	HL.DMKA..HNZ.D.GR-1999-0001.ACC.MP	5.9	19.6	767	ESM
2	RSN1065_NORTHR_RHE090	RSN1065_NORTHR_RHE360	RSN1065_NORTHR_RHE-UP	6.69	44.9	473	NGA
2	20161113_110324_HAVS_20_x	20161113_110324_HAVS_20_y	20161113_110324_HAVS_20_z	7.85	63.0	1000	GNS
2	RSN9489_10410337_CIGORHNN	RSN9489_10410337_CIGORHNE	RSN9489_10410337_CIGORHNZ	4.7	134.2	559	NGA
2	RSN9108_14151344_CISWSHHN	RSN9108_14151344_CISWSHHE	RSN9108_14151344_CISWSHHZ	5.2	95.0	503	NGA
2	RSN12693_14330056_CJRC2HHN	RSN12693_14330056_CJRC2HHE	RSN12693_14330056_CJRC2HHZ	4.34	19.2	623	NGA
2	RSN497_NAHANNI_S3270	RSN497_NAHANNI_S3360	RSN497_NAHANNI_S3-UP	6.76	4.9	605	NGA
2	20130816_023124_EBPS_20_x	20130816_023124_EBPS_20_y	20130816_023124_EBPS_20_z	6.6	65.8	540	GNS
2	RSN18868_71336726_NJSFBHNN	RSN18868_71336726_NJSFBHNE	RSN18868_71336726_NJSFBHNZ	4.05	34.2	432	NGA
2	RSN18085_14519780_CIFURHNN	RSN18085_14519780_CIFURHNE	RSN18085_14519780_CIFURHNZ	5.19	86.8	433	NGA
2	20150424_033700_NNZ_20_x	20150424_033700_NNZ_20_y	20150424_033700_NNZ_20_z	6.05	96.4	1200	GNS

2	RSN18146_14519780_CSPG2HNN	RSN18146_14519780_CSPG2HNE	RSN18146_14519780_CSPG2HNZ	5.19	83.6	924	NGA
2	RSN1098_NORTHR_WRI090	RSN1098_NORTHR_WRI180	RSN1098_NORTHR_WRI-UP	6.69	71.5	477	NGA
2	RSN2048_YLINDA_13068360	RSN2048_YLINDA_13068090	RSN2048_YLINDA_13068-UP	4.27	6.5	485	NGA
3	RSN9048_14151344_ALVA2HHN	RSN9048_14151344_ALVA2HHE	RSN9048_14151344_ALVA2HHZ	5.2	17.9	682	NGA
3	RSN12578_51207740_58238004	RSN12578_51207740_58238094	RSN12578_51207740_58238-UP	4.1	44.7	414	NGA
3	RSN10588_10370141_13922360	RSN10588_10370141_13922090	RSN10588_10370141_13922-UP	4.45	48.0	581	NGA
3	IT.MLC..HNE.D.IT-2012-0010.ACC.MP	IT.MLC..HNN.D.IT-2012-0010.ACC.MP	IT.MLC..HNZ.D.IT-2012-0010.ACC.MP	5.5	100.9	430	ESM
3	RSN2144_BEARCTY_2013A090	RSN2144_BEARCTY_2013B360	RSN2144_BEARCTY_2013C-UP	4.92	44.9	426	NGA
3	IT.ASP..HGE.D.EMSC-20160824_0000006.ACC.MP	IT.ASP..HGN.D.EMSC-20160824_0000006.ACC.MP	IT.ASP..HGZ.D.EMSC-20160824_0000006.ACC.MP	6	31.4	436	ESM
3	IT.SIG..HGE.D.EMSC-20161030_0000029.ACC.MP	IT.SIG..HGN.D.EMSC-20161030_0000029.ACC.MP	IT.SIG..HGZ.D.EMSC-20161030_0000029.ACC.MP	6.5	53.3	689	ESM
3	RSN1747_SKULLMTN_LSM8000	RSN1747_SKULLMTN_LSM8270	RSN1747_SKULLMTN_LSM8-UP	5.65	98.1	579	NGA
3	IT.PGG..HGE.D.EMSC-20161026_0000095.ACC.MP	IT.PGG..HGN.D.EMSC-20161026_0000095.ACC.MP	IT.PGG..HGZ.D.EMSC-20161026_0000095.ACC.MP	5.9	65.6	694	ESM
3	RSN8365_YLINDA_N5331021	RSN8365_YLINDA_N5331111	RSN8365_YLINDA_N5331-UP	4.27	55.2	643	NGA
3	IT.CLO..HGE.D.EMSC-20161026_0000095.ACC.MP	IT.CLO..HGN.D.EMSC-20161026_0000095.ACC.MP	IT.CLO..HGZ.D.EMSC-20161026_0000095.ACC.MP	5.9	3.2	420	ESM
3	RSN9071_14151344_AZPFOHLN	RSN9071_14151344_AZPFOHLE	RSN9071_14151344_AZPFOHLZ	5.2	12.8	763	NGA
3	RSN8845_14383980_CSBB2HNN	RSN8845_14383980_CSBB2HNE	RSN8845_14383980_CSBB2HNZ	5.39	80.9	1131	NGA
3	RSN1742_SKULLMTN_LSM3000	RSN1742_SKULLMTN_LSM3270	RSN1742_SKULLMTN_LSM3-UP	5.65	45.2	404	NGA
3	RSN6045_SIERRA.MEX_SLR360	RSN6045_SIERRA.MEX_SLR-90	RSN6045_SIERRA.MEX_SLR-UP	7.2	163.1	499	NGA
4	RSN11082_40187964_N1806HNN	RSN11082_40187964_N1806HNE	RSN11082_40187964_N1806HNZ	4.5	49.8	688	NGA
4	RSN555_CHALFANT.A_A-MAM020	RSN555_CHALFANT.A_A-MAM290	RSN555_CHALFANT.A_A-MAM-UP	6.19	34.9	529	NGA
4	IV.RM05..HNE.D.IT-2009-0102.ACC.MP	IV.RM05..HNN.D.IT-2009-0102.ACC.MP	IV.RM05..HNZ.D.IT-2009-0102.ACC.MP	5.5	20.5	617	ESM
4	HL.DMKA..HN2.D.GR-1999-0001.ACC.MP	HL.DMKA..HN3.D.GR-1999-0001.ACC.MP	HL.DMKA..HNZ.D.GR-1999-0001.ACC.MP	5.9	19.6	767	ESM
4	RSN12577_51207740_58219360	RSN12577_51207740_58219090	RSN12577_51207740_58219-UP	4.1	22.9	517	NGA
4	RSN1662_NORTH001_TEM000	RSN1662_NORTH001_TEM090	RSN1662_NORTH001_TEM-UP	6.05	26.8	452	NGA
4	RSN12693_14330056_CJRC2HHN	RSN12693_14330056_CJRC2HHE	RSN12693_14330056_CJRC2HHZ	4.34	19.2	623	NGA
4	RSN9010_14151344_CIDPPHHN	RSN9010_14151344_CIDPPHHE	RSN9010_14151344_CIDPPHHZ	5.2	67.2	611	NGA
4	IT.TER..HGE.D.EMSC-20161026_0000095.ACC.MP	IT.TER..HGN.D.EMSC-20161026_0000095.ACC.MP	IT.TER..HGZ.D.EMSC-20161026_0000095.ACC.MP	5.9	45.3	887	ESM
4	RSN8970_14383980_NS720360	RSN8970_14383980_NS720090	RSN8970_14383980_NS720-UP	5.39	72.8	493	NGA

4	20130721_050943_FAIS_20_x	20130721_050943_FAIS_20_y	20130721_050943_FAIS_20_z	6.58	64.9	760	GNS
4	RSN10528_10370141_CISLRHNN	RSN10528_10370141_CISLRHNE	RSN10528_10370141_CISLRHNZ	4.45	55.3	499	NGA
4	RSN3739_WHITTIER.B_B-GLE180	RSN3739_WHITTIER.B_B-GLE270	RSN3739_WHITTIER.B_B-GLE-UP	5.27	27.6	402	NGA
4	RSN5830_SIERRA.MEX_RSL000	RSN5830_SIERRA.MEX_RSL090	RSN5830_SIERRA.MEX_RSL--V	7.2	43.6	524	NGA
4	RSN13356_10285533_23292360	RSN13356_10285533_23292090	RSN13356_10285533_23292-UP	4.2	10.6	403	NGA
5	RSN19045_40238431_PGWRDHNN	RSN19045_40238431_PGWRDHNE	RSN19045_40238431_PGWRDHNZ	4.39	21.2	649	NGA
5	20110613_022049_D14C_x	20110613_022049_D14C_y	20110613_022049_D14C_z	5.99	11.0	1000	GNS
5	RSN3776_NORTH392_CO2092	RSN3776_NORTH392_CO2182	RSN3776_NORTH392_CO2-UP	5.28	8.5	400	NGA
5	IT.FSS..HGE.D.EMSC-20161030_0000029.ACC.MP	IT.FSS..HGN.D.EMSC-20161030_0000029.ACC.MP	IT.FSS..HGZ.D.EMSC-20161030_0000029.ACC.MP	6.5	86.9	932	ESM
5	RSN12577_51207740_58219360	RSN12577_51207740_58219090	RSN12577_51207740_58219-UP	4.1	22.9	517	NGA
5	RSN1666_NORTH001_PKC090	RSN1666_NORTH001_PKC360	RSN1666_NORTH001_PKC-UP	6.05	6.6	508	NGA
5	RSN10528_10370141_CISLRHNN	RSN10528_10370141_CISLRHNE	RSN10528_10370141_CISLRHNZ	4.45	55.3	499	NGA
5	RSN9074_14151344_CIPSDHHN	RSN9074_14151344_CIPSDHHE	RSN9074_14151344_CIPSDHHZ	5.2	31.3	408	NGA
5	20130721_050943_WANS_20_x	20130721_050943_WANS_20_y	20130721_050943_WANS_20_z	6.58	62.6	1000	GNS
5	IV.T1299..HNE.D.EMSC-20161030_0000029.ACC.MP	IV.T1299..HNN.D.EMSC-20161030_0000029.ACC.MP	IV.T1299..HNZ.D.EMSC-20161030_0000029.ACC.MP	6.5	9.8	641	ESM
5	RSN9071_14151344_AZPFOHLN	RSN9071_14151344_AZPFOHLE	RSN9071_14151344_AZPFOHLZ	5.2	12.8	763	NGA
5	RSN1098_NORTHR_WRI090	RSN1098_NORTHR_WRI180	RSN1098_NORTHR_WRI-UP	6.69	71.5	477	NGA
5	RSN12578_51207740_58238004	RSN12578_51207740_58238094	RSN12578_51207740_58238-UP	4.1	44.7	414	NGA
5	RSN226_ANZA_TVY045	RSN226_ANZA_TVY135	RSN226_ANZA_TVY-UP	5.19	5.9	618	NGA
5	RSN4069_PARK2004_JACK-90	RSN4069_PARK2004_JACK360	RSN4069_PARK2004_JACK-UP	6	9.1	576	NGA
6	RSN9048_14151344_ALVA2HHN	RSN9048_14151344_ALVA2HHE	RSN9048_14151344_ALVA2HHZ	5.2	17.9	682	NGA
6	IV.TERO..HNE.D.EMSC-20161030_0000029.ACC.MP	IV.TERO..HNN.D.EMSC-20161030_0000029.ACC.MP	IV.TERO..HNZ.D.EMSC-20161030_0000029.ACC.MP	6.5	27.9	1002	ESM
6	RSN12343_40194055_01823360	RSN12343_40194055_01823090	RSN12343_40194055_01823-UP	4.23	9.9	469	NGA
6	IV.T1201..HNE.D.EMSC-20161026_0000095.ACC.MP	IV.T1201..HNN.D.EMSC-20161026_0000095.ACC.MP	IV.T1201..HNZ.D.EMSC-20161026_0000095.ACC.MP	5.9	22.3	426	ESM
6	RSN11501_10275733_13096360	RSN11501_10275733_13096090	RSN11501_10275733_13096-UP	4.73	19.8	646	NGA
6	RSN8784_14383980_CIDGRHNN	RSN8784_14383980_CIDGRHNE	RSN8784_14383980_CIDGRHNZ	5.39	74.4	576	NGA
6	RSN226_ANZA_TVY045	RSN226_ANZA_TVY135	RSN226_ANZA_TVY-UP	5.19	5.9	618	NGA
6	RSN11333_9064092_CISVDHHN	RSN11333_9064092_CISVDHHE	RSN11333_9064092_CISVDHHZ	4.78	15.8	699	NGA

6	IV.T1244..HNE.D.EMSC-20161026_0000095.ACC.MP	IV.T1244..HNN.D.EMSC-20161026_0000095.ACC.MP	IV.T1244..HNZ.D.EMSC-20161026_0000095.ACC.MP	5.9	13.6	923	ESM
6	IV.T1216..HNE.D.EMSC-20161030_0000029.ACC.MP	IV.T1216..HNN.D.EMSC-20161030_0000029.ACC.MP	IV.T1216..HNZ.D.EMSC-20161030_0000029.ACC.MP	6.5	3.1	805	ESM
6	RSN12045_14116972_N5036360	RSN12045_14116972_N5036090	RSN12045_14116972_N5036-UP	4.42	7.0	631	NGA
6	RSN277_MAMMOTH.AH_H-XCV075	RSN277_MAMMOTH.AH_H-XCV165	RSN277_MAMMOTH.AH_H-XCV-UP	4.85	5.4	454	NGA
6	20120525_024450_PARS_x	20120525_024450_PARS_y	20120525_024450_PARS_z	5.07	2.7	760	GNS
6	20140120_025307_WAZ_20_x	20140120_025307_WAZ_20_y	20140120_025307_WAZ_20_z	6.31	116.0	690	GNS
6	RSN10610_10370141_23084360	RSN10610_10370141_23084090	RSN10610_10370141_23084-UP	4.45	7.5	428	NGA
7	RSN9048_14151344_ALVA2HHN	RSN9048_14151344_ALVA2HHE	RSN9048_14151344_ALVA2HHZ	5.2	17.9	682	NGA
7	IV.TERO..HNE.D.EMSC-20161030_0000029.ACC.MP	IV.TERO..HNN.D.EMSC-20161030_0000029.ACC.MP	IV.TERO..HNZ.D.EMSC-20161030_0000029.ACC.MP	6.5	27.9	1002	ESM
7	RSN9099_14151344_CISLRHLN	RSN9099_14151344_CISLRHLE	RSN9099_14151344_CISLRHLZ	5.2	37.9	499	NGA
7	IV.T1213..HNE.D.EMSC-20161030_0000029.ACC.MP	IV.T1213..HNN.D.EMSC-20161030_0000029.ACC.MP	IV.T1213..HNZ.D.EMSC-20161030_0000029.ACC.MP	6.5	4.4	588	ESM
7	RSN11501_10275733_13096360	RSN11501_10275733_13096090	RSN11501_10275733_13096-UP	4.73	19.8	646	NGA
7	RSN9840_51182810_54933360	RSN9840_51182810_54933090	RSN9840_51182810_54933-UP	4.6	15.0	523	NGA
7	RSN10610_10370141_23084360	RSN10610_10370141_23084090	RSN10610_10370141_23084-UP	4.45	7.5	428	NGA
7	RSN6076_YLINDA_05409-H1	RSN6076_YLINDA_05409-H2	RSN6076_YLINDA_05409-UP	4.27	43.7	414	NGA
7	IV.T1244..HNE.D.EMSC-20161026_0000095.ACC.MP	IV.T1244..HNN.D.EMSC-20161026_0000095.ACC.MP	IV.T1244..HNZ.D.EMSC-20161026_0000095.ACC.MP	5.9	13.6	923	ESM
7	RSN11755_9069986_CISVDHHN	RSN11755_9069986_CISVDHHE	RSN11755_9069986_CISVDHHZ	4.5	33.6	699	NGA
7	RSN250_MAMMOTH.L_L-LUL000	RSN250_MAMMOTH.L_L-LUL090	RSN250_MAMMOTH.L_L-LUL-UP	5.94	9.7	537	NGA
7	RSN10585_10370141_13916360	RSN10585_10370141_13916090	RSN10585_10370141_13916-UP	4.45	22.8	582	NGA
7	IT.VAL..HGE.D.EMSC-20160824_0000006.ACC.MP	IT.VAL..HGN.D.EMSC-20160824_0000006.ACC.MP	IT.VAL..HGZ.D.EMSC-20160824_0000006.ACC.MP	6	53.6	459	ESM
7	RSN277_MAMMOTH.AH_H-XCV075	RSN277_MAMMOTH.AH_H-XCV165	RSN277_MAMMOTH.AH_H-XCV-UP	4.85	5.4	454	NGA
7	RSN939_BIGBEAR_WWN090	RSN939_BIGBEAR_WWN180	RSN939_BIGBEAR_WWN-UP	6.46	59.1	506	NGA
8	RSN13357_10285533_23958360	RSN13357_10285533_23958090	RSN13357_10285533_23958-UP	4.2	6.4	423	NGA
8	4A.MI02..HNE.D.IT-2009-0102.ACC.MP	4A.MI02..HNN.D.IT-2009-0102.ACC.MP	4A.MI02..HNZ.D.IT-2009-0102.ACC.MP	5.5	2.6	445	ESM
8	RSN89_SFERN_TEH090	RSN89_SFERN_TEH180	RSN89_SFERN_TEHDWN	6.61	61.8	669	NGA
8	RSN603_WHITTIER.A_A-VIR200	RSN603_WHITTIER.A_A-VIR290	RSN603_WHITTIER.A_A-VIR-UP	5.99	52.8	404	NGA
8	RSN11501_10275733_13096360	RSN11501_10275733_13096090	RSN11501_10275733_13096-UP	4.73	19.8	646	NGA
8	RSN401_COALINGA_C-PLM270	RSN401_COALINGA_C-PLM360	RSN401_COALINGA_C-PLM-UP	5.18	9.9	458	NGA

8	RSN9048_14151344_ALVA2HHN	RSN9048_14151344_ALVA2HHE	RSN9048_14151344_ALVA2HHZ	5.2	17.9	682	NGA
8	RSN112_OROVILLE_D-EBH000	RSN112_OROVILLE_D-EBH090	RSN112_OROVILLE_D-EBHDWN	4.7	6.0	427	NGA
8	IV.T1244..HNE.D.EMSC-20161026_0000095.ACC.MP	IV.T1244..HNN.D.EMSC-20161026_0000095.ACC.MP	IV.T1244..HNZ.D.EMSC-20161026_0000095.ACC.MP	5.9	13.6	923	ESM
8	RSN12652_14403732_12092360	RSN12652_14403732_12092090	RSN12652_14403732_12092-UP	4.11	6.3	407	NGA
8	IV.RM03..HNE.D.IT-2009-0102.ACC.MP	IV.RM03..HNN.D.IT-2009-0102.ACC.MP	IV.RM03..HNZ.D.IT-2009-0102.ACC.MP	5.5	0.3	512	ESM
8	RSN9388_14155260_CIPERHHN	RSN9388_14155260_CIPERHHE	RSN9388_14155260_CIPERHHZ	4.88	28.4	418	NGA
8	RSN4069_PARK2004_JACK-90	RSN4069_PARK2004_JACK360	RSN4069_PARK2004_JACK-UP	6	9.1	576	NGA
8	RSN12279_40194055_BBRIBHLN	RSN12279_40194055_BBRIBHLE	RSN12279_40194055_BBRIBHLZ	4.23	4.4	490	NGA
8	IT.SIG..HGE.D.EMSC-20161026_0000095.ACC.MP	IT.SIG..HGN.D.EMSC-20161026_0000095.ACC.MP	IT.SIG..HGZ.D.EMSC-20161026_0000095.ACC.MP	5.9	45.6	689	ESM
9	RSN226_ANZA_TVY045	RSN226_ANZA_TVY135	RSN226_ANZA_TVY-UP	5.19	5.9	618	NGA
9	RSN225_ANZA_PFT045	RSN225_ANZA_PFT135	RSN225_ANZA_PFT-UP	5.19	12.2	725	NGA
9	IV.RM05..HNE.D.IT-2009-0102.ACC.MP	IV.RM05..HNN.D.IT-2009-0102.ACC.MP	IV.RM05..HNZ.D.IT-2009-0102.ACC.MP	5.5	20.5	617	ESM
9	IT.PCB..HGE.D.EMSC-20160824_0000006.ACC.MP	IT.PCB..HGN.D.EMSC-20160824_0000006.ACC.MP	IT.PCB..HGZ.D.EMSC-20160824_0000006.ACC.MP	6	10.7	655	ESM
9	RSN119_OROVILLE_D-OR6035	RSN119_OROVILLE_D-OR6125	RSN119_OROVILLE_D-OR6DWN	4.7	4.8	549	NGA
9	RSN45_LYTLECR_DCF090	RSN45_LYTLECR_DCF180	RSN45_LYTLECR_DCFDWN	5.33	18.4	667	NGA
9	RSN112_OROVILLE_D-EBH000	RSN112_OROVILLE_D-EBH090	RSN112_OROVILLE_D-EBHDWN	4.7	6.0	427	NGA
9	RSN9071_14151344_AZPFOHLN	RSN9071_14151344_AZPFOHLE	RSN9071_14151344_AZPFOHLZ	5.2	12.8	763	NGA
9	20130721_050940_MKBS_20_x	20130721_050940_MKBS_20_y	20130721_050940_MKBS_20_z	6.58	49.6	1000	GNS
9	RSN4069_PARK2004_JACK-90	RSN4069_PARK2004_JACK360	RSN4069_PARK2004_JACK-UP	6	9.1	576	NGA
9	RSN9332_14155260_CICFSHLN	RSN9332_14155260_CICFSHLE	RSN9332_14155260_CICFSHLZ	4.88	25.0	444	NGA
9	RSN12279_40194055_BBRIBHLN	RSN12279_40194055_BBRIBHLE	RSN12279_40194055_BBRIBHLZ	4.23	4.4	490	NGA
9	IT.ASP..HGE.D.EMSC-20160824_0000006.ACC.MP	IT.ASP..HGN.D.EMSC-20160824_0000006.ACC.MP	IT.ASP..HGZ.D.EMSC-20160824_0000006.ACC.MP	6	31.4	436	ESM
9	RSN414_COALINGA_D-CSU000	RSN414_COALINGA_D-CSU090	RSN414_COALINGA_D-CSU-UP	5.77	9.8	617	NGA
9	RSN1698_NORTH392_VIR200	RSN1698_NORTH392_VIR290	RSN1698_NORTH392_VIR-UP	5.28	19.1	404	NGA
10	RSN226_ANZA_TVY045	RSN226_ANZA_TVY135	RSN226_ANZA_TVY-UP	5.19	5.9	618	NGA
10	XO.AM05..HNE.D.EMSC-20161026_0000095.ACC.MP	XO.AM05..HNN.D.EMSC-20161026_0000095.ACC.MP	XO.AM05..HNZ.D.EMSC-20161026_0000095.ACC.MP	5.9	15.5	824	ESM
10	RSN13357_10285533_23958360	RSN13357_10285533_23958090	RSN13357_10285533_23958-UP	4.2	6.4	423	NGA
10	RSN12519_51207740_NCCRHHNN	RSN12519_51207740_NCCRHHNE	RSN12519_51207740_NCCRHHNZ	4.1	0.4	481	NGA

10	IT.AMT..HGE.D.EMSC-20160824_0000006.ACC.MP	IT.AMT..HGN.D.EMSC-20160824_0000006.ACC.MP	IT.AMT..HGZ.D.EMSC-20160824_0000006.ACC.MP	6	1.4	670	ESM
10	RSN386_COALINGA_A-SKH270	RSN386_COALINGA_A-SKH360	RSN386_COALINGA_A-SKH-UP	5.09	0.3	480	NGA
10	RSN116_OROVILLE_D-OR7180	RSN116_OROVILLE_D-OR7270	RSN116_OROVILLE_D-OR7DWN	4.7	0.8	515	NGA
10	IV.RM03..HNE.D.IT-2009-0102.ACC.MP	IV.RM03..HNN.D.IT-2009-0102.ACC.MP	IV.RM03..HNZ.D.IT-2009-0102.ACC.MP	5.5	0.3	512	ESM
10	RSN3719_WHITTIER.B_B-NYA090	RSN3719_WHITTIER.B_B-NYA180	RSN3719_WHITTIER.B_B-NYA-UP	5.27	22.1	412	NGA
10	RSN9388_14155260_CIPERHHN	RSN9388_14155260_CIPERHHE	RSN9388_14155260_CIPERHHZ	4.88	28.4	418	NGA
10	RSN399_COALINGA_C-OLF270	RSN399_COALINGA_C-OLF360	RSN399_COALINGA_C-OLF-UP	5.18	6.7	474	NGA
10	RSN12279_40194055_BBRIBHLN	RSN12279_40194055_BBRIBHLE	RSN12279_40194055_BBRIBHLZ	4.23	4.4	490	NGA
10	RSN4064_PARK2004_DONNA-90	RSN4064_PARK2004_DONNA360	RSN4064_PARK2004_DONNA-UP	6	4.3	657	NGA
10	IV.RM14..HNE.D.IT-2009-0102.ACC.MP	IV.RM14..HNN.D.IT-2009-0102.ACC.MP	IV.RM14..HNZ.D.IT-2009-0102.ACC.MP	5.5	7.2	755	ESM
10	RSN9332_14155260_CICFSHLN	RSN9332_14155260_CICFSHLE	RSN9332_14155260_CICFSHLZ	4.88	25.0	444	NGA

Table 5: Selected records at rock (record set 15 for PGA) with causative parameters

7.1. Hazard consistency verifications of the bedrock ground motions

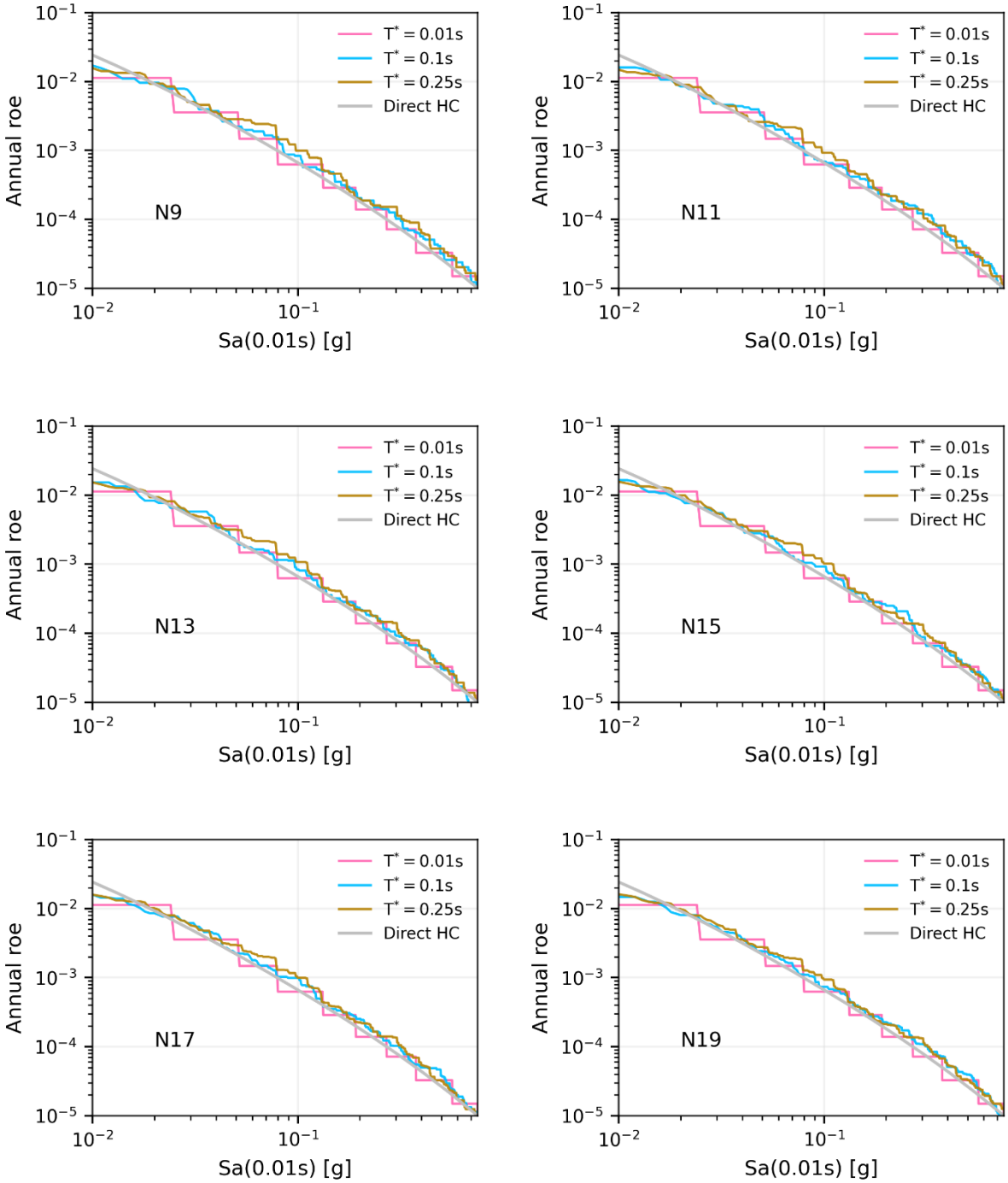

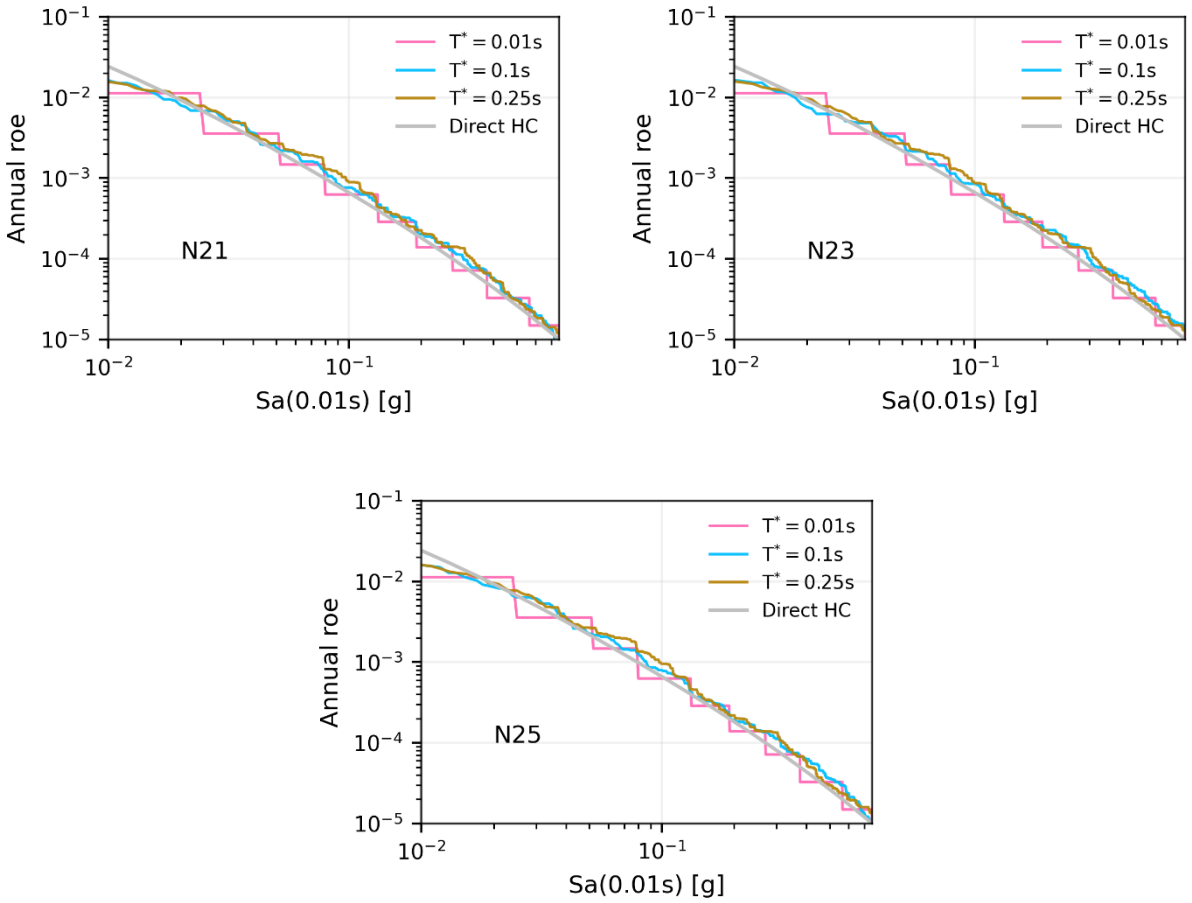

Figure 42: Hazard consistency checks for the PGA (SA [0.01s]) set

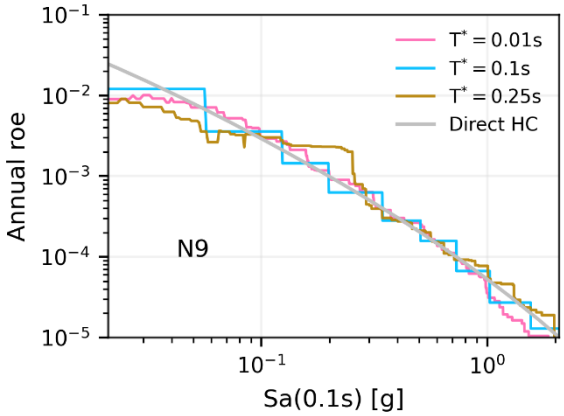
Annual roe
Sa(0.1s) [g]
T* = 0.01s
T* = 0.1s
T* = 0.25s
Direct HC
N9

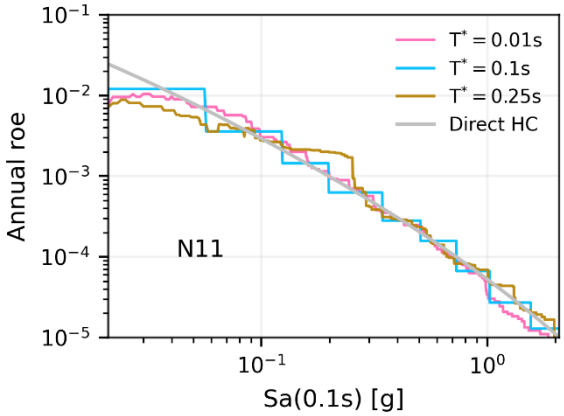
Annual roe
Sa(0.1s) [g]
T* = 0.01s
T* = 0.1s
T* = 0.25s
Direct HC
N11

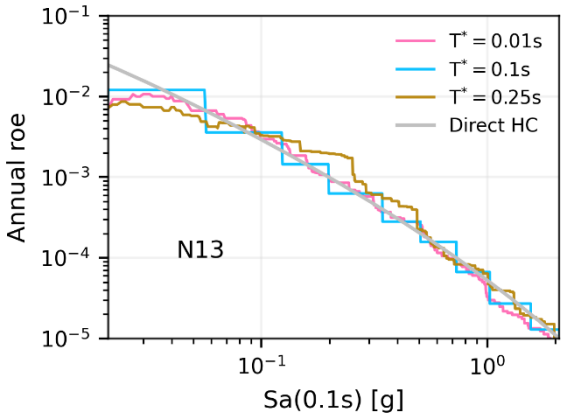
Annual roe
Sa(0.1s) [g]
T* = 0.01s
T* = 0.1s
T* = 0.25s
Direct HC
N13

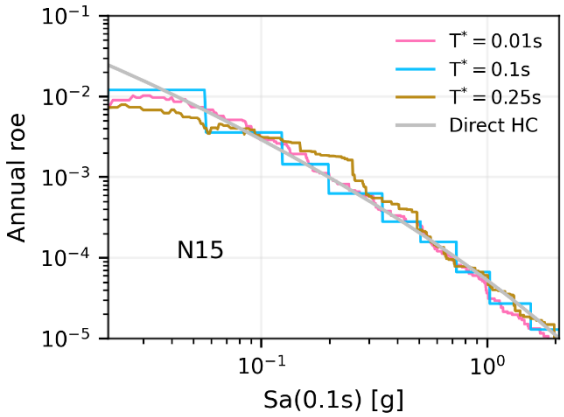
Annual roe
Sa(0.1s) [g]
T* = 0.01s
T* = 0.1s
T* = 0.25s
Direct HC
N15

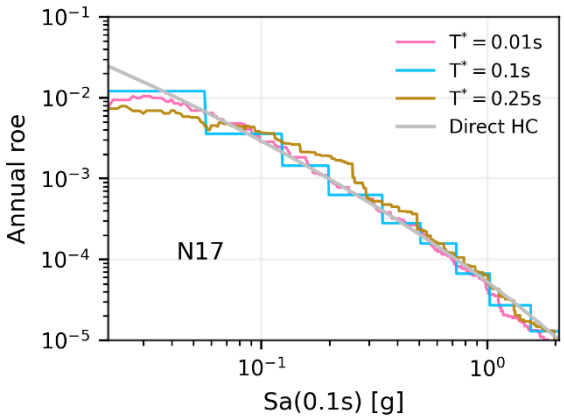
Annual roe
Sa(0.1s) [g]
T* = 0.01s
T* = 0.1s
T* = 0.25s
Direct HC
N17

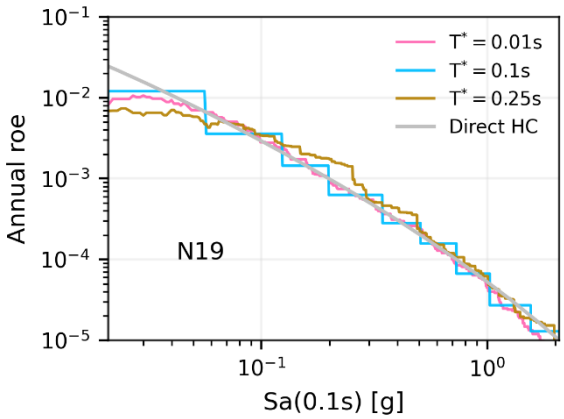
Annual roe
Sa(0.1s) [g]
T* = 0.01s
T* = 0.1s
T* = 0.25s
Direct HC
N19

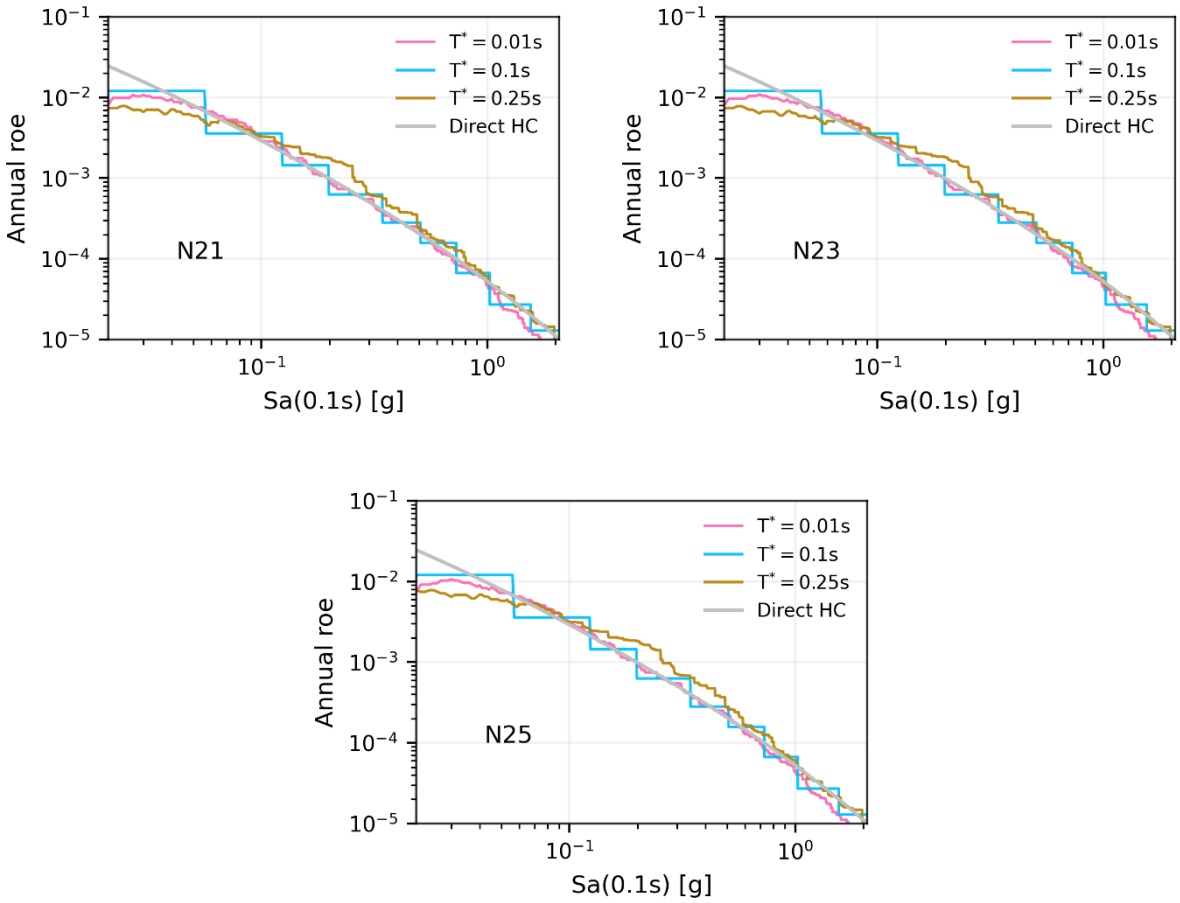

Figure 43: Hazard consistency checks for the SA (0.1s) set

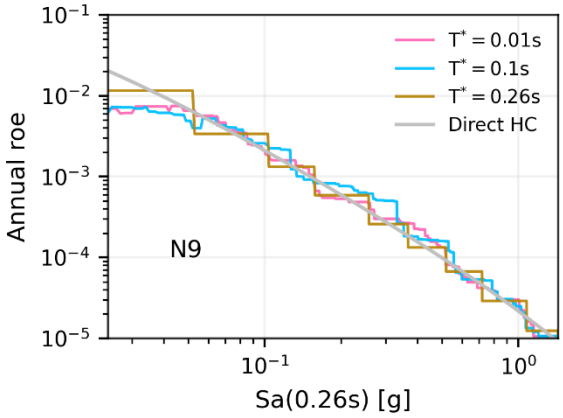
Annual roe
Sa(0.26s) [g]
N9
T* = 0.01s
T* = 0.1s
T* = 0.26s
Direct HC

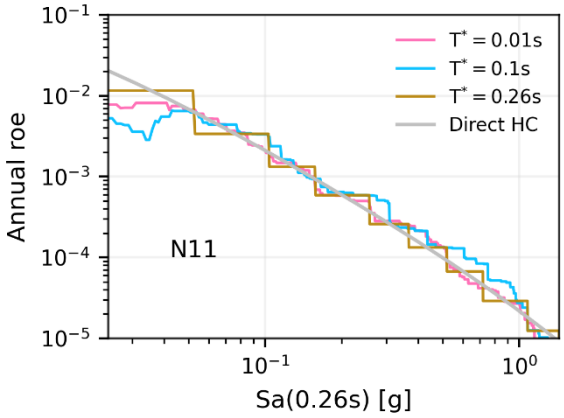
Annual roe
Sa(0.26s) [g]
N11
T* = 0.01s
T* = 0.1s
T* = 0.26s
Direct HC

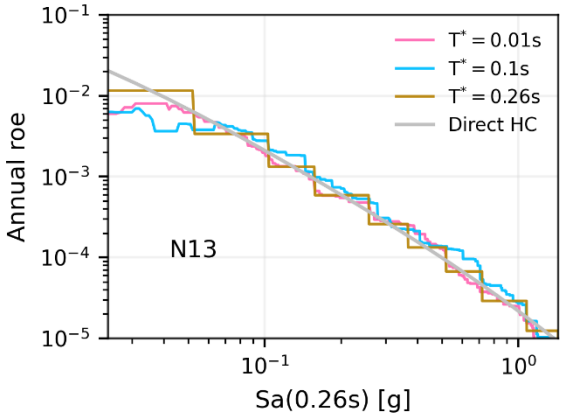
Annual roe
Sa(0.26s) [g]
N13
T* = 0.01s
T* = 0.1s
T* = 0.26s
Direct HC

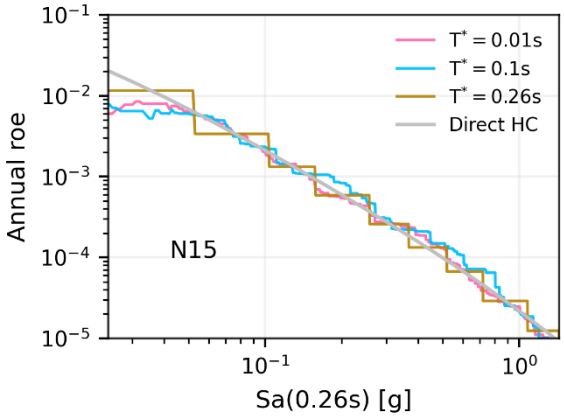
Annual roe
Sa(0.26s) [g]
N15
T* = 0.01s
T* = 0.1s
T* = 0.26s
Direct HC

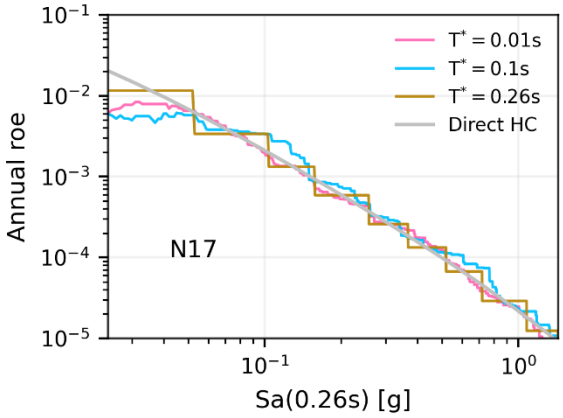
Annual roe
Sa(0.26s) [g]
N17
T* = 0.01s
T* = 0.1s
T* = 0.26s
Direct HC

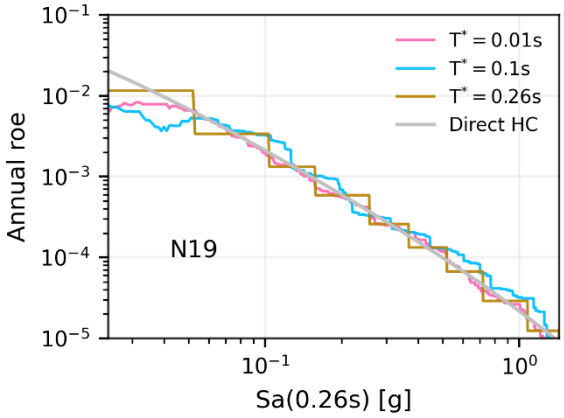
Annual roe
Sa(0.26s) [g]
N19
T* = 0.01s
T* = 0.1s
T* = 0.26s
Direct HC

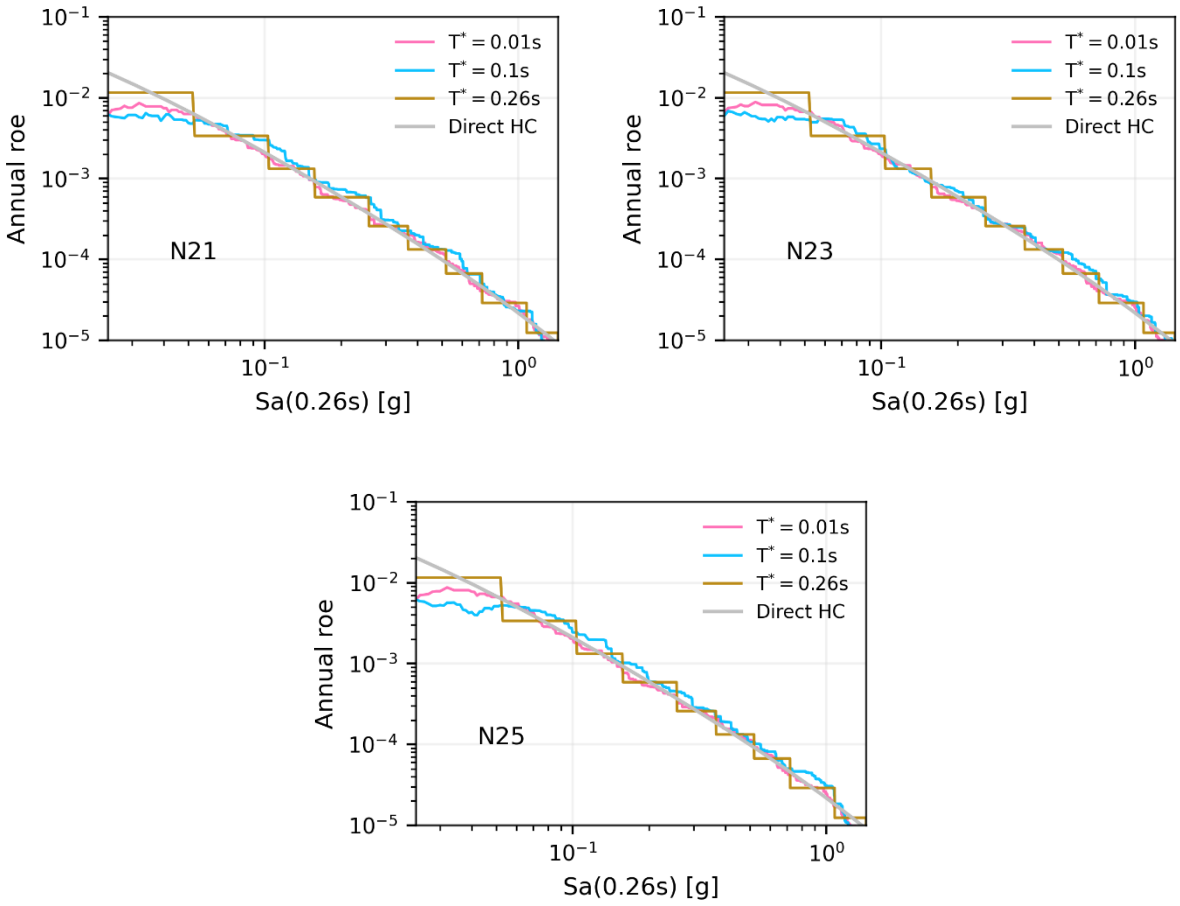

Figure 44: Hazard consistency checks for the SA (0.26s) actual SA(0.25s) set